PNAS
www.pnas.org

Supplementary Information Appendix for

Assessment of enzyme active site positioning and tests of catalytic mechanisms through X-ray-derived conformational ensembles

Filip Yabukarski[1], Justin T Biel[6], Margaux M Pinney[1], Tzanko Doukov[7], Alexander S Powers[2,4,5,], James S Fraser[6], Daniel Herschlag[1,3,5]

[1]Department of Biochemistry, [2]Department of Chemistry, [3]Department of Chemical Engineering, [4]Department of Computer Science, [5]Stanford ChEM-H, Stanford University, Stanford, California 94305, United States, [6]Department of Bioengineering and Therapeutic Sciences, University of California, San Francisco, San Francisco, United States, [7]Stanford Synchrotron Radiation Light Source, SLAC National Accelerator Laboratory, Menlo Park, California 94025, United States.

*correspondence: Daniel Herschlag, Filip Yabukarski

Email: herschla@stanford.edu, fyabukar@stanford.edu

This PDF file includes:

Supplementary text and detailed Materials and Methods

Figures S1 to S32

Tables S1 to S60

Supplementary information References

Supplementary text #1

Obtaining conformational ensemble information from cryo X-ray crystallography structural data

Cryo X-ray crystallography conformational ensembles have been built and used (1–4), but the question can be raised, how well do multiple cryo X-ray structures replicate the actual conformational heterogeneity experienced by a protein in solution at physiological temperature?

Crystals differ in crystallization conditions, the details of vitrification, and ligands and mutations that may be present, and the premise of ensembles obtained from cryo X-ray crystallography structural models is that these variations lead to capturing states that approximate different states of the protein's conformational landscape (1, 2, 4–6). For this to hold, the conformational heterogeneity must be substantially dampened at cryo temperatures (7–9) and the induced changes must be limited and local enough to not vastly reconfigure the overall conformational landscape. Indeed, prior data indicate good agreement between disorder of each residue obtained from cryo X-ray ensembles and measured by NMR (2). While this agreement is encouraging, it does not indicate that the actual atomic coordinates of a cryo ensemble are accurate, and inaccuracies could arise in several ways, including from changes during the vitrification process and transition to temperatures below the glass transition, crystallization condition and crystal contact effects, as well as mutants included in an ensemble that might have long-range effects (7–12). *Fortunately, the data presented herein provide additional strong support for and additional information about the accuracy of cryo X-ray ensembles as we can compare with RT data and ensembles*. The following observations support the accuracy of cryo X-ray ensembles:

i. The cryo ensemble (referred to as "pseudo" ensemble herein) and RT ensemble are very similar, as judged by several criteria (Figs. S17 and S18), including R^2 of 0.84 and 0.87 for Cα and Cβ positions of across the entire sequence.

ii. The residue-level atomic ensembles were highly similar from the cryo pseudo and RT ensembles. In the main text and *SI Appendix* we show these ensembles for the active site, Y16, D103, and D40 (Figs. 5 and 7 and Figs. S21 and S23). The directions and extent of the conformational heterogeneity is similar, with the exception that the Y16 motions are more extended and less symmetrical in the RT *vs.* the cryo pseudo-ensemble (Fig. S23). This difference does not impact any of the conclusions herein and may result from restricted conformational freedom at temperatures below the glass transition.

iii. Sub-setting the cryo X-ray data or using only higher resolution data do not significantly alter the overall conformational heterogeneity (Figs. S6 and S7), providing support for the robustness of the derived ensemble information.

iv. While there are not extensive changes from the KSI mutations (see above), we do see and learn from local rearrangements. In particular we show that the sub-ensemble missing the Y16-

Y57 hydrogen bond occupies new states and also has increased heterogeneity, rather than a simple conformational switch (Fig. S32).

v. Some mutations that could be reasonably expected to cause local rearrangements and that may represent states not sampled in the WT conformational ensemble were excluded from the full pseudo-ensemble to obtain a reduced pseudo-ensemble (Table S2). Both the overall and local conformational heterogeneity properties of the reduced cryo pseudo-ensemble are nevertheless highly similar to both the full cryo pseudo-ensemble and the RT ensemble (Figs. S17 and S18).

In summary, our data strongly support the ability to obtain conformational ensemble information from combinations of cryo X-ray structures and further indicate that we can learn more by judicious sub-setting of these ensembles. In the future, identifying mutations that result in conformational outliers may reveal sites of allosteric communication. These experiments are likely to be carried out more and more using RT X-ray data, given the ability to obtain conformational heterogeneity from single diffraction datasets as opposed to the large set of structures needed with cryo structures.

Supplementary text #2

The relationship of KSI transition state analog ensembles to the reaction's transition state.

As no transition state analog (TSA) is a perfect mimic, it is important to evaluate the properties of an analog that may and may not be expected to reflect properties of the actual transition state (13–15). Below we address the two principle aspects of KSI transition state and TSA analog behavior: i. oxyanion/oxyanion hole interactions and ii. proton abstraction and donation. In both cases, energetic and conformational data suggest consistent properties of the TSAs and actual transition state.

Mutations in the oxyanion hole give similar changes in binding affinity and catalysis, providing energetic evidence for analogous TSA/transition state behavior (16). From a conformational perspective, the bound TSAs explore conformational states that allow it to come within ~3.2, ~3.2, and ~3.7 Å of each position of proton abstraction/donation (Fig. 5E); the greater flexibility of the actual substrates (relative to planar, aromatic TSAs) and the apparent smoothness of the energy landscape for the TSA conformational states (Fig. 5E) provide no indication of a special barrier to the conformers required to achieve the shorter, higher-energy transition state configurations in which the proton is in flight.

The bound TSA is sufficiently mobile so that the single state represented by the single D103N structure is well within the ensemble of states captured by the KSI cryo pseudo-ensemble (Fig. S16). We also observe no difference in the conformational preferences of D40 or N40 (Fig. S21), and thus no indication of changes in positional preferences that might indicate additional conformational preferences and complications in the actual reaction coordinate.

With respect to the oxyanion hole, an energetic argument sometimes made to suggest that oxyanions are poor KSI TSAs is based on the similar *observe*d affinities for the TSA equilenin and KSI substrates but does not take into account energetic penalties in TSA binding from loss of the TSA phenolic proton and uptake of a proton by D40; these steps are needed to mimic the transition state, but do not occur in the normal reaction cycle (Fig. 1A, Fig. S1). When this proton uptake is no longer needed, equilenin oxyanion binds $3x10^4$ fold stronger to KSI (with D40N to mimic protonated D40 that is present when the oxyanion intermediate is bound) than substrates bind WT KSI (17, 18). The D40 general base appears to contribute an additional 10^5 to catalysis, relative to the corresponding solution reaction (19), so that together these factors come close to KSI's overall catalysis of 10^{11} fold (20).

Supplementary text #3

Developing and testing models about the forces and interactions that define residues' conformational ensemble preferences.

Y16. Several groups, including M84, are situated within van der Waals contact distance of Y16, whereas M31 is consistently beyond van der Waals contact distance and M116 is highly variable in its positioning with respect to Y16 (Fig. 8A, D, Fig. S27). In addition to these packing interactions, Y16 accepts a hydrogen bond from Y57, and the Y16-Y57 distance is highly conserved (Fig. 8G). The observed longer Y16/M31 distances indicate that the collection of states with tight simultaneous packing of all residues is higher in free energy than the states that are observed.

We considered two simple models to account for the absence of close Y16/M31 packing:

> *Model I*: Packing is more favorable with residues other than M31 (e.g., M84), leading to the choice to not utilize the available van der Waals interaction energy from packing with M31.
>
> *Model II*: The Y16-Y57 hydrogen bond energy and positioning dominates to constrain Y16 away from M31 and closer to M84.

Model I predicts that breaking the Y16-Y57 hydrogen bond will leave Y16 or its replacement residue in place, whereas in *Model II* predicts a rearrangement, most simply to make closer interactions with M31. To test these predictions, we compared KSI sub-ensembles with the Y16-Y57 hydrogen bond to those with mutations that removed this hydrogen bond (Fig. S32A, B, Y16-Y57 hydrogen bond intact (grey stick) and ablated (green sticks), respectively; Table S2). Without the Y16-Y57 hydrogen bond, we observed a shift in the Y16 positions, toward M31 and away from M84 (Fig. S32C-D**,** Y16-Y57 hydrogen bond intact (grey histograms) and ablated (green histograms), respectively). These results support *Model II* and an energetic and conformational trade-off between the Y16-Y57 hydrogen bond and what would otherwise be a more symmetrical packing of Y16 with both M31 and M84 (Fig. S32A-D). Nevertheless, Y16 becomes more mobile without the hydrogen bond from Y57 (Fig. S32E), and a range of Y16

distances is observed with respect to both M31 and M84, suggesting a rather flat local energy landscape in which interactions with M31 and M84 are similar in energy, whereas states rearranged to allow simultaneous packing are disfavored, presumably because the cost of losing other interactions with these side chains is too high. This flat energy landscape is then tilted by the Y16-Y57 hydrogen bond to favor Y16 positions closer to M84.

Interestingly, the increased flexibility of the ring at position 16 upon removal of the Y16–Y57 hydrogen bond does not result in any rearrangements or significant structural changes in the surrounding residues, suggesting that their positioning is dominated by interactions with residues other than Y16 (Fig. S28). Further, neither ablation of the Y16 hydrogen bonding group (e.g., Y16F mutation, Fig. S16), nor increased flexibility or apparent mispositioning of Y16 upon ablation of the Y16–Y57 hydrogen bond (Fig. S28) appear to impact D103 positioning, supporting the conclusion above that the allowed Y16 and D103 side chain orientations are not coupled (Fig. 7B).

D103. The observed conformational constraint from the Y16–Y57 hydrogen bond leads to the question of how D103 can be well-positioned in the absence of analogous hydrogen bonding. Analysis of the D103 surroundings revealed particularly close packing of the non-catalytic Oδ1 of D103 with multiple residues: F86, V101, and A118 (Fig. 8B, E). Indeed, the RT-ensemble suggested that this oxygen atom may be more restricted than the protonated catalytic oxygen (Oδ2) that sits in the oxyanion hole (Fig. 4C). This atypical arrangement in which hydrophobic interactions surround a carboxylic acid oxygen atom (21) is particularly intriguing as it appears to accomplish two objectives: *i.* positioning the catalytic group, and *ii.* increasing its pK_a so that the carboxylate group remains protonated and can act as a hydrogen bond donor at physiological pH. The protonated D103 side chain provides greater oxyanion stabilization than hydrogen bond donors with higher pK_a values, such as asparagine, as those side chains have hydrogen bonding protons with lower partial positive charges (Fig. 1; (22, 23) see "*Discussion*"). Thus, counterintuitively, interactions of a polar oxyanion atom with hydrophobic groups appear to provide important favorable interaction energy, from van der Waals interactions that sterically constrain the carboxylic acid group for function and disfavor conformational states where the carboxylic acid group can rearrange and be solvated to favor its anionic form. This model is testable—it predicts that mutations that reduce packing will decrease D103's pK_a and positioning.

D40. Above we addressed the hydrogen bonding and anion-aromatic interactions with W120 and F120. Our packing analysis reveals interactions in addition to the W120 hydrogen bond: van der Waals interactions with V38, M84, and A118 (Fig. 8C).

Intriguingly, the "other" oxygen of D40, the one involved in proton abstraction and donation, makes an anion-aromatic interaction, with F56 (Fig. 6A). The broader potential of this interaction, relative to a hydrogen bond, may help the Oδ2 oxygen atom explore the range of positions required for proton transfers. It may also destabilize the anionic form of D40, relative

to its protonated form, to increase the driving force for proton abstract and thereby facilitate catalysis.

Materials and Methods

KSI expression and purification. The ketosteroid isomerase enzymes from *Pseudomonas putida* (pKSI, referred to herein as KSI, UniProt P07445) and *Comamonas testosteroni* (tKSI, referred to herein as $KSI_{homolog}$, UniProt P00947) were expressed and purified as previously described with minor modifications (19, 24). KSI W120F and $KSI_{homolog}$ F120W (KSI numbering) variants were obtained using standard mutagenesis protocols and the presence of the desired mutations was confirmed via DNA sequencing (see Table S60). Briefly, BL21 cells transformed with plasmid carrying the desired KSI construct were grown at 37 °C to OD 0.5−0.6 in LB media (EMD Millipore Corp, Billerica, MA, USA) containing 50 μg/mL carbenicillin (Goldbio, St Lousi, MO, USA), and protein expression was induced with 1 mM isopropyl-β-D-1-thiogalactopyranoside (Goldbio, St Lousi, MO, USA). After induction, cultures were grown for 10−12 h at 37 °C. Cells were harvested by centrifugation at 5000 g for 30 min at 4 °C and lysed using sonication. Lysed cells were centrifuged at 48000 g for 30 min at 4 °C. Enzymes were purified from the soluble fraction, first using an affinity column (deoxycholate resin) followed by a size exclusion chromatography column (SEC) Superdex 200. Prior to the purification of each enzyme, the affinity column, FPLC loops, and SEC column were washed with 40 mM potassium phosphate (JT Baker, Omaha, NE, USA), 6 M guanidine (JT Baker, Omaha, NE, USA), pH 7.2 buffer, and then equilibrated with 40 mM potassium phosphate, 1 mM sodium EDTA, 2 mM DTT (Goldbio, St Lousi, MO, USA), pH 7.2 buffer.

KSI solution kinetics. KSI Michaelis–Menten parameters were obtained by monitoring the 5(10)-estrene-3,17-dione ((5(10)-EST), Steraloids, Newport, RI, USA) reaction at 248 nm (extinction coefficient 14,800 M^{-1} cm^{-1}) in a PerkinElmer Lambda 25 spectrophotometer(19). Reactions were measured at 25 °C in 4 mM sodium phosphate, pH 7.2 buffer with 2% DMSO (JT Baker, Omaha, NE, USA) added for substrate solubility. Low buffer concentrations were used to minimize the background reaction rate. Values of k_{cat} and K_M were determined by fitting the initial rates as a function of substrate concentration to the Michaelis–Menten equation. Typically, seven to eight substrate concentrations, varying from 2 to 600 μM, were used for each mutant. The k_{cat} and K_M values were averaged from two independent measurements using different enzyme concentrations varied over 2–3 fold. Averaged values and errors representing the standard deviations are given in Table S58.

KSI ^{1}H solution Nuclear Magnetic Resonance. The ^{1}H NMR spectrum of KSI D40N bound to equilenin was acquired at the Stanford Magnetic Resonance Laboratory using an 800 MHz Varian ^{UNITY}INOVA spectrometer running VNMRJ 3.1A and equipped with a Varian 5 mm triple resonance, pulsed field gradient $^1H[^{13}C,^{15}N]$ cold probe, as previously described (25). The sample contained 1.0 mM KSI and 2.0 mM equilenin (Steraloids, Newport, RI, USA) in 40 mM potassium phosphate (pH 7.2), 1 mM sodium·EDTA, 2 mM DTT, and 10% DMSO-d_6 (v/v) (Cambridge Isotope Laboratories, Tewksbury, MA, USA). DMSO-d_6 served as the deuterium

lock solvent and prevented freezing at low temperatures. The spectrum was obtained in a 5 mm Shigemi symmetrical microtube at –3.5 °C, following temperature calibration with a 100% methanol standard. The 1331 binomial pulse sequence was used to suppress the water signal with a spectral width of 35 ppm (carrier frequency set on the water resonance) and an excitation maximum between 14-18 ppm (26). The data was processed using 10 Hz line broadening and baseline correction applied over the peaks of interest. Chemical shifts were referenced internally to the water resonance.

Protein crystallization and X-ray data collection. All enzymes were crystallized (27, 28) as previously described (29). Briefly, enzyme were crystallized by mixing 1 µL of enzyme at 1 mM and 1 µL of crystallization solution (17-23% PEG 3350 (Hampton Research, Aliso Viejo, CA, USA) and 0.2 M $MgCl_2$ (JT Baker, Omaha, NE, USA)) in a vapor diffusion hanging drop setup at room temperature. For crystallization of KSI bound to the transition state analog (equilenin) or the ground-state analog (4-androstenedione (Steraloids, Newport, RI, USA)), equilenin or 4-androstenedione were first dissolved in methanol (JT Baker, Omaha, NE, USA) at 20 mM and 40 mM concentration, respectively. Each ligand was then mixed with enzyme to achieve final concentrations of 1 mM enzyme and 2 mM equilenin or 4 mM 4-androstenedione (10% methanol in the final enzyme-ligand solution). As a ground-state analog, 4-androstenedione binds more weakly than the transition-state analog equilenin, and thus higher concentration was used to achieve higher occupancy. Crystals typically appeared after 24-72 h. Prior to data collection, crystals with minimum dimensions 0.2 x 0.2 x 0.2 mm were transferred from the crystallization solution to paratone N oil (Hampton Research, Aliso Viejo, CA, USA) where excess crystallization solution was stripped and crystals where then either frozen in liquid nitrogen for 100 K data collection and then mounted on the goniometer or directly mounted on the goniometer for 250 K or 280 K data collection. Data collection temperature was controlled using a N_2 cooler/heater. Single-crystal diffraction data were collected at SSRL, beamline BL9-2, using wavelengths of either 0.787 Å or 0.886 Å. See Table S3 for diffraction data statistics.

Crystallographic data processing and model building. Data processing was carried out with in-house scripts: http://smb.slac.stanford.edu/facilities/software/xds/#autoxds_script. Briefly, data reduction was done using the XDS package (30), scaling and merging was done using *Aimless* (31, 32) and structure factor amplitudes were obtained using *Truncate* (31, 33). Initial phases were obtained via molecular replacement using *PHASER* (34) and the PDB entry 3VSY as a search model. Model building was carried out with the program *ARP/wARP* (35) and manually in *Coot* (36). Traditional, single conformation models, in which major alternative side chain and backbone conformations were modeled, were refined manually after visual inspection with *Coot* and using *phenix.refine* (37). Torsion-angle simulated annealing (as implemented in *phenix.refine*) was used during the initial stages of refinement. Riding hydrogens were added in the late stages of refinement and their scattering contribution was accounted for in the refinement. Ligand restraints were generated using the *GRADE* server (http://grade.globalphasing.org/cgi-bin/grade/server.cgi). Model quality was assessed using

Molprobity (38) as implemented in *phenix.refine* and via the PDB Validation server (https://validate-rcsb-2.wwpdb.org/). See Table S3 for refinement statistics.

Multi-conformer models were obtained from the 250 K diffraction datasets, using previously described methods (8, 27, 28, 39, 40). As a large body of work identified the 180–220 K temperature range as an inflection point above which various protein motions are activated, providing strong evidence that at and above 250 K both harmonic and anharmonic protein motions are enabled (8, 41–44), and as the 250 K diffraction data was of higher resolution than our 280 K data (Table S3), we used the higher-resolution 250 K to obtain multi-conformer models of Apo, GS-bound, and TSA-bound KSI. Briefly, the program *qFit* was used to obtain multi-conformation models (28, 39) using as input the traditional single-conformation models obtained above after removing the riding hydrogen atoms. Subsequent to the automated multi-conformer model building, ill-defined water molecules were deleted and alternative protein side and main chain conformations and orientations were edited manually after visual inspection in *Coot* and based on the fit to the electron density (45). Models were subsequently refined with *phenix.refine* (37). Riding hydrogen atoms were added in the late stages of refinement and their scattering contribution was accounted for in the refinement. Final multi-conformer model quality was checked by *MolProbity* (38) and via the PDB Validation server (https://validate-rcsb-2.wwpdb.org/) and deposited on the PDB (Table S3). See Table S3 for refinement statistics.

Crystallographic order parameters calculation. Crystallographic order parameters, S^2, were obtained from the 250 K multi-conformer models as previously described (27). These order parameters include both harmonic and anharmonic contributions as captured by the crystallographic atomic displacement parameters (B-factors) and by the occupancies of alternative rotameric states, respectively; these values correlate well with solution NMR-derived S^2 (27). The analysis was applied to the bond most closely associated with the first side-chain dihedral angle (χ_1), using Cβ—H for all amino acids other than Gly and Cα—H for Gly. Because S^2 varies from 0 to 1 as a measure of order, we used 1-S^2 as a measure of disorder.

The KSI crystals obtained in this study contained two molecules in the asymmetric unit and the average of the two molecules was used for analysis. Because the total ground-state analog (4-Androstenedione) occupancy in the final refined model of the two crystallographically-independent KSI molecules was 1.4 instead of 2.0 (corresponding to the maximum occupancy of 1.0 for each of the KSI molecules), the (1-S^2) values for each residue were corrected using the equation:

$$(1 - S^2)\, GSA_{corrected} = \left((1 - S^2)GSA_{observed} - 0.3x(1 - S^2)Apo\right) \Big/ 0.7$$

Ensemble building. To obtain KSI pseudo-ensembles, all KSI cryo crystal structures were downloaded from the PDB (46) and parsed into individual KSI monomers (Table S1). While KSI

is a dimer, we focused the analysis on the individual KSI molecule as: i) all individual KSI molecules were highly similar, with RMSDs below 0.5 Å after excluding two flexible loops (see Results); ii) KSI is known to also crystallize with one molecule in the crystallographic asymmetric unit (see Table S1), indicating that the two molecules of the dimer are identical; and iii) each monomer has the full catalytic machinery required for catalysis. All KSI molecules were aligned using PyMOL and standard commands (The PyMOL Molecular Graphics System, Version 2.0 Schrödinger, LLC.) on the protein backbone (N, Cα, C, O atoms) of residues 5-125 on either the highest resolution crystal structure of KSI bound to the transitions state analog equilenin (PDB 1OH0, (47)) or as otherwise indicated. Residues 1-4 (N-terminal) and 126-131(C-terminal) were excluded from the analyses because these residues appeared highly flexible, as is common for N/C-terminal residues, and were also not modeled in some of the KSI structures. No alignment gaps were allowed during the alignment, and allowing for gaps (default PyMOL alignment procedure) did not appreciably change the results (Fig. S9). The same approach was used to obtain $KSI_{homolog}$ pseudo-ensembles, with the backbone of residues 3-122 aligned on the highest resolution crystal structure of $KSI_{homolog}$ bound to the ground state analog 4-androstene-3,17-dione (PDB 3NHX). $KSI_{homolog}$ pseudo-ensembles excluded structures with mutations that alter the chemical nature of the general base (e.g., histidine or glycine) and mutations in the loop carrying the general base (residues 40-44, 'general base loop', KSI numbering), as these mutations alter the general base positioning (Table S21). Different sets of crystal structures were used to obtain different types of pseudo-ensembles (sub-ensembles) and the structures included in the different types of pseudo-ensembles are listed in Tables S1, 2, 20-22 and explicitly indicated in the legends of figures from the main text and supplemental information. The KSI RT-ensemble was obtained from the Apo, GS-bound, and TSA-bound RT multi-conformer models using the same alignment procedure and the Apo state as alignment template.

Calculating mean deviations. From the ensemble of aligned crystal structures or multi-conformer models, a list of *xyz* coordinates was defined for each atom using PyMOL and standard code. For *n* copies of each particular atom in the ensemble, a coordinate list of size 3*n* was obtained for this atom. The mean deviation (MDev) was then calculated by computing the spread of these points about the center point *j*:

$$mean\ deviation = \sqrt{\min_j \left(\frac{1}{n} \sum_i \left(x_i - x_j\right)^2 + \left(y_i - y_j\right)^2 + \left(z_i - z_j\right)^2 \right)}$$

Here *i* is an index over each of the *n* atoms in the ensemble and the average distance of all points to a center point from atom *j* was calculated. The center point *j* was chosen to give the minimum average distance to all other points in the given ensemble of atoms and was determined by

calculating the average distance between each atom in a given ensemble and all other atoms in the same ensemble of atoms.

Bootstrap analysis. A bootstrap analysis was used to estimate the errors associated with the sum of Cα MDev values of the Apo and the transition-state bound KSI pseudo-ensembles (ΣMDev Apo and TSA-bound, Fig. 3E from the main text). Briefly, from the number of distances, n (e.g. for the full pseudo-ensemble of 94 structures ($q = 94$), $n = q - 1$), used to calculate the Cα MDev for a given KSI residue x (where x denotes residues 5 to 125), a random number of distances, m_1, was randomly selected and excluded from n. A second small number of distances, m_2, equal to m_1, was randomly selected from n to replace the excluded m_1 and then the sum of the MDevs for residues 5-125 was calculated (ΣMDev). The procedure was repeated 300 times and the standard deviations associated with an increasing number of bootstrapped ΣMDev (n = 2, 5, 10, 20, 30, 40, 50, 100, 200 and 300 cycles, Fig. S8, Table S27) was used to estimate the standard deviation of the ΣMDev in Fig. 3E from the main text.

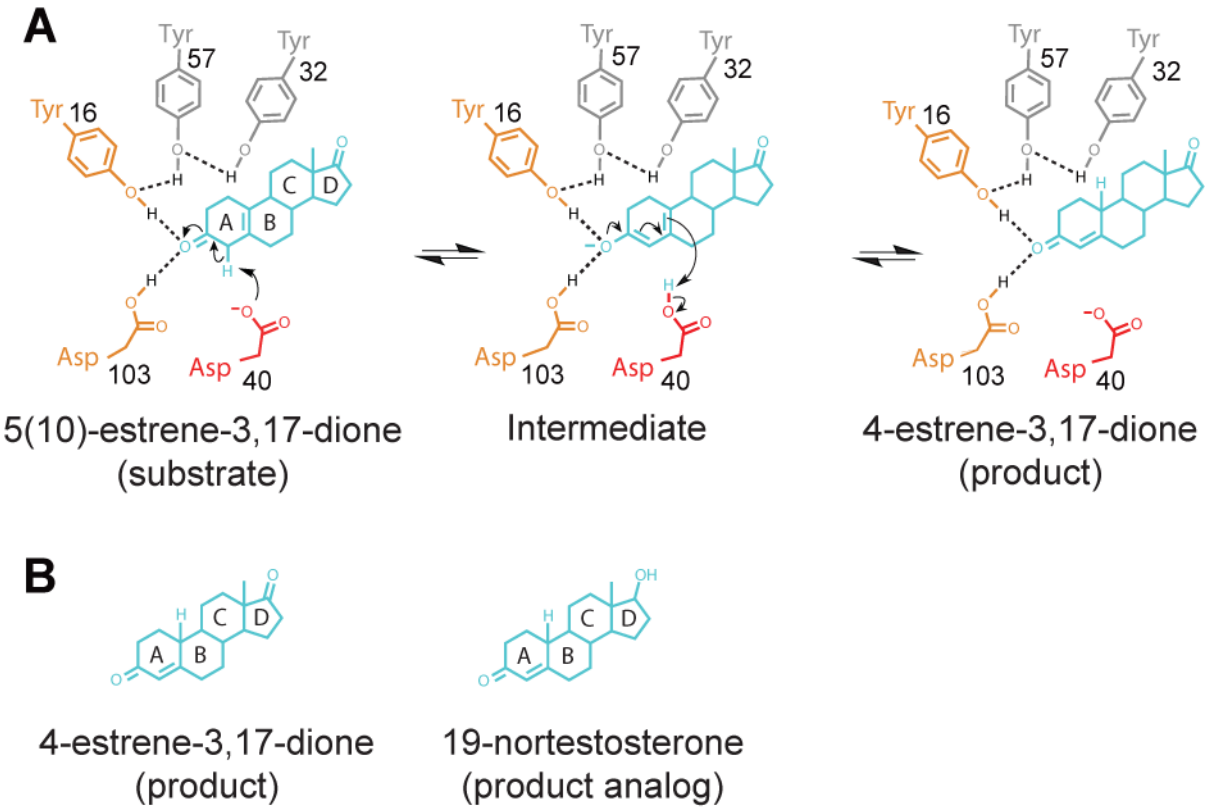

Fig. S1. The Ketosteroid Isomerase (KSI) reaction. (A) KSI catalyzes double bond isomerization of steroid substrates (shown for the substrate 5(10)-estrene-3,17-dione) utilizing a general acid/base D40 (which we refer to herein as a general base, for simplicity) and an oxyanion hole composed of the side chains of Y16 and D103 (protonated); general base and oxyanion hole residues are colored in red and orange, respectively. (B) The product in (A), 4-estrene-3,17-dione (left)**,** is the substrate of the reverse reaction and is highly similar to the 19-nortestosterone bound to the cryo structure of KSI (right, PDB code 5KP4). We note that k_{cat} values are within two-fold for substrates with four and one rings and that steroid ligands with or without bulky substituents attached to the D-ring have similar affinities for KSI (25)(48).

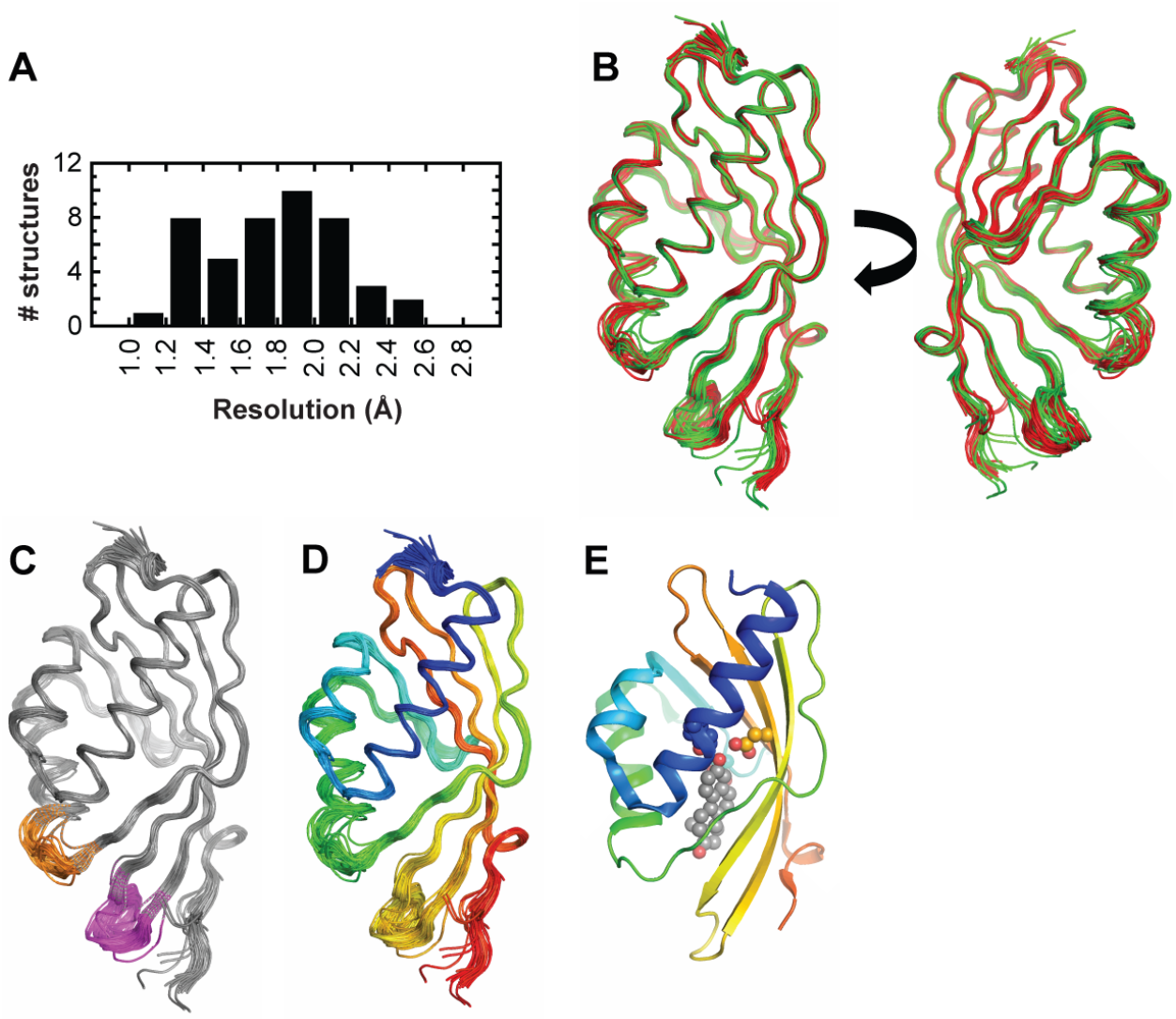

Fig. S2. The KSI pseudo-ensemble. (A) Resolution of the KSI cryo crystal structures used to obtain pseudo-ensembles (Table S1). (B-D) Individual KSI molecules are colored, as follows: (B) according to the catalytic state: Apo (green), GS-bound (blue), and TSA-bound (red); (C) in grey, with the exception of the 62-65 loop (in orange) and 91-96 loop (in magenta); and (D) from N– (blue) to C–terminal (red). (E) KSI bound to a TSA (PDB 1OH0) using the same color code as (D), with Y16 (blue), D103 (orange), D40 (teal), colored according to their associated secondary structure element, and bound TSA (grey) shown in spheres.

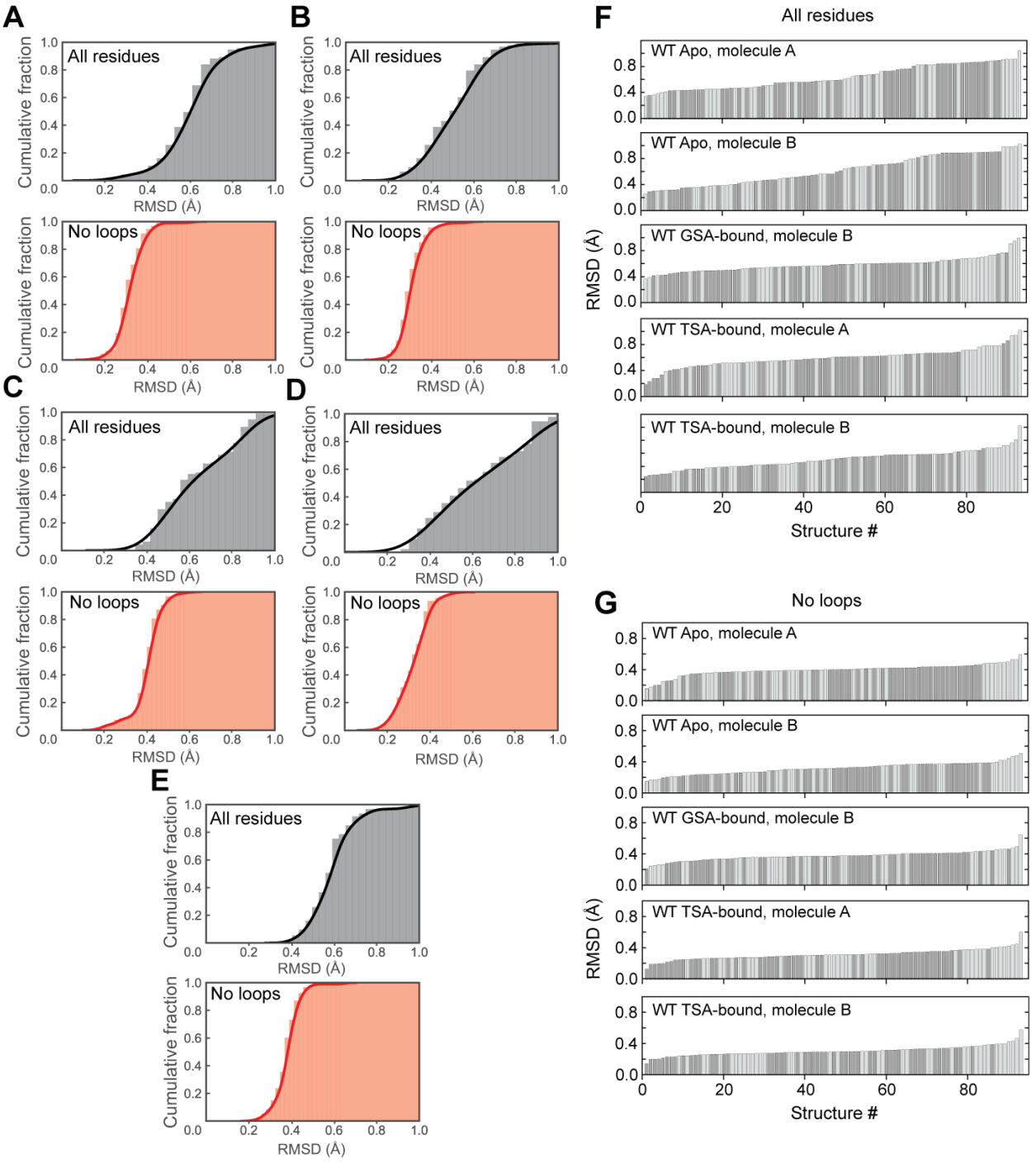

Fig. S3. RMSDs for all available KSI cryo structures. Structures were aligned on the backbone of residues 5–125. Backbone RMSDs for WT Apo (PDB 3VSY, A and B), WT GS - bound (PDB 5KP4, C), and WT TSA-bound (PDB 1OH0, D and E) relative to each of the remaining crystallographically-independent KSI molecules from the PDB (N = 95). A and B represent each of the two crystallographically-independent KSI molecules of WT Apo (PDB 3VSY) and similarly D and E represent each of the two crystallographically-independent KSI molecules of WT TSA-bound (PDB 1OH0), whereas for PDB 5KP4 (C), there is only the

crystallographically-independent KSI molecule with bound GS, molecule B. The larger RMSD values and variability in the “All residues” panels reflect the greater structural variability of the 62–65 and 91–96 loops. Backbone RMSDs from A-E have been ranked according to increasing RMSD values for (F) the entire sequence and (G) excluding loops 62–65 and 91–96. RMSDs with Apo and Ligand-bound KSI molecules are colored in light and dark grey, respectively.

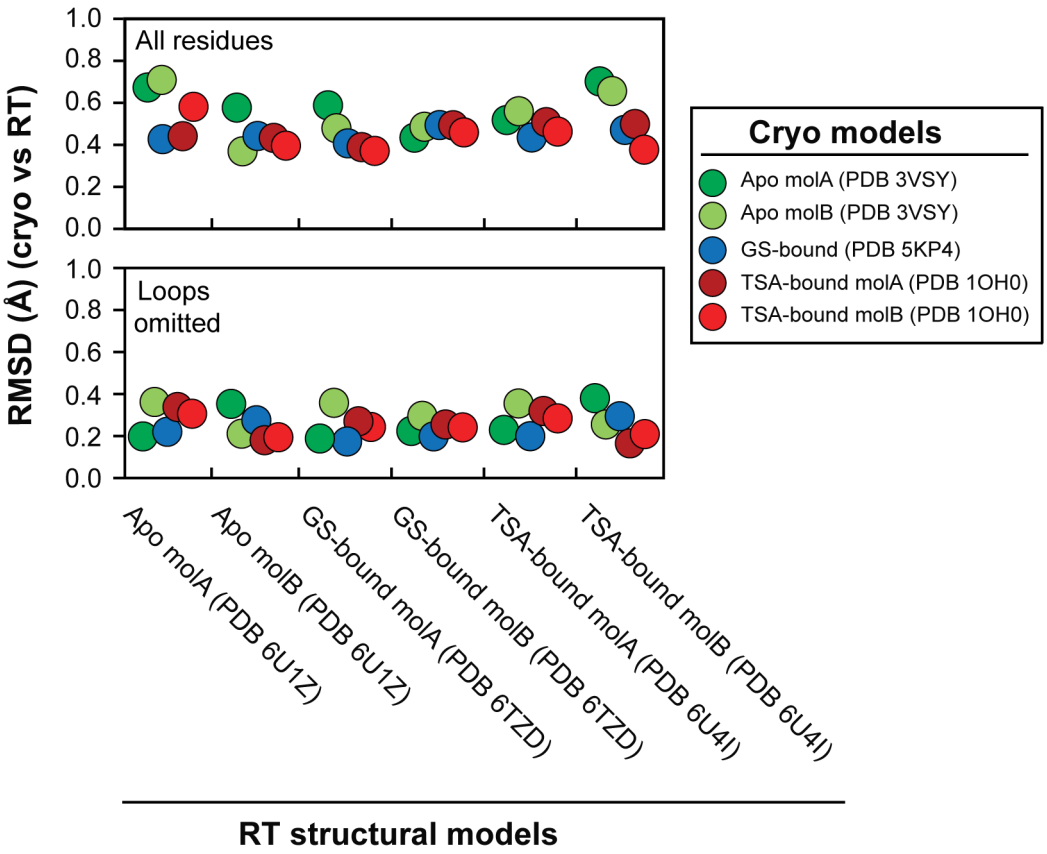

Fig. S4. Backbone RMSDs of Apo, GS-bound and TSA-bound KSI single-conformation structures obtained at RT (280 K, this study; x-axis) *vs.* the highest-resolution cryo (100 K, from the PDB; y-axis). There are two crystallographically-independent molecules for each enzymes state, for both RT and cryo structures, except for the GS -bound cryo structure, for which there was only one GS -bound molecule. Each circle represents the RMSD between each of the two independent KSI molecules from the RT structures (x-axis) and each of the independent molecules from the cryo structures (color coded in legend). Fig. 2 from the main text represents the average RMSD between each of the two independent monomers from the KSI dimer from the RT structures and each of the two independent monomers from the KSI dimer the cryo structures.

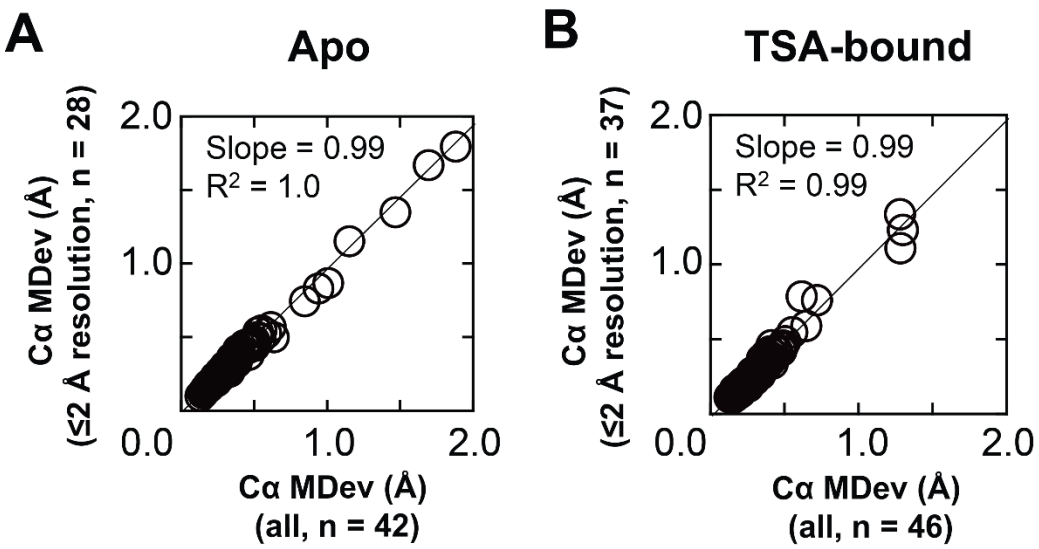

Fig. S5. Exclusion of lower resolution structures does not alter the KSI pseudo-ensemble properties. Correlation between Cα MDevs for the full pseudo-ensemble *vs.* a pseudo-ensemble including only higher-resolution Apo structures for (A) Apo pseudo-ensembles (42 and 28 structures, respectively) and (B) TSA-bound pseudo-ensembles (46 and 37 structures, respectively). High-resolution structures are defined as structures with resolutions ≤2 Å. For a given atom in a structure, the MDev describes the average displacement of equivalent atoms within the ensemble of structures, with lower and higher values representing smaller and larger positional fluctuations, respectively, corresponding to less or more conformational heterogeneity (also see Materials and Methods for a more complete definition of MDev).

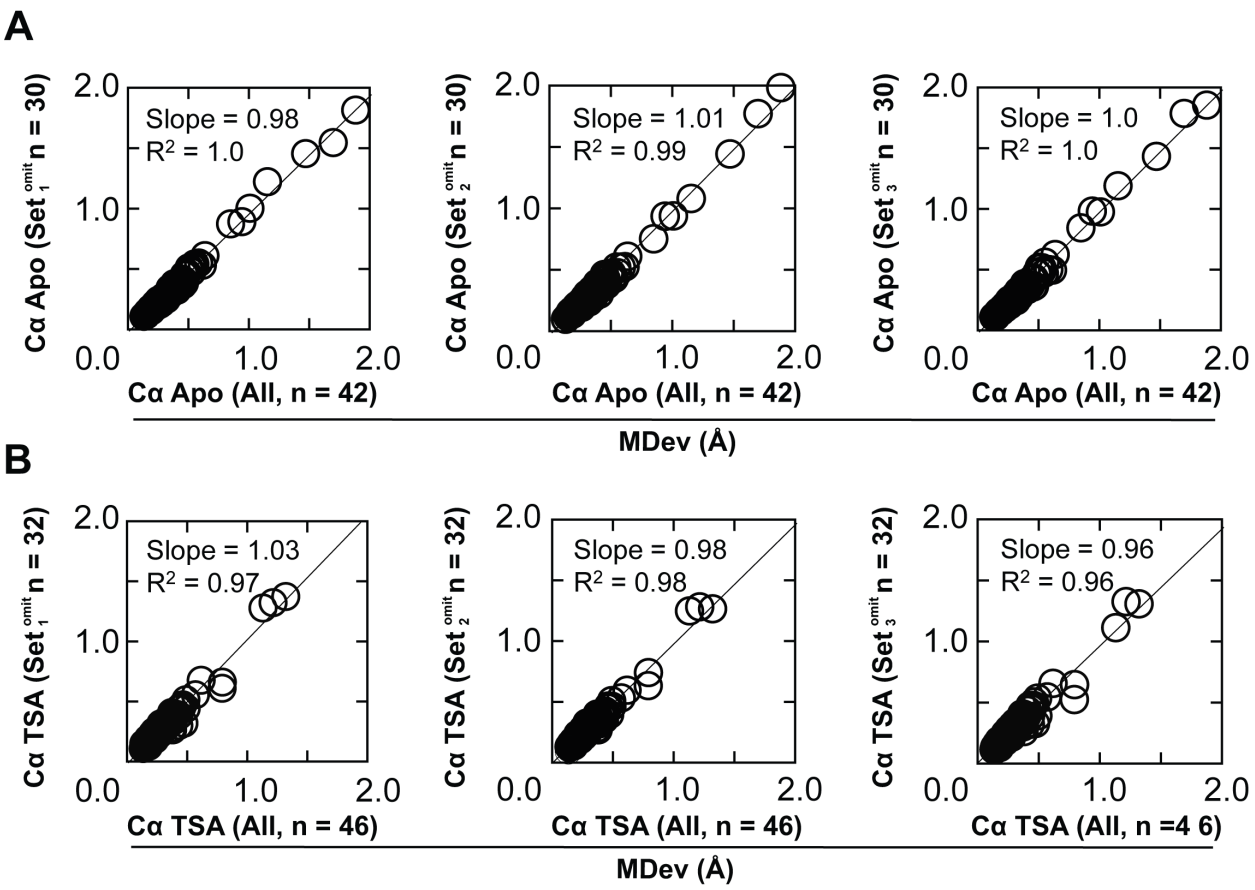

Fig. S6. Random omission of KSI molecules does not alter the pseudo-ensemble properties. Comparison of Cα MDevs for (A) Apo and (B) TSA-bound from the full pseudo-ensembles (obtained from 42 (Apo) and 46 (TSA-bound) KSI molecules, respectively) and pseudo-ensembles from which 30% of the structures were randomly omitted (12 out of 42 and 14 out of 46 KSI molecules, respectively); random selection and exclusion of molecules was repeated three times to generate three independent sets (Set1-3); Table S8).

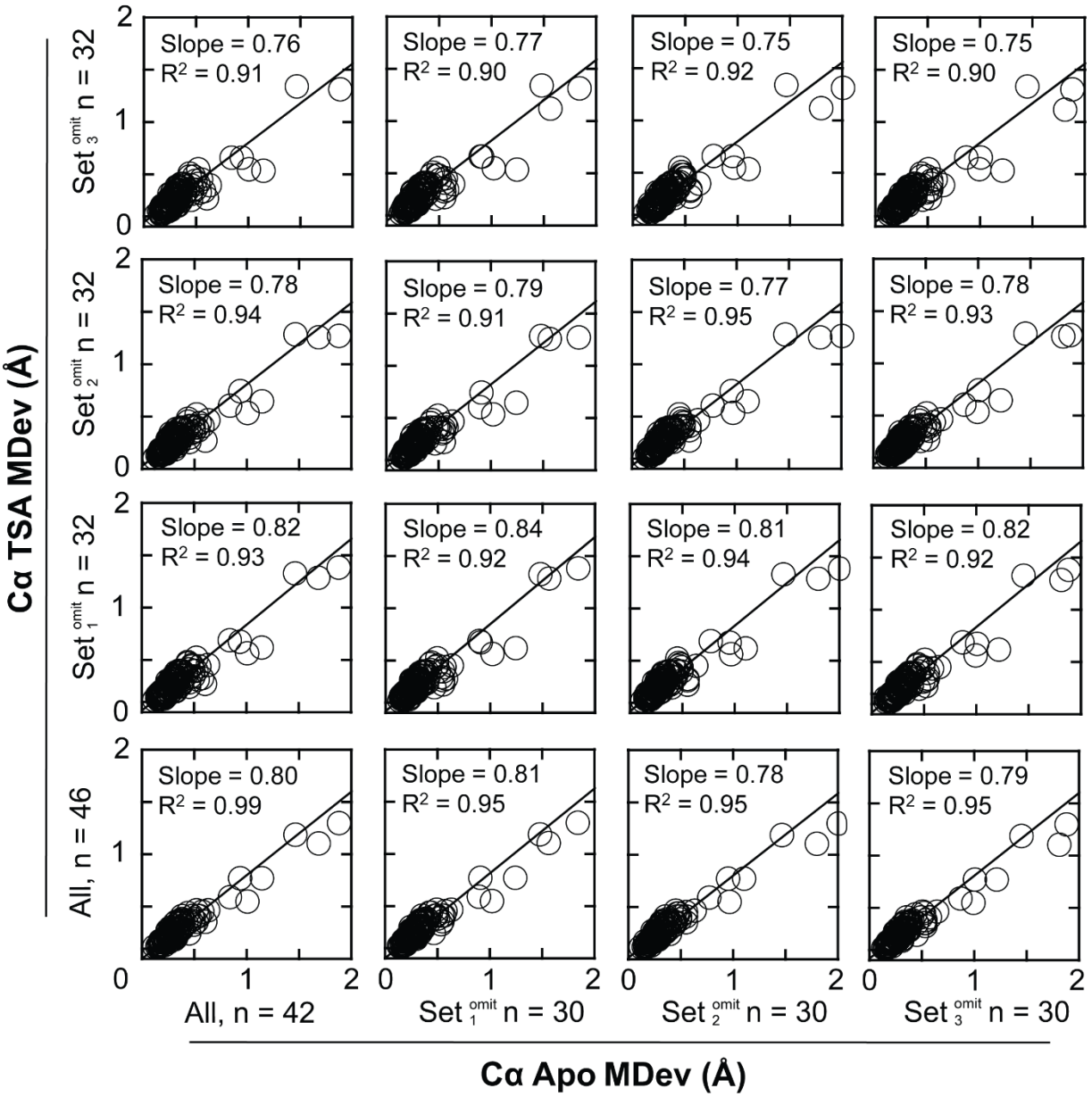

Fig. S7. Random omission of KSI molecules from pseudo-ensembles has no significant impact on the conformational heterogeneity dampening in Apo KSI upon TSA binding. Comparison of correlation plots between Cα MDevs for Apo and TSA-bound pseudo-ensembles composed of all structures (42 and 46 KSI molecules, respectively) and pseudo-ensembles from which 30% of the structures have been randomly omitted (12 out of 42 and 14 out of 46 KSI molecules, respectively; data from Fig. S5, Tables S8 and S9). The average slope is 0.79 ± 0.02 and average R^2 is 0.93 ± 0.02.

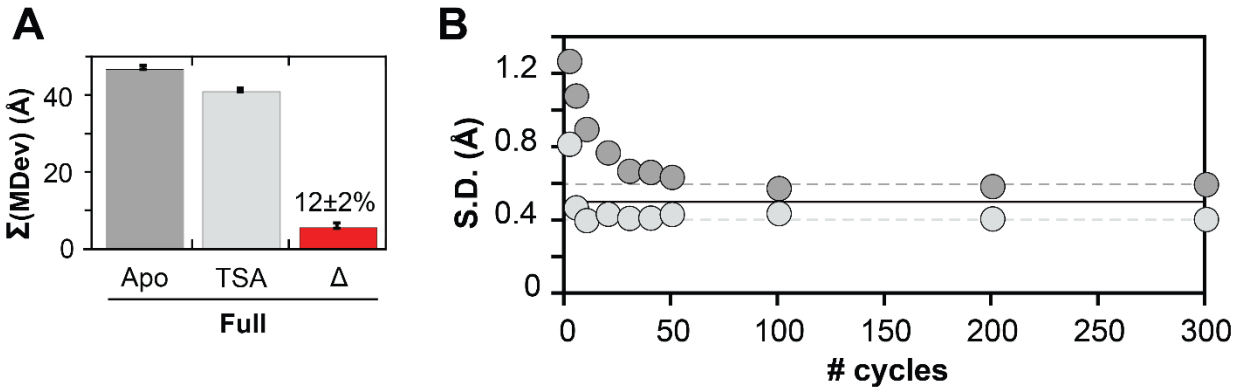

Fig. S8. Estimating the error in the sum of Cα MDevs from the Apo and TSA-bound pseudo-ensembles. (A) Sum of Cα MDevs for Apo (dark grey bars), TSA-bound (light grey bars) and the sum of their difference (Δ, red bars) for the entire enzyme (reproduced from Fig. 3E from main text). The error bars in (A) were estimated using a bootstrap analysis. Briefly, ΣMDev Apo and TSA-bound were obtained by summing the Cα MDevs for residues 5-125 in Apo and TSA-bound pseudo-ensembles, respectively. The Cα MDev for each residue is the average distance of all Cα atoms within the Cα ensemble for a given residues, to the center of the same Cα ensemble. For a number of distances *n*, (in either the Apo or the TSA-bound pseudo-ensemble), a random number of distances, m_1, was randomly selected and replaced by second number of distances, m_2, equal in number to m_1, and randomly selected from the same ensemble. A new Cα ΣMDev for residues 5–125 was then obtained and the procedure was repeated 300 times (see Materials and Methods for a more complete description). (B) The standard deviation (S.D.) over an increasing number of bootstrapped Cα ΣMDevs. The S.D. levels off as the number of bootstrapped Cα ΣMDevs increases, as expected (dark and light grey dashed lines for Apo and TSA-bound pseudo-ensembles, respectively). The solid black line indicates the average, 0.5 Å, which was used as a measure of the error in (A) and in the Fig. 3E of the main text.

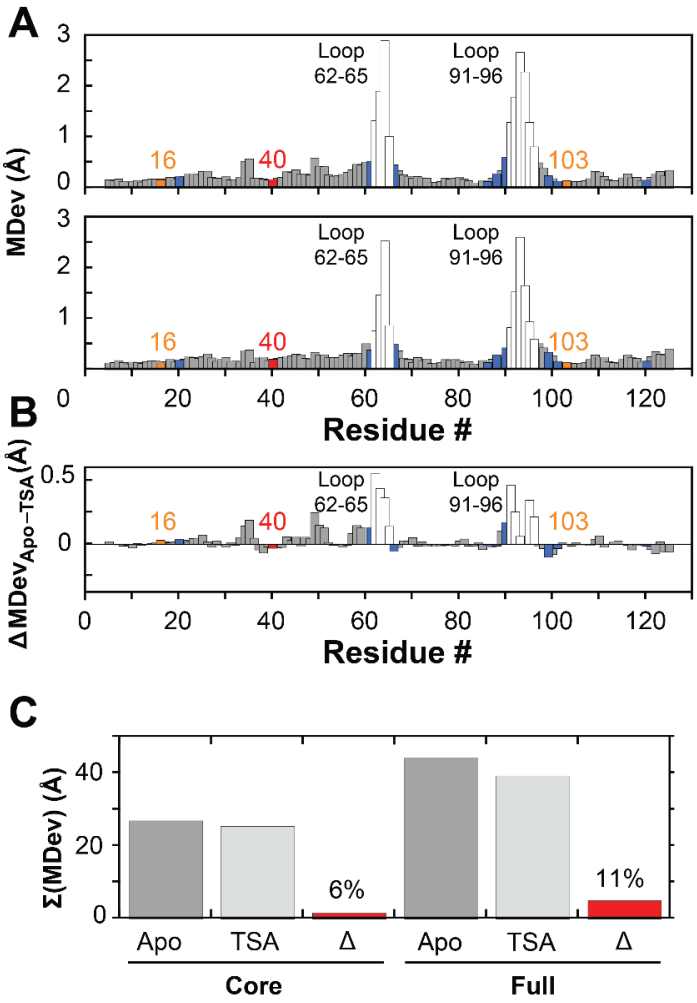

Fig. S9. The alignment procedure does not impact the change in conformational heterogeneity for Apo *vs.* TSA-bound KSI obtained from pseudo-ensembles. Apo and TSA-bound KSI pseudo-ensembles were obtained using an alignment procedure different from the alignment procedure used in the main text (see Materials and Methods). (A) Cα MDevs for KSI Apo (top) and TSA–bound (bottom) states. (B) Difference Cα MDev values between the Apo and TSA-bound states ($MDevs_{Apo-TSA}$), such that positive values indicate lower MDevs for the TSA-bound state. The differences are similar throughout the enzyme, except for larger changes in the 62-65 and 91-96 loops (white bars). (C) Sum of Cα MDevs for Apo, TSA-bound and their difference. The color code is the same as in Fig. 3 of the main text.

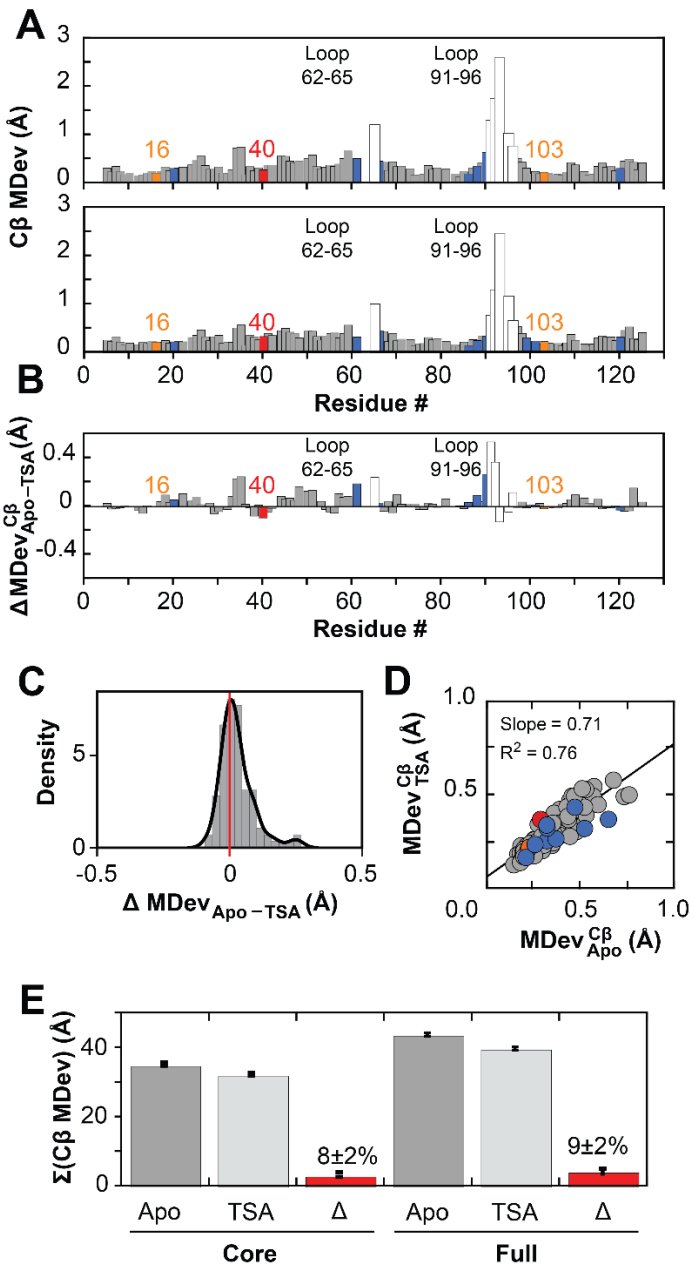

Fig. S10. Quantifying changes in conformational heterogeneity through the KSI catalytic cycle via pseudo-ensemble Cβ MDevs. (A) Cβ MDevs for KSI Apo (top) and TSA–bound (bottom) states. (B) Difference Cβ MDev values between the Apo and TSA-bound states ($MDevs_{Apo-TSA}$), such that positive values indicate lower MDevs for the TSA-bound state. Note that the ΔMDev for the loop represents a small difference between large values (note the different scale of the y-axis in A *vs.* B). (C) Histogram of MDev differences from part (B; $MDevs_{Apo-TSA}$) for the enzyme core (i.e., loops excluded). (D) Correlation plot of Apo and TSA-bound Cβ MDevs (excluding loops 62–65 and 91–96). (E) Sum of Cα MDevs for Apo, TSA-bound and their difference; colors as in Fig. 4 main text. The slightly lower dampening of conformational heterogeneity for the full enzyme estimated using Cβ MDevs *vs.* Cα MDevs (12±2% and 9±2% *vs.* 8±2% and 9±2%, respectively) arises at least in part because both 62–65

and 91–96 loops contain Gly residues (3 and 1 Gly residues, respectively) which do not have Cβ atoms. Color code as in Fig. 3 of the main text.

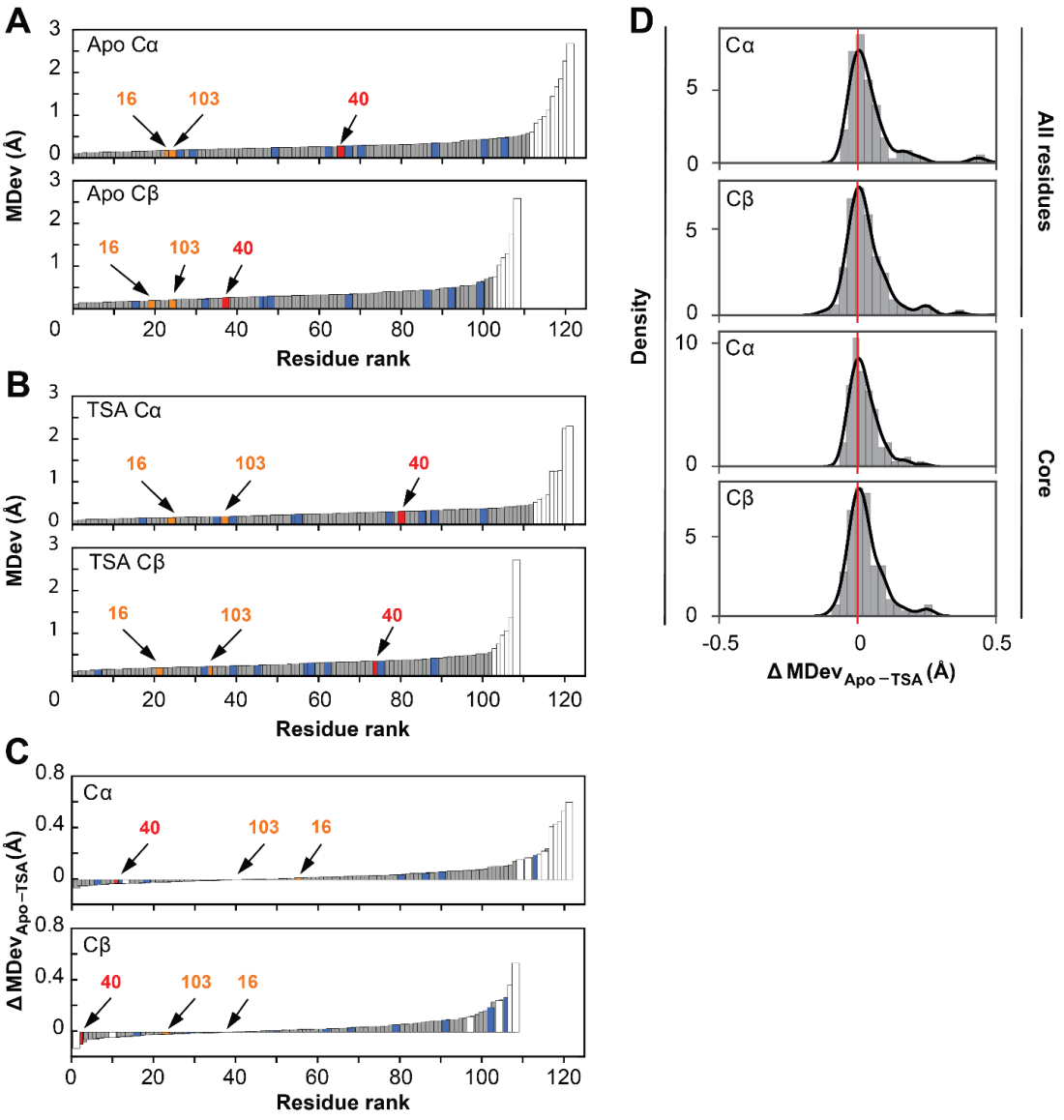

Fig. S11. Conformational heterogeneity through the KSI catalytic cycle obtained from pseudo-ensembles. MDevs for KSI Apo (A) and TSA–bound state (B) Cα (top) and Cβ (bottom) in rank order. (C) Difference Cα (top) and Cβ (bottom) MDev values between the Apo and TSA-bound states ($MDevs_{Apo-TSA}$) ordered according to increasing $MDevs_{Apo-TSA}$ values. Positive values indicate lower MDevs for the TSA-bound state. The largest changes occur in the 62–65 and 91–96 loops (white bars). (D) Histogram of $\Delta MDev_{Apo-TSA–bound}$ values for all residues (two top panels) and for the enzyme core (two bottom panels). Color code as in Fig. 4 of the main text.

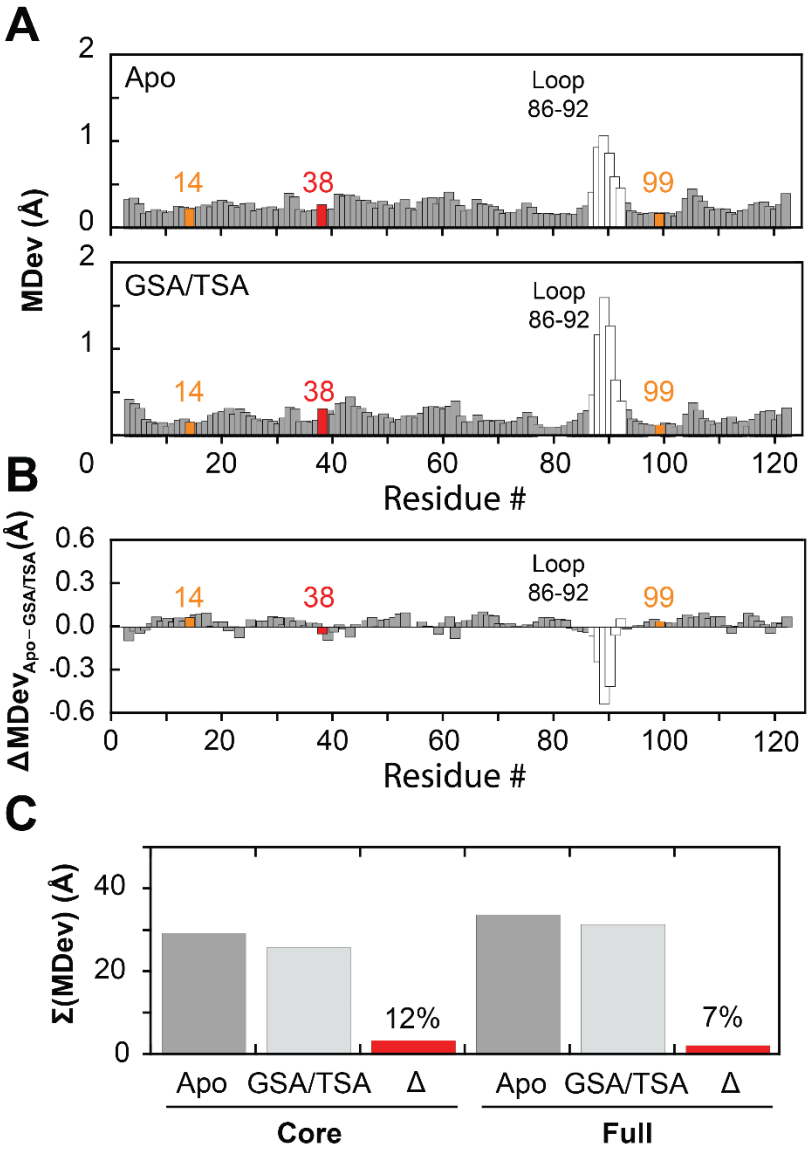

Fig. S12. Quantifying changes in conformational heterogeneity for a homologous KSI ($KSI_{homolog}$) catalytic cycle via pseudo-ensembles. (A) Cα MDevs for KSI Apo (n = 24, top) and GS /TSA–bound (n = 18, bottom) states. GSA-bound and TSA-bound structures were pooled due to the low number of GSA-bound and TSA-bound molecules (9 and 9, respectively) from PDB crystal structures (Table S21-23). The flexible 86–92 loop is presented as white bars; positions 14 and 99 (oxyanion hole, corresponding to positons 16 and 103, respectively in the main text) in orange and position 38 (general base; D40 in main text) in red. (B) Difference Cα MDev values between the Apo and GS /TSA-bound states ($\Delta MDevs_{Apo-TSA}$), such that positive values indicate lower MDevs for the GSA/TSA-bound state. (C) Sum of Cα MDevs for Apo, GSA/TSA-bound and their difference (Δ); colors as in Fig. 4 of the main text. From the above comparisons it appears that the 86–92 loop becomes more flexible upon GSA/TSA binding; nevertheless note that the ΔMDev for the loop represents a small difference between large values (note the different scale of the y-axis in A *vs.* B).

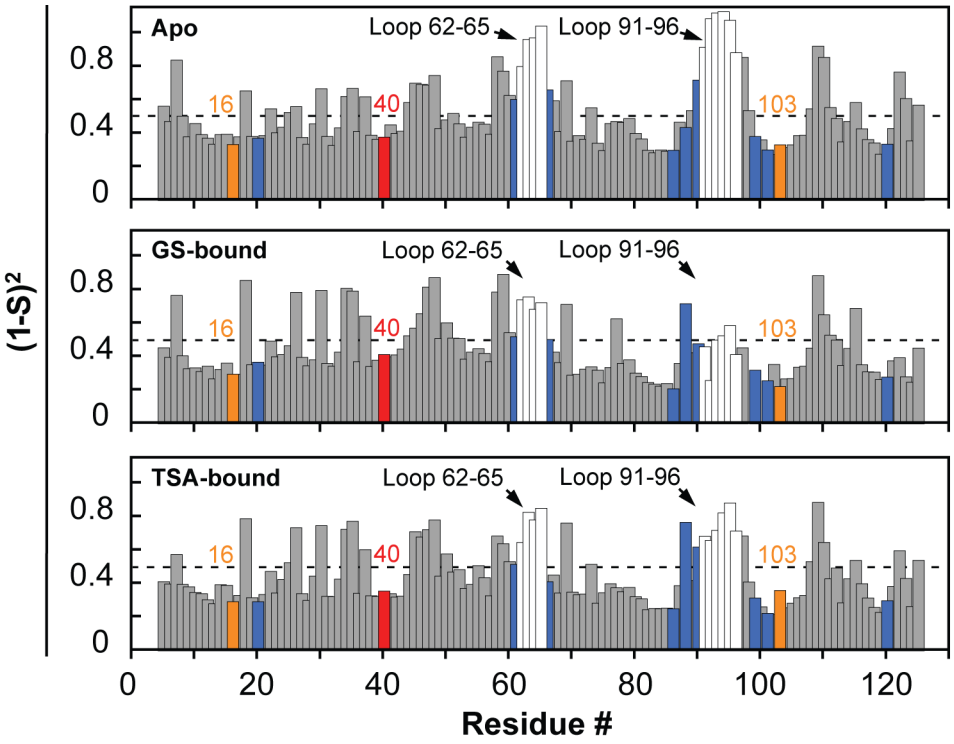

Fig. S13. Conformational heterogeneity in KSI catalytic states from RT X-ray data. Disorder parameters, ($1-S^2$), obtained from multi-conformer models for KSI Apo (top), GS -bound (middle) and TSA-bound (bottom). ($1-S^2$) for the GS -bound state corrected for 70% GS occupancy (see Fig. S14 for uncorrected values). Dashed lines represent average ($1-S^2$) values: 0.52, 0.45, and 0.46 for Apo, GS - and TSA-bound, respectively. Y16 and D103 are in orange; D40 in red; binding residues in blue; and loop residues in white, as in Fig. 3A from main text.

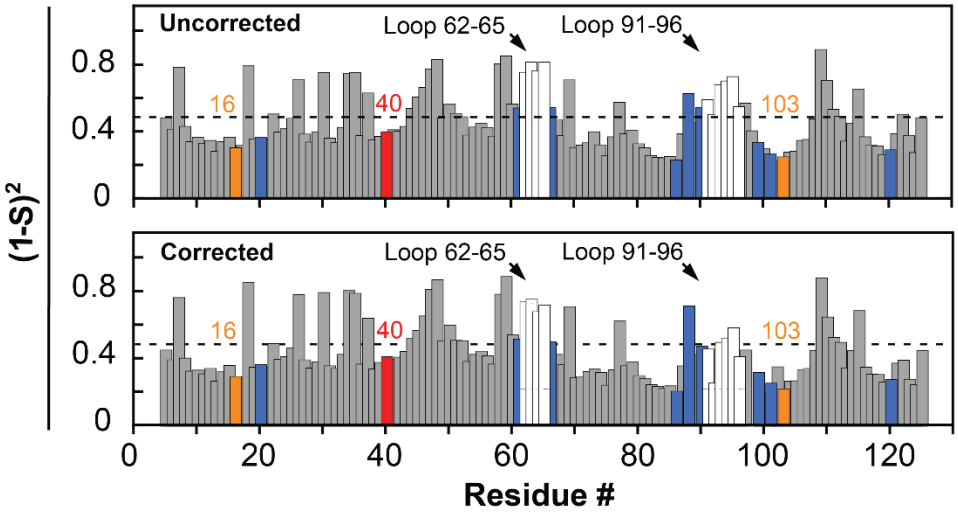

Fig. S14. Correcting for incomplete occupancy does not appreciably alter the conformational heterogeneity in the KSI GS -bound multi-conformer model. The observed (uncorrected, top) and GS occupancy–corrected (70% occupancy, bottom) GS-bound ($1-S^2$) obtained from the 250 K multi-conformer model are highly similar and give analogous results and conclusions (see Table S32). The bottom panel is repeated from the Fig. S13 (middle). Color code as in Fig. 3A from main text.

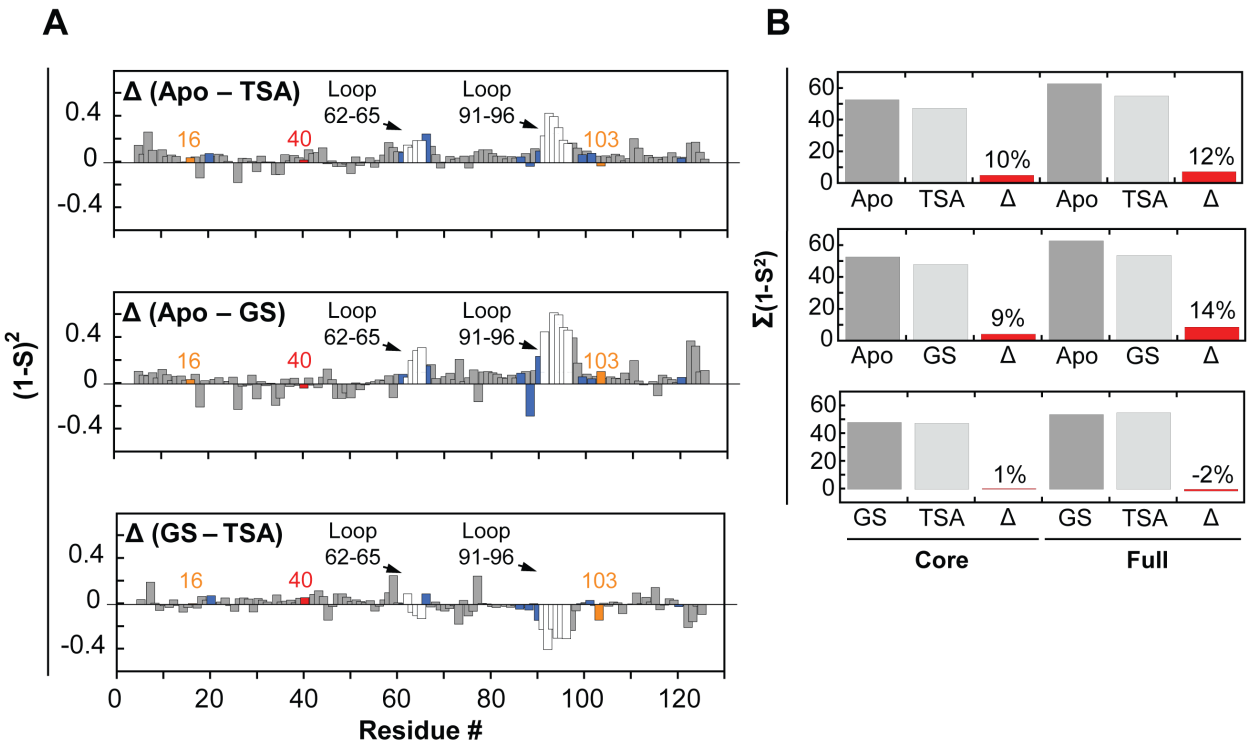

Fig. S15. Changes in KSI conformational heterogeneity during its catalytic cycle from RT X-ray data. (A) Difference ($1-S^2$) between Apo and TSA-bound (top), Apo and GS-bound (middle) and GS and TSA-bound (bottom). Y16 and D103 in orange, D40 in red, and binding residues in blue. (B) Sum of ($1-S^2$) values for the different catalytic states (grey bars) and their difference (Δ, red bars). Each panel in B is the summed ($1-S^2$) value or difference (Δ) from the respective panel in A. Color code as in Fig. 3A from main text.

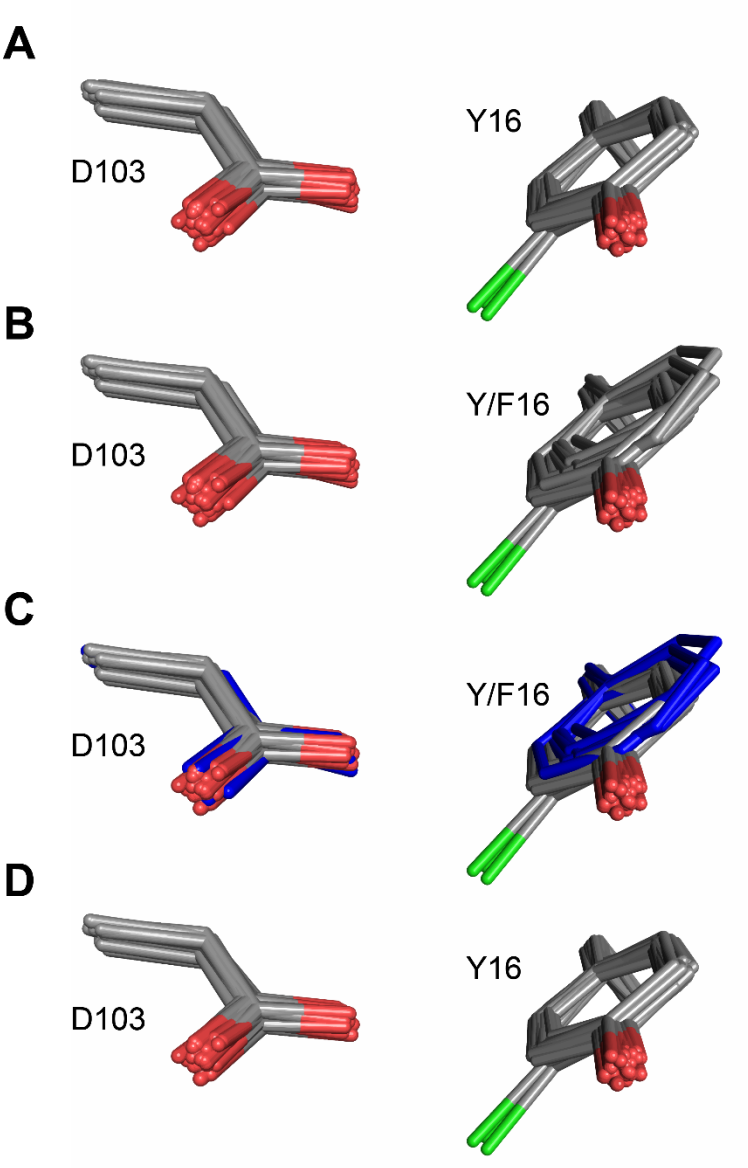

Fig. S16. Ablation of the Y16 hydrogen bonding group does not alter D103 positioning. (**A**) The oxyanion hole D103 and Y16 reduced pseudo-ensemble, which does not include structures with i) mutations in the oxyanion hole that alter the chemical nature of the hydrogen bonding groups or ii) mutations in the Y16 hydrogen bond network (e.g. Y57F) (Table S2). Phenylalanine residues at position 16 are omitted in this panel. Chlorine atoms in chemically modified tyrosine residues are shown in green. (B) The reduced pseudo-ensemble with phenylalanine residues at position 16 included (Table S2). (C) The reduced pseudo-ensemble from B in which structures with phenylalanine residues at position 16 are colored in blue. The aspartate residues from structures with phenylalanine at position 16 (blue) are within the ensemble of aspartate residues from structures with tyrosine at position 16. (D) The reduced pseudo-ensemble from which all structures with phenylalanine residues at position 16 have been excluded.

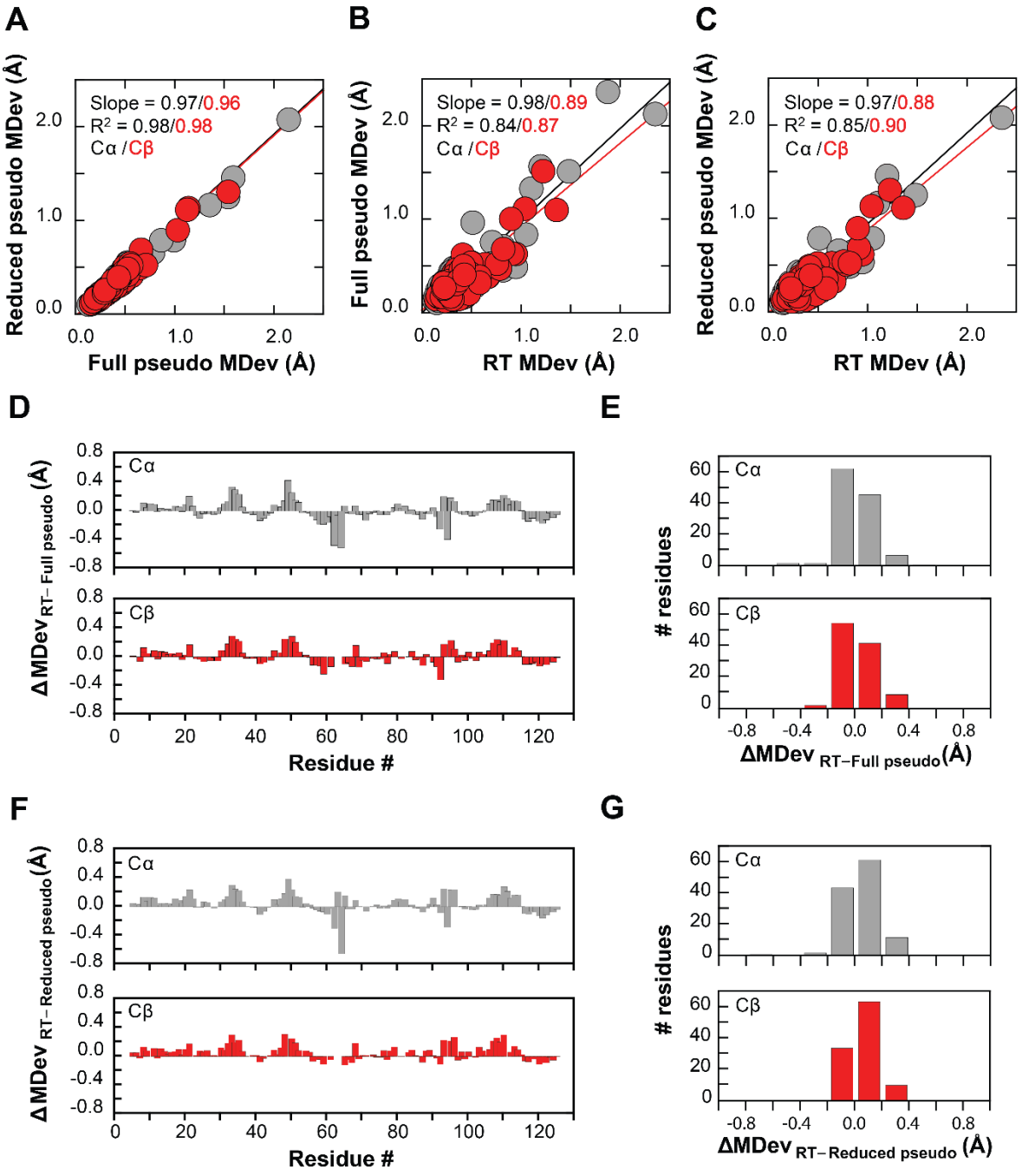

Fig. S17. Similar overall KSI conformational heterogeneity is obtained from the full pseudo-ensemble, the reduced pseudo-ensemble, and the RT-ensemble (see Table S2 and Materials and Methods). Correlation plots of MDev values for the full pseudo-ensemble and reduced pseudo-ensembles (A), for RT-ensemble and full pseudo-ensembles, (B) and for RT-ensemble and reduced pseudo-ensembles (C); backbone (Cα, grey symbols) and side-chain (Cβ, red symbols) MDevs. ΔMDevs between (D) RT-ensemble and full pseudo-ensemble and (F) RT-ensemble and reduced pseudo-ensemble backbone (Cα, grey, top panels) and side-

chain (Cβ, red bottom panels). The histograms in (E) and (G) represent the ΔMDevs from D and F, respectively.

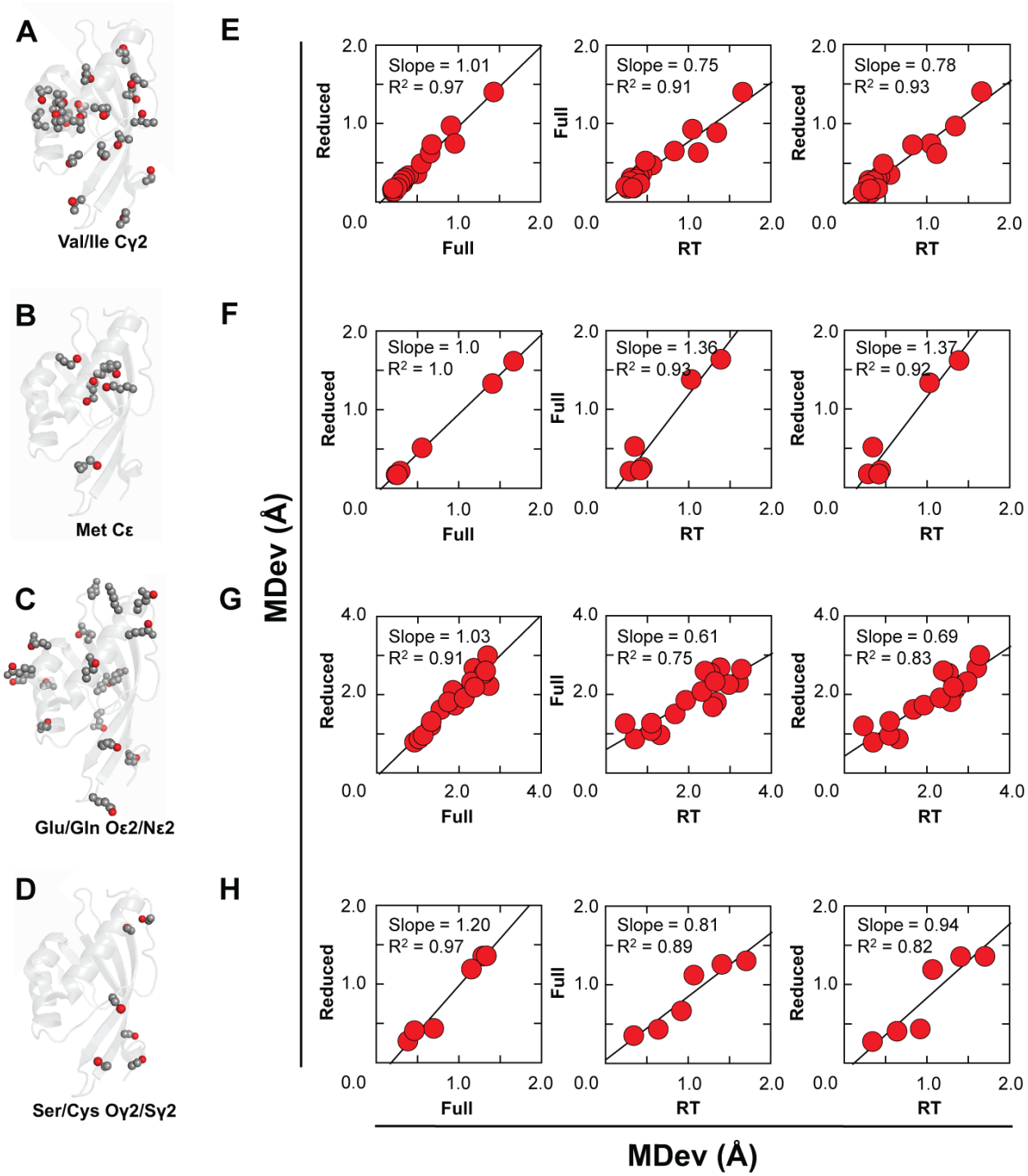

Fig. S18. High correlation coefficients indicate similar KSI side chain conformational heterogeneity obtained from the full pseudo-ensemble, the reduced pseudo-ensemble, and the RT-ensemble. Cartoon representation of the KSI structure (PDB 1OH0) in which different classes of side-chains are depicted as spheres: Ile/Val and Met (hydrophobic, (A) and (B), respectively) and Glu/Gln and Ser/Cys (polar/charged, (C) and (D), respectively). Side chains are colored in grey and the red color indicates specific atoms for which conformational heterogeneity from the different types of KSI ensembles has been quantified and compared in

E-H. Correlation plots of full pseudo-ensemble and reduced pseudo-ensemble (left row), RT-ensemble and full pseudo-ensemble (middle row) and RT-ensemble and reduced pseudo-ensemble (right row) MDevs for representative side chain atoms: valine/isoleucine Cγ2 (E), glutamate/glutamine Oε2/Nε2 (F), serine/cysteine Oγ2/Sγ2 (G), and methionine Cε (H).

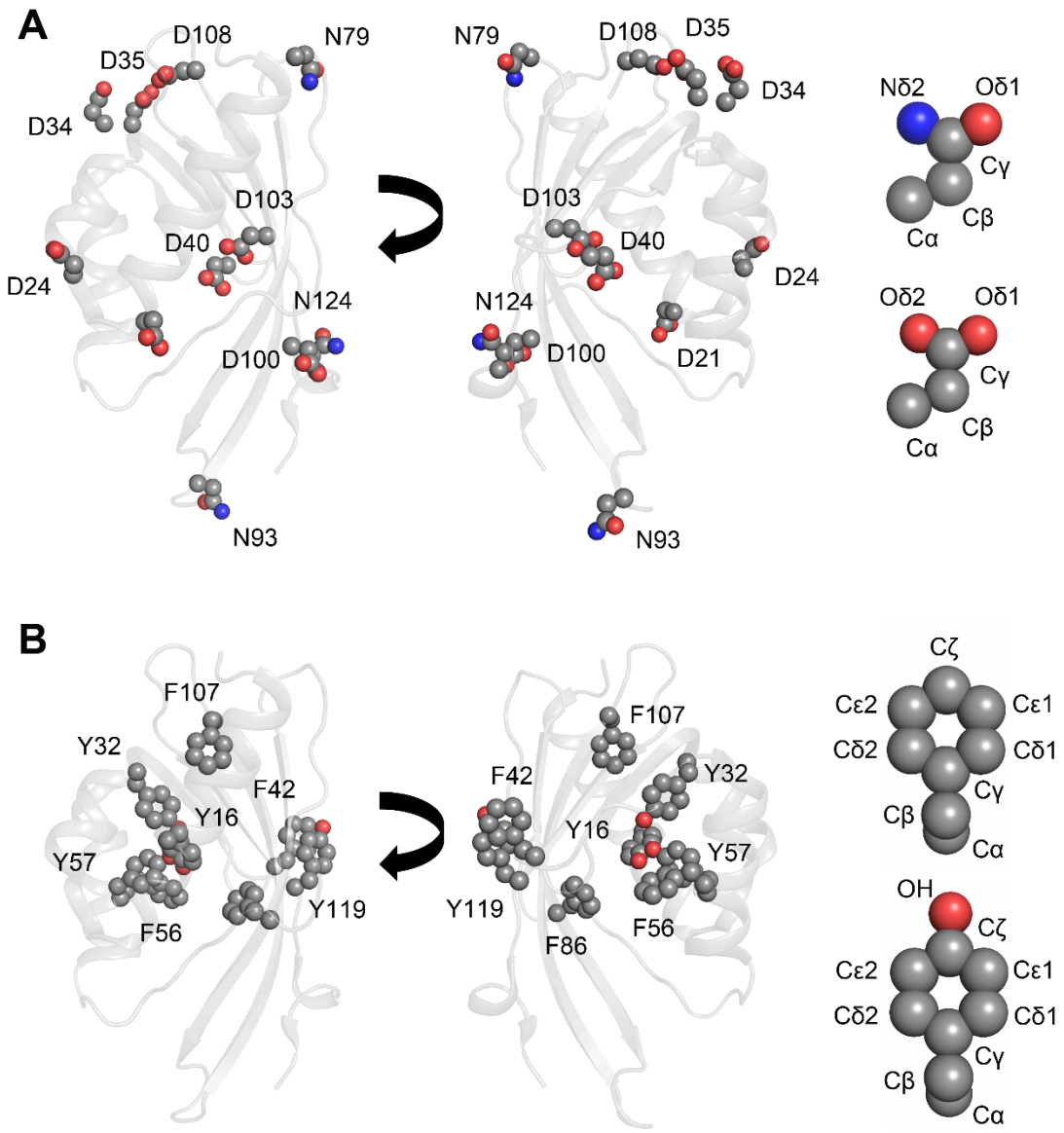

Fig. S19. Cartoon depiction of KSI (PDB 1OH0) with all aspartate and asparagine residues (A) and all tyrosine and phenylalanine residues (B) represented as spheres. Right panels show aspartate, asparagine, tyrosine and phenylalanine side-chains and atom nomenclature. The assignment of Oδ1 *vs.* Oδ2 in aspartate residues is arbitrary, but consistent across all KSI crystal structures. N93 was not included in the analyses in this work, as it is situated within the flexible 91–96 loop.

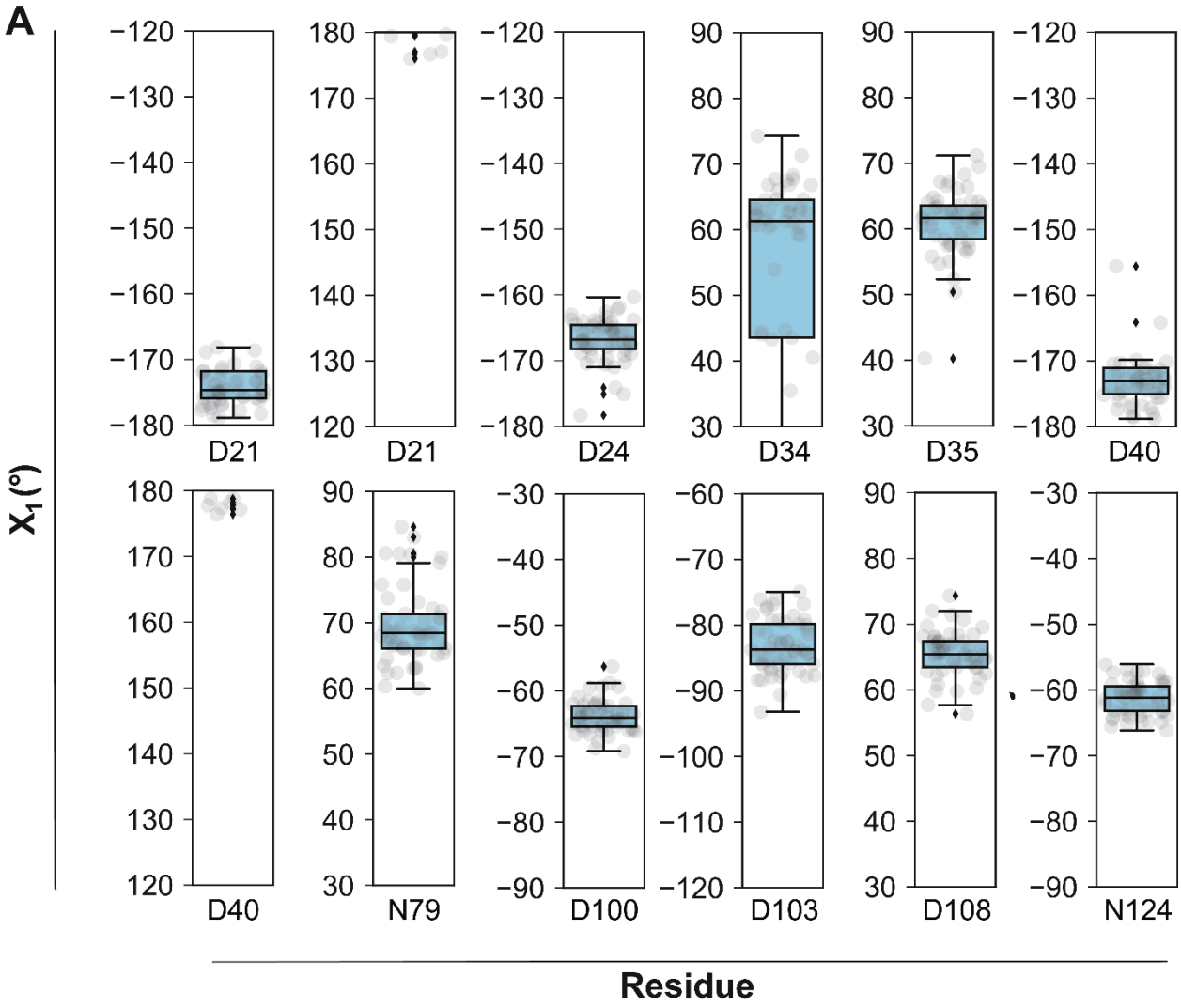
A
X_1 (°)
D21
D21
D24
D34
D35
D40
D40
N79
D100
D103
D108
N124
Residue

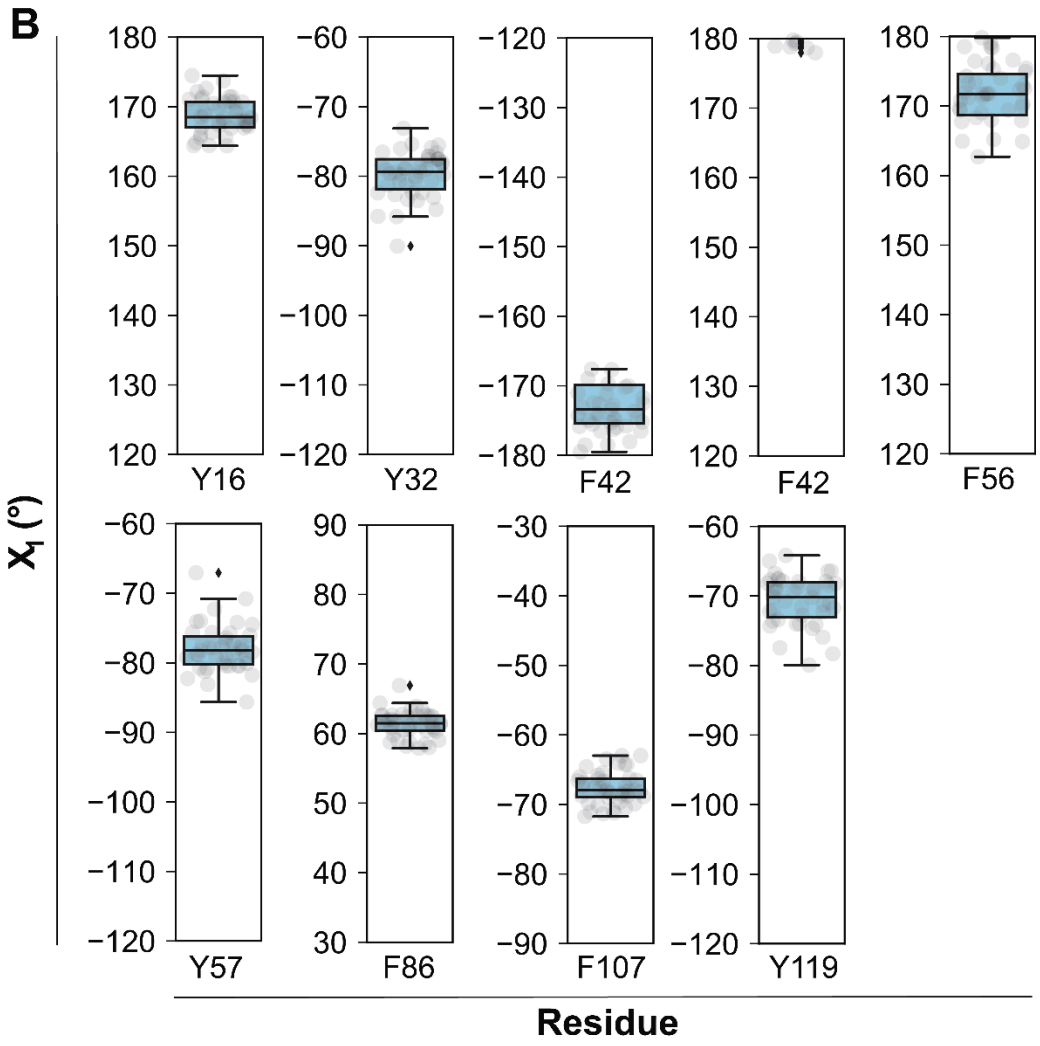

Fig. S20. Sidechain dihedral angles analysis provides additional evidence against exceptional positioning of oxyanion hole Y16 and D103 and general base D40. Side chain χ1 dihedral angles for (A) all aspartate and asparagine residues and (B) tyrosine and phenylalanine residues from the reduced pseudo-ensemble. Asparagine residues at position 2 and position 93 have been excluded from the analysis because these residues are situated in the highly flexible N-terminus and 91-96 loop, respectively. χ1 angles for position 16 include tyrosine residues only (phenylalanine substitutions have been omitted).

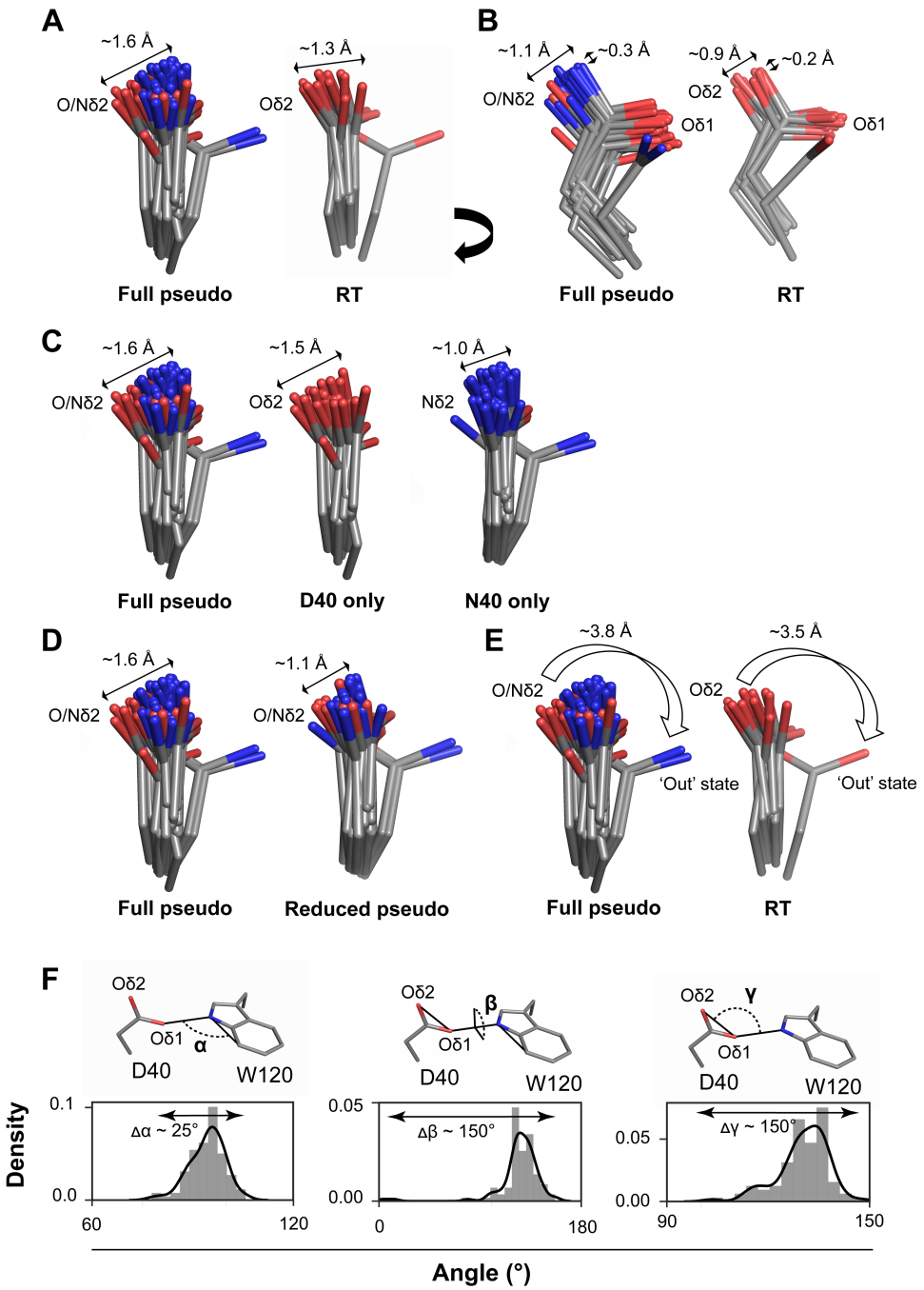

Fig. S21. Estimating the precision in positioning of the KSI general base. Comparison of the general base D40 full pseudo-ensemble (left) and RT-ensemble (right) (A and B show orthogonal orientations); asparagine at position 40 mimics the protonated (intermediate) state of the KSI general base (18, 25). (C) Comparison of the full general base pseudo-ensemble (left) with sub-ensembles composed of aspartate only (middle) or asparagine only (right) at position 40. These ensembles exhibit similar extents of motion. (D) The full pseudo-ensemble (left) and the reduced pseudo-ensemble (right) exhibit similar extents of motion (Table S2). (E) The pseudo-ensemble and the RT-ensemble both provide evidence for general base 'out' state, suggesting that the KSI general base can undergo motion of up to ~4 Å. (F) General base D40/W120 angular sidechain orientations obtained from the pseudo-ensemble.

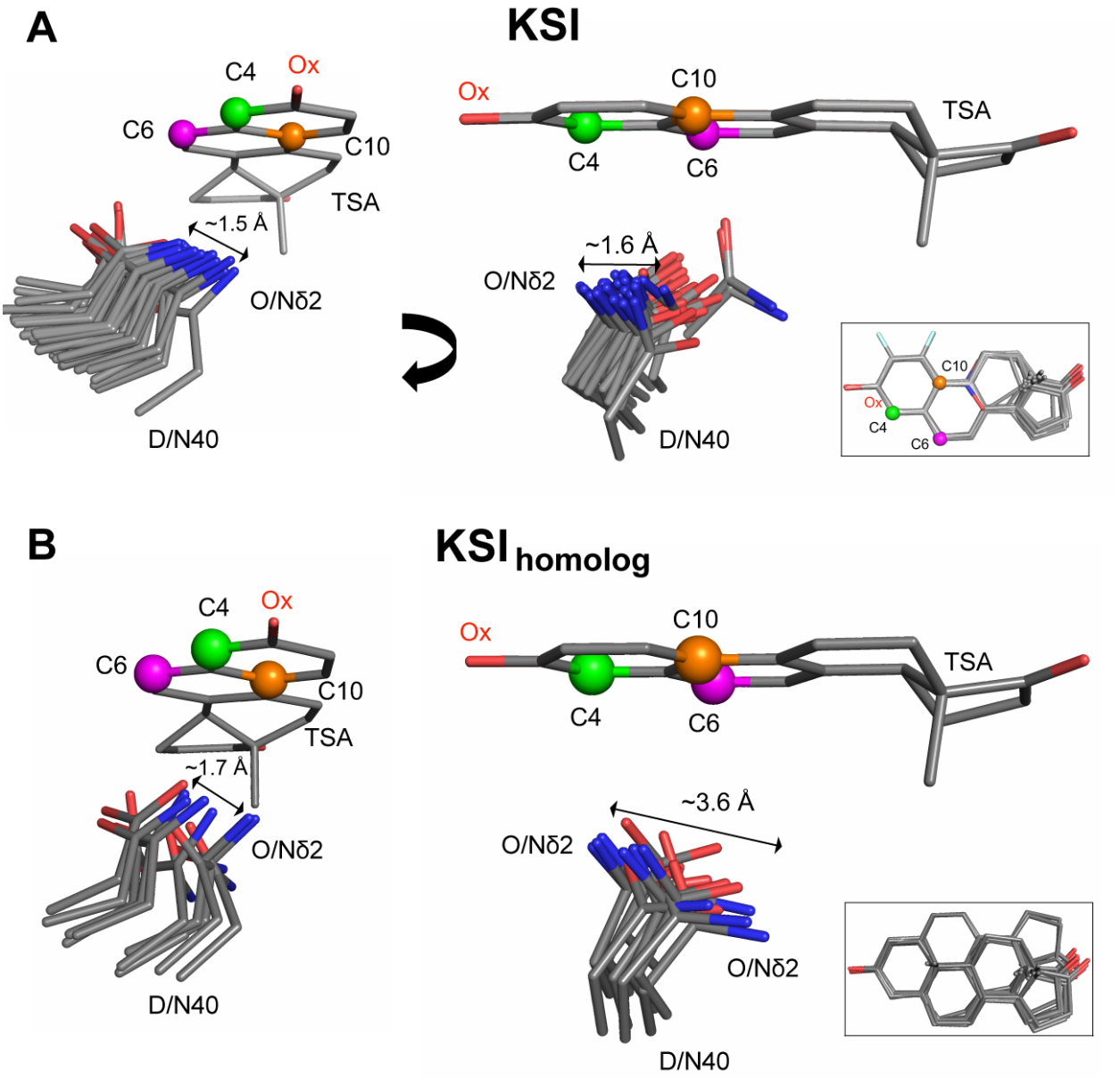

Fig. S22. The KSI general base is highly precise positioned. A bound TSA as "seen" by the KSI (A) and $KS_{Ihomolog}$ (B) general base in a TSA-bound ensemble of cryo crystal structures (n = 36 and 11, respectively) (see Table S2 for structures in (A) and Table S22 for structures in (B) (for (B) only $KSI_{homolog}$-TSA bound complexes for which the steroid is bound with its ring A facing the oxyanion hole are included (PDB codes 1OHP, 1QJG, 3NHX, 3NUV)). Panel A is reproduced from Fig. 5D from the main text. The TSAs (equilenin and various phenols) have been aligned on the A ring with only one (PDB 1OH0) shown for clarity. The carbon positions between which protons are shuffled in KSI reactions are represented as green, magenta, and orange spheres (see Fig. 1 and Fig. S30 for the reaction mechanisms). The insets show the aligned TSAs.

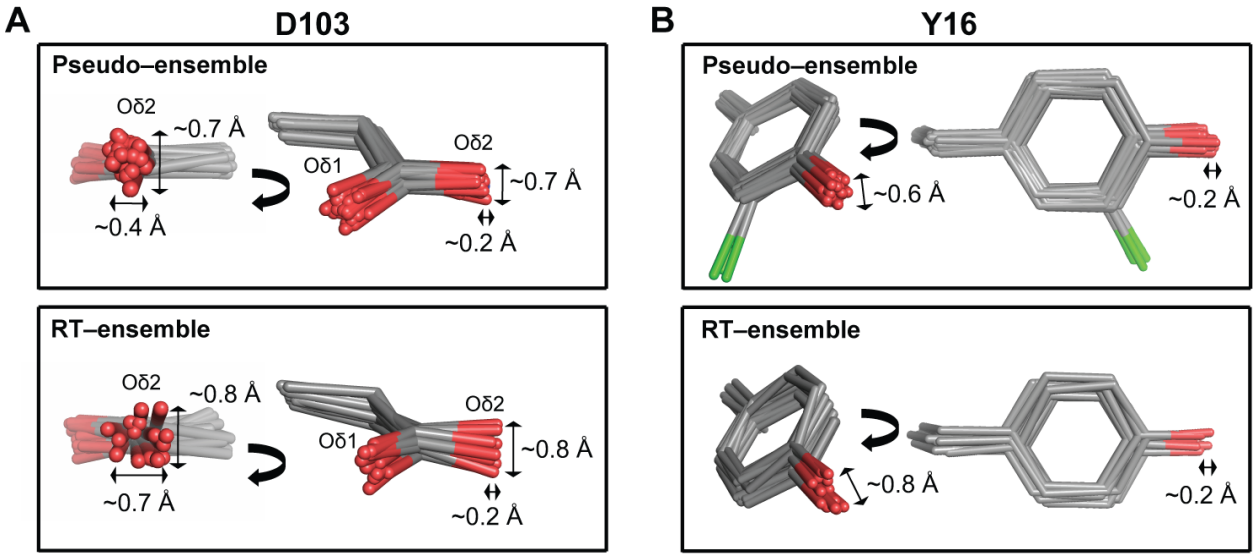

Fig. S23. Estimating the precision in positioning within the KSI oxyanion hole. The oxyanion hole Y16 (A) and D103 (B) reduced pseudo-ensemble (top panels) and RT-ensembles (bottom panels). Chlorine atoms of Cl-tyrosine residues are colored in green.

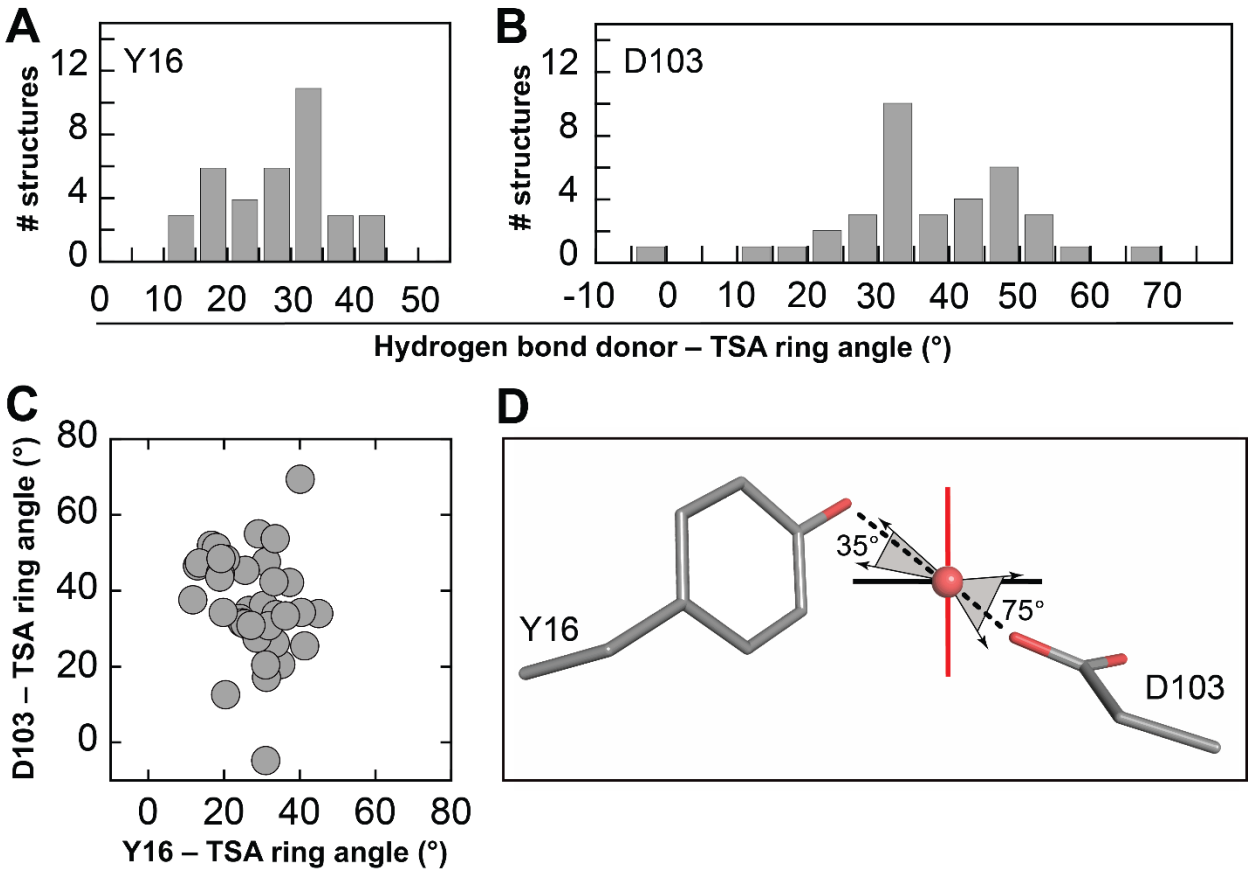

Fig. S24. The KSI oxyanion hole does not appear to be precisely positioned for ground state (sp^2) *vs.* transition state (sp^3) geometric discrimination. Distribution of the angles between the hydrogen bond donors Y16 (A) and D103 (B) and the plane of steroid ligands from KSI crystal structures of variants with WT-like activity bound to TSAs (Table S2); angles range from 10° to 45° and from -5° to 75°, respectively. (C) Plot of the Y16 and D103 angles from A and B showing lack of correlation between Y16 and D103 hydrogen bond angles. (D) Cartoon representing the range of angles from (A) and (B) and the plane of a steroid ligand (black solid line). The black and red solid lines represent planes that are parallel and orthogonal to the steroid ring, respectively; the red line indicates the extreme plane from which sp^3 ligands could be more stabilized than sp^2 ligands. We note that rotation around C–O(H) bond in Y16 and D103 will allow the hydrogen bonding H (H is only expected to be observed in crystal structure of resolution better than 0.6-0.8 Å and therefore not observed in the crystal structures used in this work) to approach the ligand oxyanion from an additional range of angles, which could potentially contribute to the range of angles made with the plane of the steroid.

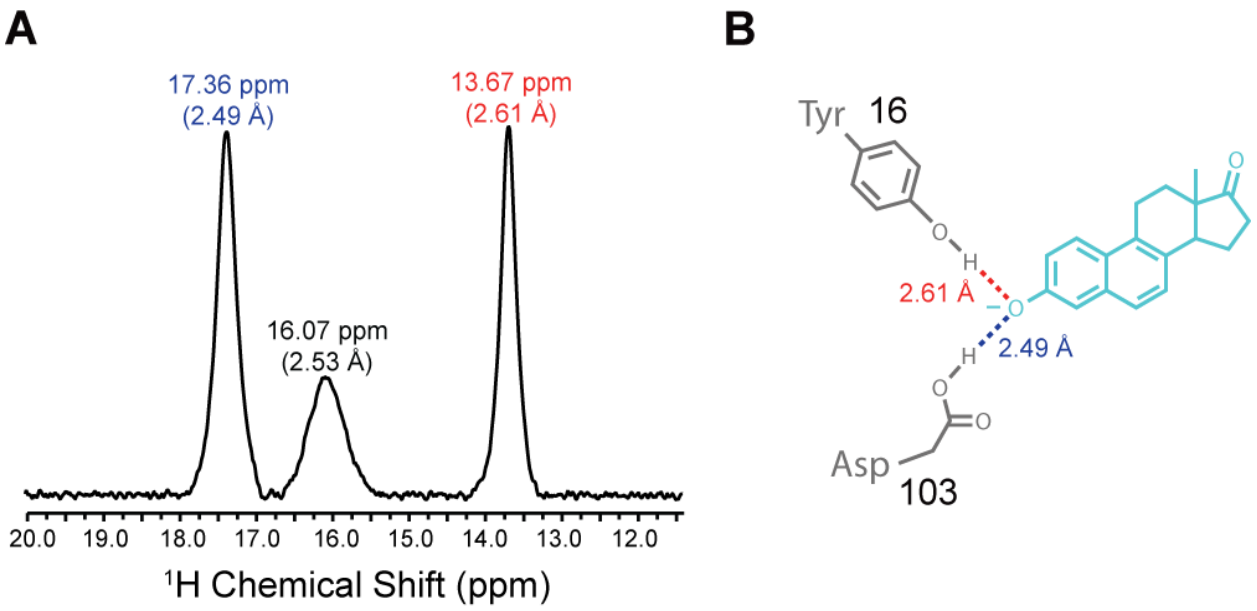

Fig. S25. Measuring Y16 and D103 hydrogen bond lengths in a KSI–TSA complex in solution by ^{1}H NMR. (A) ^{1}H NMR spectra of KSI D40N variant bound to the TSA equilenin (see Materials and Methods for data collection). The D40N substitution mimics the protonated (intermediate) general base state and has been used to increase TSA affinity (18, 25). Shown are the chemical shifts for the ^{1}H peaks (in ppm) in the downfield region of the spectrum. The respective hydrogen bonds lengths were calculated from the chemical shifts and using standard procedures (Harris & Mildvan, 1999; Pinney et al., 2018) (Materials and Methods). Three peaks are observed in the downfield region of the ^{1}H spectrum. Comparison with previously published ^{1}H NMR spectra of KSI bound to a variety of TSAs and consideration of the coupling between the hydrogen bond lengths suggests that the 13.67 ppm and the 17.36 ppm peaks (2.61 Å and 2.49 Å lengths, respectively) correspond to the Y16–TSA and D103–TSA hydrogen bonds, respectively (25, 29) Alternative assignments are possible but do not alter any of the conclusions in the main text. We note that the peak at 16.07 ppm could originate from alternative hydrogen bonding conformations or from a non-active site hydrogen bond, possibilities that will be investigated in future work. (B) Schematic depiction of the oxyanion hole residues Y16 and D103 (in grey) and the bound TSA (in cyan) and the assigned hydrogen bond lengths (Y16–TSA in red and D103–TSA in blue).

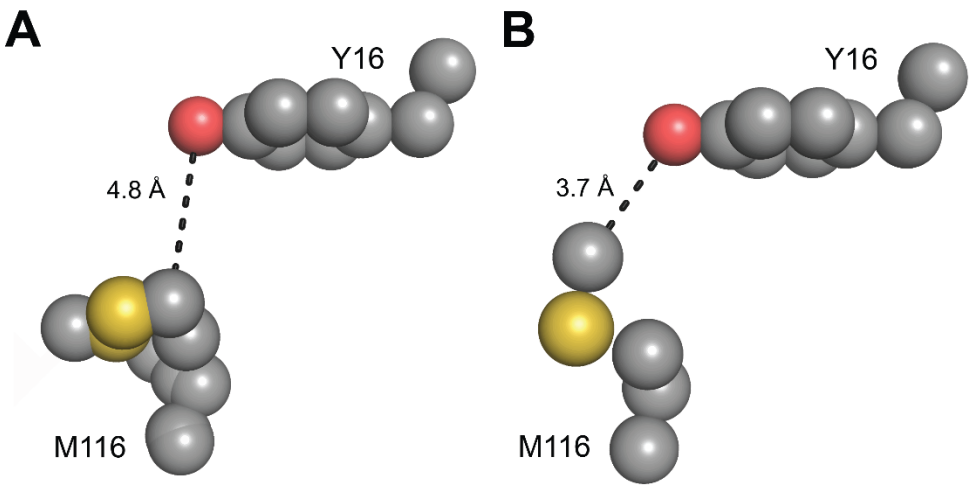

Fig. S26. Packing interactions cannot be uniquely evaluated from single X-ray crystallography models. Distance between M116 and Y16 could be interpreted as beyond van der Waals contact radius ('loose' packing, (A), PDB 5D81) or within this contact radius ('tight' packing, (B), PDB 5D83), depending on the analyzed crystal structure. The r_{vdw} methyl is ~2.0 Å, r_{vdw} oxygen is 1.4–1.7 Å (see Table S48).

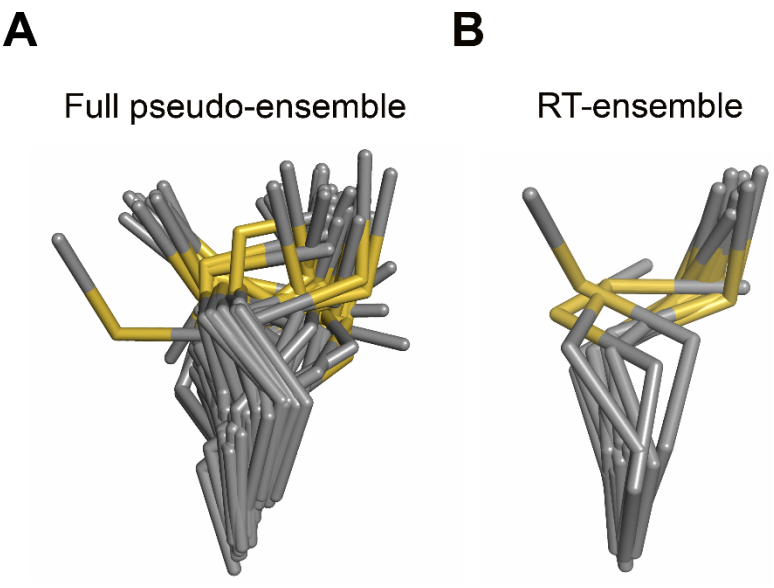

Fig. S27. M116 has a broad conformational ensemble. (A) The M116 full pseudo-ensemble and (B) and RT-ensemble.

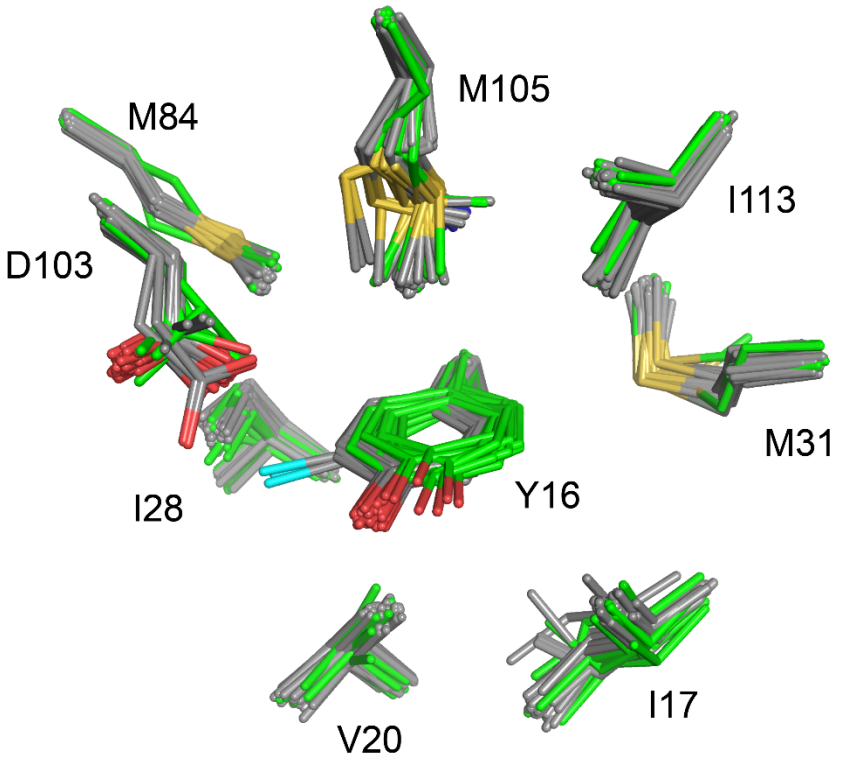

Fig. S28. Ablation of the Y16–Y57 hydrogen bond and the increased flexibility of the residue at position 16 does not lead to significant rearrangements or enhanced mobility in the surrounding residues. Shown are all structures with intact (grey, n = 70) or ablated (green, n = 15) Y16–Y57 hydrogen bond; position 103 includes various substitutions (see also Figures S16 and 29).

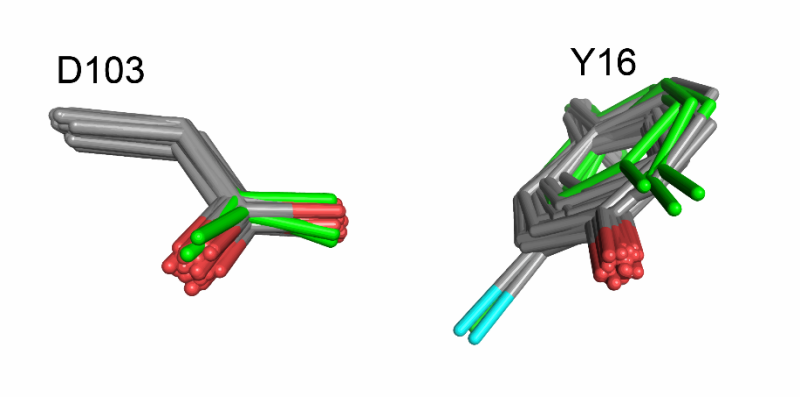

Fig. S29. Increased flexibility or mispositioning of Y16 does not impact D103 positioning. Shown are the reduced pseudo-ensemble (grey, Table S2) and a subset of KSI structures with intact Y16 and D103, in which the Y16-Y57 hydrogen bond is ablated via Y57 substitutions (green; PDB 1DMM, Y57F and PDB 1K41, Y57S).

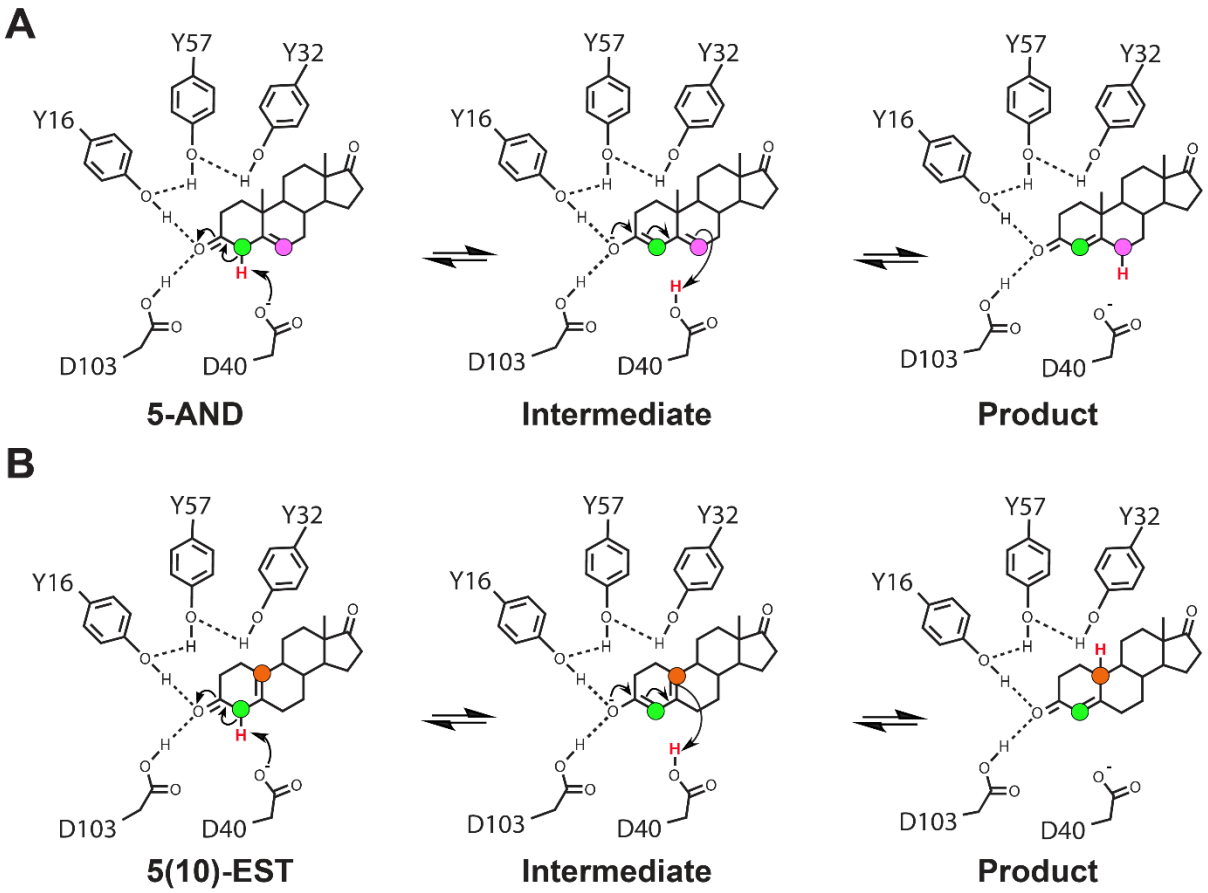

Fig. S30. KSI reaction mechanism with the steroid substrates 5-androstenedione (5-AND, (A)) and 5(10)-estrene-3,17-dione (5(10)-EST, (B)). The shuffled proton is colored in red. The donating and accepting protons (forward reaction) are colored in green and magenta for 5-AND, respectively, and green and orange for 5(10)-EST, respectively; the same colors are used in Fig. 5 in the main text to map donating and accepting carbon positions onto KSI-bound TSAs.

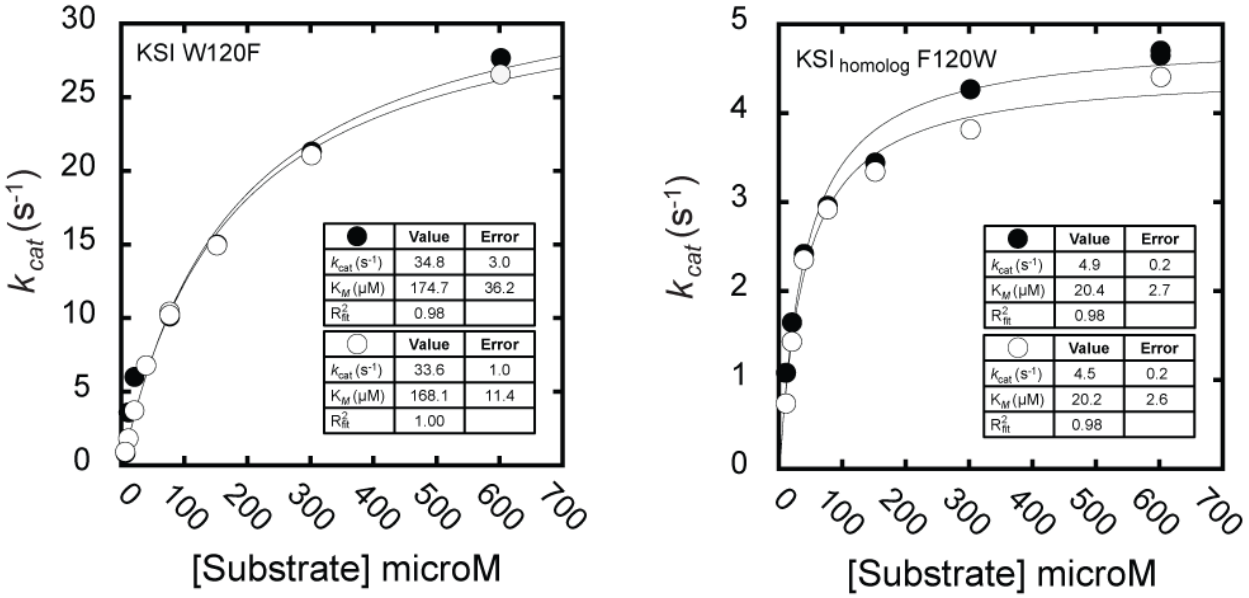

Fig. S31. Michaelis-Menten kinetics of KSI W120F and $KSI_{homolog}$ F120W. Kinetics were measured with the substrate 5(10)-Estrene-3,17-dione as the chemical step for this substrate is rate limiting (49). Kinetics were measured in duplicate (both shown) with the enzyme concentration varied ~3 fold (Table S58).

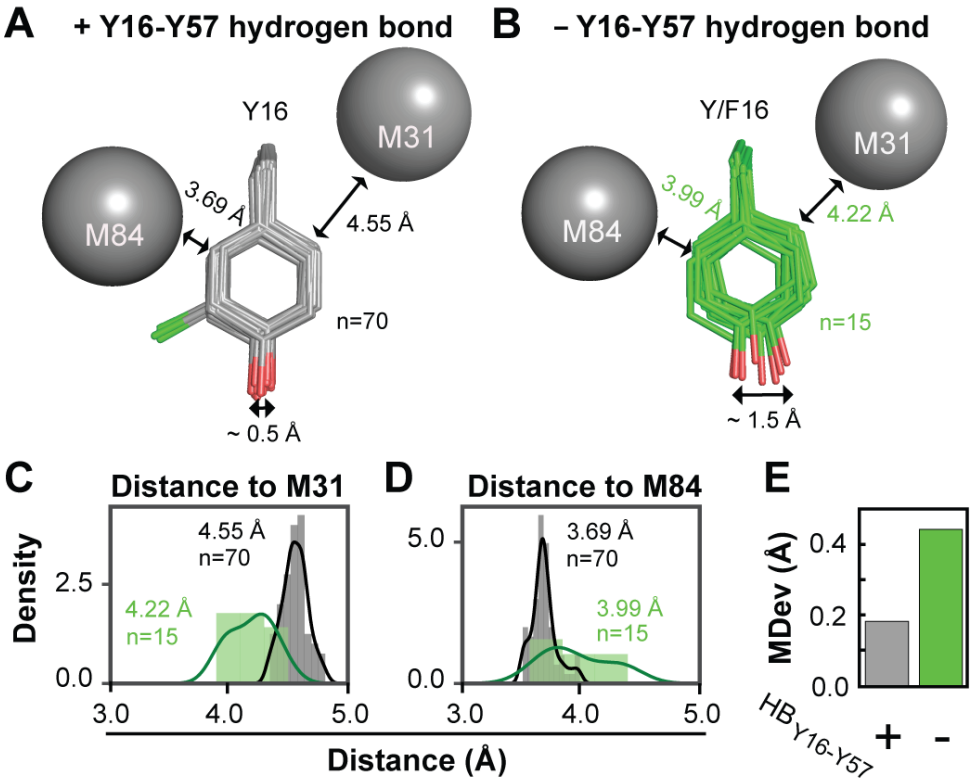

Fig. S32. Testing models for the asymmetric packing of Y16. Y16 residues with intact Y16–Y57 hydrogen bond (A, in grey) or Y/F16 residues with the Y16–Y57 hydrogen bond ablated (B, in green) (Table S2). Residues M31 and M84 are shown as grey spheres with the mean distances between M84 and Y16 or M31 and Y16 given (n = 70 and 15 for intact and ablated Y16-Y57 hydrogen bonds, respectively). Chlorine substitutions in a subset of tyrosines in A are colored light green. (C, D) Histogram of the distribution of Y16–M31 and Y16–M84 distances for the ensembles from panels (A) and (B), respectively. (E) MDev for the Cζ atom of the phenyl ring for the ensemble from panel (A) in grey and from panel (B) in green (see Fig. S19 for definition of the Cζ atom).

Structure (PDB code)	Mutations	Ligand	Resolution (Å)	Space group	# molecules asymmetric unit
1DMM	Y57F	-	1.9	$C222_1$	1
1DMN	Y32F/Y57F	-	2.05	$C222_1$	1
1DMQ	Y32F	-	2.15	$C222_1$	1
1E97	Y16F/Y32F/Y57F	-	2.0	$C222_1$	1
1EA2	Y16F	-	1.8	$C222_1$	1
1GS3	Y32F/Y57F/Y119F/D40N	Equilenin	2.1	$C222_1$	1
1OHO	Y16F/D40N	Equilenin	1.9	$C222_1$	1
1OPY	WT	-	1.9	$C222_1$	1
1W02	Y16F/D103L	-	2.3	$C222_1$	1
1W6Y	W92A	Equilenin	2.1	$C222_1$	1
2INX	D40N	2,6-difluorophenol	1.5	$C222_1$	1
3CPO	D40N	2-fluorophenol	1.24	$C222_1$	1
3RGR	M116A	-	1.59	$C222_1$	1
3SED	M105A	-	1.3	$C222_1$	1
4K1V	Y16F/Y57F	-	1.8	$C222_1$	1
5AI1	Y32F/Y57F/Y119F/D40N	Equilenin	2.1	$C222_1$	1
1CQS	D103E/D40N	Equilenin	1.9	$C2_1$	2
1E3R	D40N	Androsten-3β-ol-17-one	2.5	$C2_1$	2
1E3V	WT	Deoxycholate	2.0	$P2_12_12_1$	2
1K41	Y57S	-	2.2	$C2_1$	2
1OGX	D40N	Equilenin	2.0	$C2_1$	2
1OH0	WT	Equilenin	1.1	$C2_1$	2
1VZZ	Y32F/D103L	-	2.3	$P2_12_12_1$	2
1W00	D103L	-	2.2	$P2_12_12_1$	2
1W01	Y57F/D103L	-	2.2	$P2_12_12_1$	2
3FZW	D40N/D103N	Equilenin	1.32	C21	2
3OWS	D40N/C69S/C81S/C97S/M116C-CN	Equilenin	1.71	$C2_1$	4
3OWU	D40N/C69S/C81S/C97S/F86C-CN	Equilenin	1.7	$P2_1$	4
3VGN	D40N	3-fluoro-4-nitrophenol	1.3	$P2_12_12_1$	2
3VSY	WT	-	1.5	$P2_12_12_1$	2
4K1U	Y16F/Y32F	-	2.0	$P2_12_12_1$	2
5D83	D40N, Y32 (Cl-Y)	-	1.7	$P2_12_12_1$	2
5D82	D40N, Y16 (Cl-Y)	-	1.37	$P2_12_12_1$	2
5D81	D40N, Y57 (Cl-Y)	-	1.39	$C222_1$	1
5KP4	WT	19-nortestosterone	1.71	$P2_12_12_1$	2
2PZV	D40N	Phenol	1.25	P1	4
3IPT	Y16S/D40N	Equilenin	1.63	$P2_1$	4
3OWY	D40N/C69S/C81S/C97S/M105C-CN	Equilenin	2.3	$P2_1$	8
3OX9	D40N/C69S/C81S/C97S/F86C-CN	-	2.0	$P2_1$	4
3OXA	D40N/C69S/C81S/C97S/M116C-CN	-	1.89	$P2_1$	4
3T8N	Y16AD103A	-	1.47	$C2_1$	4
5KP1	D40N, Y16(Cl-Y)	Equilenin	1.22	P1	4
5KP3	D40N, Y57(Cl-Y)	Equilenin	1.7	$P2_12_12_1$	2
5G2G	M116K	Equilenin	1.6	$P2_12_12_1$	2
1C7H	R75A	-	2.5	$C2_12_12_1$	1

Table S1. KSI cryo crystal structures available from the Protein Data Bank (PDB).

PDB	Pseudo-ensemble							
	Full	Apo	TSA-bound	Reduced	TSA-bound*	Intact Y16–Y57 Hbond	Ablated Y16–Y57 Hbond#	Equilenin-bound%
1DMM	X	X					X	
1DMN	X	X					X	
1DMQ	X	X				X		
1E97	X	X		X			X	
1EA2	X	X		X			X	
1GS3	X		X		X		X	
1OHO	X		X	X			X	
1OPY	X	X		X		X		
1W02	X	X					X	
1W6Y	X		X		X	X		X
2INX	X		X	X		X		
3CPO	X		X	X	X	X		
3RGR	X	X		X		X		
3SED	X	X		X		X		
4K1V	X	X		X			X	
5AI1	X		X		X		X	
1CQS	X		X			X		
1E3R	X					X		
1E3V	X			X		X		
1K41	X	X					X	
1OGX	X		X	X	X	X		X
1OH0	X		X	X	X	X		X
1VZZ	X	X				X		
1W00	X	X				X		
1W01	X	X					X	
3FZW	X		X	X	X	X		
3OWS	X		X	X	X	X		X
3OWU	X		X		X	X		X
3VGN	X		X	X	X	X		
3VSY	X	X		X		X		
4K1U	X	X		X			X	
5D83	X	X		X		X		
5D82	X	X		X		X		
5D81	X	X		X		X		
5KP4	X			X[2]		X[2]		
2PZV	X		X	X	X	X		
3IPT	X		X	X				
3OWY	X	X[1]	X		X	X		X
3OX9	X	X				X		
3OXA	X	X		X		X		
3T8N	X	X						
5KP1	X		X	X	X	X		
5KP3	X		X	X	X	X		
5G2G	X		X	X		X		
1C7H	X	X				X		
# KSI monomers	94	42	46	54	36	70	15	19

*TSA-bound structures with activity within ~10–fold from WT and containing both Asp and Asn residues at position 40. TSAs include equilenin and various phenols. Even though D40N substitution leads to a rate decrease, the Asn at position 40 mimics the protonated (intermediate) state of the general base and increases the KSI affinity for TSAs (18, 25); # KSI crystals structures in

which Y16 – Y57 hydrogen bond (Hbond) is ablated but the phenyl ring at position 16 is preserved (Y16F or Y57X substitutions, X being any residue). % Equilenin-bound structures with intact oxyanion hole residues, activity within ~10–fold from WT and containing both Asp and Asn residues at position 40. [1] Although the structure has been reported as TSA-bound, two out of the 8 KSI molecules in the asymmetric unit were Apo and were thus included in the Apo pseudo-ensemble. [2] The asymmetric unit of this crystal structure contains two molecules and the molecule B was not bound to a GS. Further, in molecule B, Y16 orientation appears misaligned when compared to all known KSI crystal structures to date and was not included in the pseudo-ensembles in this work.

Table S2. KSI crystal structures used to obtain the various pseudo-ensembles in this work. To most accurately estimate the precision in positioning in the KSI oxyanion hole and remove potential artifacts, the KSI reduced pseudo-ensemble does not include structures with i) mutations in the oxyanion hole that alter the chemical nature of the hydrogen bonding groups (e.g. D103L mutations); ii) mutations in the Y16 hydrogen bond network (e.g. Y57F) as these mutations have been suggested to alter Y16 positioning (50); iii) resolution worse than 2.0 Å. We did not exclude structures with Y16F mutations, as this mutation did not appear to alter D103 positioning (Fig. S16), further suggesting that Y16 and D103 hydrogen bonding orientations are not coupled.

	Apo		GS-bound			TSA-bound	
	250 K	**280 K**	**100 K**	**250 K**	**280 K**	**250 K**	**280 K**
PDB code	**6UCW**	**6U1Z**	**6UBQ**	**6UCY**	**6TZD**	**6UCN**	**6U4I**
Data collection*							
Wavelength (Å)	0.88557	0.88557	0.78719	0.88557	0.88557	0.88557	0.88557
Resolution range	36.72-1.25 (1.27-1.25)	36.97-1.5 (1.53-1.50)	37.16-1.30 (1.32-1.30)	36.06-1.15 (1.17-1.15)	37.19-1.45 (1.48-1.45)	35.91-1.32 (1.34-1.32)	36.83-1.55 (1.58-1.55)
Space group	$P2_12_12_1$	$P2_12_12_1$	$P2_12_12_1$	$P2_12_12_1$	$P2_12_12_1$	$P2_12_12_1$	$P2_12_12_1$
Unit cell	35.85 73.44 95.99 90 90 90	36.03 73.94 95.69 90 90 90	36.21 74.32 95.56 90 90 90	36.06 73.85 95.62 90 90 90	36.23 74.39 95.35 90 90 90	35.91 73.72 95.73 90 90 90	35.54 73.66 95.68 90 90 90
Total reflections	336888 (16253)	227920 (10482)	851076 (37730)	594265 (27460)	256187 (12435)	286924 (13737)	162032 (7526)
Unique reflections	70573 (3438)	41654 (1902)	64423 (3045)	89597 (4212)	46456 (2224)	58753 (2829)	37064 (1762)
Multiplicity	4.8 (4.7)	5.5 (5.5)	13.2 (12.4)	6.6 (6.5)	5.5 (5.6)	4.9 (4.9)	4.4 (4.3)
Completeness (%)	99.5 (98.6)	98.6 (95.3)	99.8 (97.4)	98.1 (94.4)	99.8 (99.1)	97.3 (95.2)	99.4 (98.0)
Mean I/sigma(I)	9.9 (1.1)	10.9 (1.1)	19.4 (1.4)	11.8 (1.2)	18.0 (1.1)	12.4 (1.0)	11.8 (1.1)
R-merge	0.076 (1.459)	0.074 (1.737)	0.062 (1.972)	0.069 (1.504)	0.048 (1.685)	0.066 (1.446)	0.075 (1.457)
R-meas	0.085 (1.644)	0.082 (1.916)	0.064 (2.058)	0.075 (1.632)	0.054 (1.863)	0.074 (1.621)	0.085 (1.658)
R-pim	0.038 (0.746)	0.035 (0.796)	0.018 (0.577)	0.029 (0.626)	0.023 (0.783)	0.033 (0.720)	0.040 (0.776)
$CC_{1/2}$	0.997 (0.410)	0.997 (0.466)	0.995 (0.586)	0.999 (0.583)	0.999 (0.557)	0.999 (0.430)	0.999 (0.505)
Refinement*							
Model type	Multi-conformer	Traditional	Traditional	Multi-conformer	Traditional	Multi-conformer	Traditional
Resolution range	36.72-1.25 (1.27-1.25)	36.97-1.50 (1.53-1.50)	34.64-1.30 (1.32- 1.30)	32.40-1.15 (1.16-1.15)	34.65-1.45 (1.48-1.45)	32.29-1.32 (1.34-1.32)	36.84-1.55 (1.59-1.55)
Unique reflections used in refinement**	70423 (2569)	41570 (2498)	64304 (2532)	88966 (2689)	46342 (2652)	58644 (2549)	36978 (2629)
Unique reflections used for R-free	3491 (145)	2035 (136)	3176 (135)	4435 (145)	2273 (135)	2894 (137)	1847 (138)
R-work	0.1488 (0.2943)	0.1360 (0.2528)	0.1520 (0.2681)	0.1456 (0.2672)	0.1456 (0.2915)	0.1444 (0.3078)	0.1367 (0.2465)
R-free	0.1731 (0.2771)	0.1668 (0.2965)	0.1699 (0.3067)	0.1636 (0.2595)	0.1741 (0.3415)	0.1738 (0.3323)	0.1752 (0.3190)
non-hydrogen atoms	5018	2480	2565	5351	2436	5294	2420
macromolecules	4719	2317	2228	4970	2265	4949	2223
ligands	4	3	45	67	45	84	43
solvent	295	160	292	314	126	261	154
Protein residues	255	254	254	259	252	255	254
RMS(bonds)	0.008	0.009	0.008	0.009	0.008	0.009	0.010
RMS(angles)	1.25	0.91	0.97	1.11	0.94	1.06	1.00
Ramachandran favored (%)	97.5	98.8	97.6	95.7	98.8	97.6	98.0
Ramachandran allowed (%)	2.5	1.2	2.4	4.2	1.2	2.4	2.0
Ramachandran outliers (%)	0.0	0.0	0.0	0.1[#]	0.0	0.0	0.0
Average B-factor	17.9	28.7	27.0	15.4	30.6	17.2	24.9
macromolecules	17.1	28.0	25.9	14.6	29.9	16.5	24.0
ligands	20.0	29.1	31.5	20.4	39.2	19.5	29.2
solvent	29.5	39.1	34.5	27.6	39.4	30.2	35.9

* values in parenthesis are for the highest resolution shell; ** values in parenthesis indicate the number of reflections (working set) in the highest resolution shell; [#] 1 out of 629 peptide bonds represents an outlier with clear electron density.

Table S3. X-ray diffraction data collection and model refinement statistics. All structures have been deposited on the PDB and will be released upon publication.

280 K 100K	6U1Z A (Apo)	6U1Z B (Apo)	6TZD A (GS)	6TZD B (GS)	6U4I A (TSA)	6U4I B (TSA)
3VSY A (Apo)	0.67	0.58	0.59	0.43	0.52	0.70
3VSY B (Apo)	0.71	0.37	0.48	0.49	0.56	0.66
5KP4 B (GS)	0.43	0.44	0.41	0.49	0.44	0.47
1OH0 A (TSA)	0.44	0.43	0.39	0.49	0.51	0.50
1OH0 B (TSA)	0.58	0.40	0.37	0.46	0.46	0.38

Table S4. RMSDs between crystal structures for different KSI catalytic states obtained at cryo (100 K) and room temperature (280 K). Cryo KSI Apo, GS-bound and TSA-bound structures have been obtained from the PDB (PDB 3VSY, 5KP4 and 1OH0 for Apo, GS-bound and TSA-bound, respectively), while the corresponding RT (280 K) structures were obtained in this study (PDB 6U1Z, 6TZD and 6U4I for Apo, GS-bound and TSA-bound, respectively). KSI models were aligned on the backbone of residues 5–125 and RMSDs obtained for all residues.

280 K 100K	6U1Z A (Apo)	6U1Z B (Apo)	6TZD A (GS)	6TZD B (GS)	6U4I A (TSA)	6U4I B (TSA)
3VSY A (Apo)	0.20	0.35	0.36	0.22	0.23	0.38
3VSY B (Apo)	0.36	0.21	0.24	0.30	0.36	0.26
5KP4 B (GS)	0.22	0.28	0.27	0.20	0.20	0.29
1OH0 A (TSA)	0.34	0.18	0.17	0.26	0.32	0.17
1OH0 B (TSA)	0.31	0.19	0.19	0.24	0.28	0.21

Table S5. RMSDs between crystal structures for different KSI catalytic states obtained at cryo (100 K) and room temperature (280 K). Cryo KSI Apo, GS-bound and TSA-bound structures have been obtained from the PDB (PDB 3VSY, 5KP4 and 1OH0 for Apo, GS-bound and TSA-bound, respectively), while the corresponding RT (280 K) structures were obtained in this study (PDB 6U1Z, 6TZD and 6U4I for Apo, GS-bound and TSA-bound, respectively). KSI models were aligned on the backbone of residues 5–125 and RMSDs obtained for all residues excluding loops 62–65 and 91–96.

PDB	Mutations	Ligand	Resolution	Space group	# molecules AU
1DMM	Y57F	-	1.9	$C222_1$	1
1E97	Y16F/Y32F/Y57F	-	2.0	$C222_1$	1
1EA2	Y16F	-	1.8	$C222_1$	1
1OPY	WT	-	1.9	$C222_1$	1
3RGR	M116A	-	1.59	$C222_1$	1
3SED	M105A	-	1.3	$C222_1$	1
4K1V	Y16F/Y57F	-	1.8	$C222_1$	1
3VSY	WT	-	1.5	$P2_12_12_1$	2
4K1U	Y16F/Y32F	-	2.0	$P2_12_12_1$	2
5D83	D40N, Y32 (Cl-Y)	-	1.7	$P2_12_12_1$	2
5D82	D40N, Y16 (Cl-Y)	-	1.37	$P2_12_12_1$	2
5D81	D40N, Y57 (Cl-Y)	-	1.39	$C222_1$	1
3OX9	D40N/C69S/C81S/C97S/ F86C-CN	-	2.0	$P2_1$	4
3OXA	D40N/C69S/C81S/C97S/ M116C-CN	-	1.89	$P2_1$	4
3T8N	Y16AD103A	-	1.47	$C2_1$	4

Table S6. Cryo KSI Apo crystal structures of high-resolution (≤ 2 Å) available from the PDB.

PDB	Mutations	Ligand	Resolution	Space group	# molecules AU
1OHO	Y16F/D40N	Equilenin	1.9	$C222_1$	1
2INX	D40N	2,6-difluorophenol	1.5	$C222_1$	1
3CPO	D40N	2-fluorophenol	1.24	$C222_1$	1
1CQS	D103E/D40N	Equilenin	1.9	$C2_1$	2
1OGX	D40N	Equilenin	2.0	$C2_1$	2
1OH0	WT	Equilenin	1.1	$C2_1$	2
3FZW	D40N/D103N	Equilenin	1.32	$C2_1$	2
3OWS	D40N/C69S/C81S/C97S/ M116C-CN	Equilenin	1.71	$P2_1$	4
3OWU	D40N/C69S/C81S/C97S/ F86C-CN	Equilenin	1.7	$P2_1$	4
3VGN	D40N	3-fluoro-4-nitrophenol	1.3	$P2_12_12_1$	2
2PZV	D40N	Phenol	1.25	P1	4
3IPT	Y16S/D40N	Equilenin	1.63	$P2_1$	4
5KP1	D40N, Y16(Cl-Y)	Equilenin	1.22	P1	4
5KP3	D40N, Y57(Cl-Y)	Equilenin	1.7	$P2_12_12_1$	2
5G2G	M116K	Equilenin	1.6	$P2_12_12_1$	2

Table S7. Cryo KSI TSA-bound crystal structures of high-resolution (≤ 2 Å) available from the PDB.

Apo			TSA-bound		
Set_1^{omit}	Set_2^{omit}	Set_3^{omit}	Set_1^{omit}	Set_2^{omit}	Set_3^{omit}
1C7H	1C7H	1C7H	1GS3	1GS3	1GS3
1DMM	1DMM	1DMM	1OHO	1OHO	1OHO
1DMN	1DMN	1DMN	1W6Y	1W6Y	1W6Y
1DMQ	1DMQ	1DMQ	2INX	2INX	2INX
1E97	1E97	1E97	3CPO	3CPO	3CPO
1EA2	1EA2	1EA2	5AI1	5AI1	5AI1
1OPY	1OPY	1OPY	1OH0_A	1OH0_A	1OH0_A
1W02	1W02	1W02	1OH0_B	1OH0_B	1OH0_B
3RGR	3RGR	3RGR	1CQS_A	1CQS_A	1CQS_A
3SED	3SED	3SED	1OGX_A	1OGX_A	1OGX_A
4K1V	4K1V	4K1V	3FZW_A	3FZW_A	3FZW_A
5D81	5D81	5D81	3VGN_A	3VGN_A	3VGN_A
3VSY_A	3VSY_A	3VSY_A	5KP3_A	5KP3_A	5KP3_A
3VSY_B	3VSY_B	3VSY_B	5G2G_A	5G2G_A	5G2G_A
1K41_A	1K41_A	1K41_A	1CQS_B	1CQS_B	1CQS_B
1VZZ_A	1VZZ_A	1VZZ_A	1OGX_B	1OGX_B	1OGX_B
1W00_A	1W00_A	1W00_A	3FZW_B	3FZW_B	3FZW_B
1W01_A	1W01_A	1W01_A	3VGN_B	3VGN_B	3VGN_B
4K1U_A	4K1U_A	4K1U_A	5KP3_B	5KP3_B	5KP3_B
5D82_A	5D82_A	5D82_A	5G2G_B	5G2G_B	5G2G_B
5D83_A	5D83_A	5D83_A	3OWS_A	3OWS_A	3OWS_A
1K41_B	1K41_B	1K41_B	3OWS_B	3OWS_B	3OWS_B
1VZZ_B	1VZZ_B	1VZZ_B	3OWS_C	3OWS_C	3OWS_C
1W00_B	1W00_B	1W00_B	3OWS_D	3OWS_D	3OWS_D
1W01_B	1W01_B	1W01_B	3OWU_A	3OWU_A	3OWU_A
4K1U_B	4K1U_B	4K1U_B	3OWU_B	3OWU_B	3OWU_B
5D82_B	5D82_B	5D82_B	3OWU_C	3OWU_C	3OWU_C
5D83_B	5D83_B	5D83_B	3OWU_D	3OWU_D	3OWU_D
3OWY_F	3OWY_F	3OWY_F	2PZV_A	2PZV_A	2PZV_A
3OWY_G	3OWY_G	3OWY_G	2PZV_B	2PZV_B	2PZV_B
3OX9_A	3OX9_A	3OX9_A	2PZV_C	2PZV_C	2PZV_C
3OX9_B	3OX9_B	3OX9_B	2PZV_D	2PZV_D	2PZV_D
3OX9_C	3OX9_C	3OX9_C	3IPT_A	3IPT_A	3IPT_A
3OX9_D	3OX9_D	3OX9_D	3IPT_B	3IPT_B	3IPT_B
3OXA_A	3OXA_A	3OXA_A	3IPT_C	3IPT_C	3IPT_C
3OXA_B	3OXA_B	3OXA_B	3IPT_D	3IPT_D	3IPT_D
3OXA_C	3OXA_C	3OXA_C	3OWY_A	3OWY_A	3OWY_A
3OXA_D	3OXA_D	3OXA_D	3OWY_B	3OWY_B	3OWY_B
3T8N_A	3T8N_A	3T8N_A	3OWY_C	3OWY_C	3OWY_C
3T8N_B	3T8N_B	3T8N_B	3OWY_D	3OWY_D	3OWY_D
3T8N_D	3T8N_D	3T8N_D	3OWY_E	3OWY_E	3OWY_E
3T8N_F	3T8N_F	3T8N_F	3OWY_H	3OWY_H	3OWY_H
			5KP1_A	5KP1_A	5KP1_A
			5KP1_B	5KP1_B	5KP1_B
			5KP1_C	5KP1_C	5KP1_C
			5KP1_D	5KP1_D	5KP1_D

Table S8. KSI molecules used to obtain Apo and TSA-bound pseudo-ensembles in which ~30% of all molecules have been randomly omitted (light grey, 12 out of 42 and 14 out of 46 KSI molecules omitted, respectively); random selection and exclusion of molecules was repeated three times to generate three independent sets ($\mathrm{Set}_{1-3}^{\mathrm{omit}}$) for both Apo and TSA-bound.

	Cα Apo MDev (Å)				CαTSA MDev (Å)			
Residues	**Full**	Set_1^{omit}	Set_2^{omit}	Set_3^{omit}	**Full**	Set_1^{omit}	Set_2^{omit}	Set_3^{omit}
5	0.284	0.267	0.292	0.287	0.262	0.285	0.263	0.261
6	0.242	0.231	0.248	0.237	0.263	0.278	0.266	0.272
7	0.273	0.264	0.288	0.272	0.294	0.318	0.307	0.315
8	0.220	0.216	0.225	0.223	0.228	0.253	0.238	0.248
9	0.165	0.165	0.174	0.168	0.166	0.172	0.171	0.164
10	0.190	0.191	0.189	0.196	0.202	0.203	0.207	0.208
11	0.222	0.218	0.224	0.226	0.193	0.202	0.199	0.196
12	0.168	0.170	0.177	0.172	0.170	0.191	0.175	0.168
13	0.178	0.185	0.183	0.184	0.170	0.174	0.174	0.171
14	0.193	0.202	0.186	0.192	0.184	0.181	0.190	0.200
15	0.212	0.226	0.210	0.219	0.193	0.195	0.214	0.193
16	0.200	0.205	0.204	0.205	0.185	0.204	0.192	0.193
17	0.216	0.221	0.201	0.219	0.182	0.186	0.190	0.187
18	0.248	0.222	0.209	0.224	0.175	0.180	0.183	0.167
19	0.259	0.232	0.237	0.235	0.225	0.239	0.230	0.228
20	0.306	0.273	0.284	0.271	0.256	0.261	0.256	0.263
21	0.304	0.264	0.267	0.259	0.238	0.248	0.237	0.239
22	0.309	0.274	0.255	0.274	0.206	0.205	0.198	0.215
23	0.346	0.313	0.290	0.317	0.248	0.246	0.245	0.254
24	0.377	0.351	0.359	0.369	0.305	0.296	0.324	0.305
25	0.422	0.372	0.369	0.385	0.366	0.365	0.372	0.366
26	0.448	0.420	0.436	0.446	0.409	0.422	0.413	0.410
27	0.318	0.291	0.324	0.318	0.344	0.349	0.347	0.344
28	0.241	0.219	0.224	0.225	0.264	0.255	0.264	0.283
29	0.242	0.231	0.230	0.238	0.291	0.301	0.278	0.314
30	0.258	0.240	0.265	0.261	0.322	0.323	0.320	0.338
31	0.194	0.193	0.195	0.194	0.204	0.208	0.204	0.220
32	0.183	0.182	0.187	0.184	0.186	0.184	0.185	0.192
33	0.216	0.220	0.208	0.210	0.153	0.147	0.159	0.153
34	0.533	0.541	0.536	0.487	0.391	0.314	0.372	0.338
35	0.572	0.565	0.536	0.516	0.401	0.333	0.411	0.344
36	0.210	0.217	0.199	0.196	0.155	0.142	0.153	0.147
37	0.240	0.248	0.232	0.241	0.273	0.276	0.297	0.231
38	0.258	0.254	0.246	0.251	0.307	0.313	0.342	0.301
39	0.283	0.275	0.277	0.282	0.304	0.313	0.308	0.316
40	0.296	0.290	0.300	0.298	0.327	0.340	0.318	0.348
41	0.358	0.357	0.376	0.375	0.387	0.398	0.390	0.421
42	0.376	0.376	0.403	0.376	0.386	0.394	0.387	0.421
43	0.492	0.506	0.487	0.524	0.414	0.408	0.402	0.450
44	0.471	0.473	0.484	0.489	0.440	0.450	0.420	0.489
45	0.475	0.481	0.465	0.488	0.431	0.457	0.412	0.481
46	0.358	0.337	0.316	0.338	0.353	0.355	0.334	0.378
47	0.337	0.332	0.303	0.333	0.288	0.308	0.287	0.305
48	0.317	0.294	0.297	0.302	0.212	0.204	0.218	0.203
49	0.602	0.546	0.540	0.511	0.363	0.278	0.284	0.277
50	0.442	0.384	0.386	0.372	0.334	0.293	0.299	0.317
51	0.452	0.399	0.414	0.378	0.367	0.353	0.344	0.360
52	0.328	0.310	0.320	0.293	0.312	0.314	0.301	0.346
53	0.287	0.263	0.249	0.263	0.270	0.268	0.280	0.314
54	0.318	0.304	0.299	0.307	0.332	0.340	0.338	0.367
55	0.352	0.352	0.355	0.362	0.390	0.406	0.395	0.411
56	0.342	0.325	0.308	0.340	0.375	0.384	0.385	0.380
57	0.392	0.339	0.317	0.349	0.318	0.323	0.323	0.333
58	0.514	0.536	0.446	0.530	0.399	0.408	0.397	0.419
59	0.539	0.557	0.490	0.576	0.436	0.452	0.439	0.466
60	0.513	0.491	0.448	0.504	0.493	0.529	0.525	0.551
61	0.492	0.524	0.432	0.535	0.335	0.352	0.363	0.361

62	1.141	1.237	1.095	1.205	0.605	0.624	0.649	0.540
63	1.684	1.561	1.786	1.802	1.271	1.293	1.264	1.128
64	2.697	2.591	2.559	2.641	2.264	2.209	2.124	1.993
65	0.835	0.888	0.767	0.860	0.636	0.691	0.610	0.672
66	0.369	0.394	0.365	0.400	0.392	0.404	0.404	0.408
67	0.319	0.314	0.318	0.337	0.367	0.393	0.391	0.392
68	0.244	0.255	0.232	0.258	0.203	0.197	0.202	0.202
69	0.279	0.282	0.268	0.273	0.286	0.290	0.291	0.296
70	0.269	0.261	0.268	0.269	0.232	0.229	0.234	0.232
71	0.333	0.304	0.348	0.321	0.304	0.329	0.301	0.319
72	0.273	0.259	0.273	0.269	0.207	0.208	0.223	0.215
73	0.239	0.255	0.231	0.250	0.221	0.222	0.221	0.225
74	0.139	0.145	0.134	0.138	0.142	0.136	0.142	0.149
75	0.153	0.152	0.152	0.154	0.175	0.182	0.174	0.176
76	0.172	0.166	0.154	0.168	0.184	0.188	0.188	0.203
77	0.280	0.281	0.273	0.284	0.248	0.233	0.230	0.264
78	0.265	0.243	0.250	0.256	0.247	0.252	0.261	0.275
79	0.265	0.234	0.270	0.247	0.261	0.270	0.275	0.290
80	0.248	0.243	0.253	0.265	0.198	0.204	0.196	0.194
81	0.218	0.216	0.219	0.223	0.169	0.168	0.160	0.154
82	0.179	0.168	0.174	0.170	0.190	0.190	0.182	0.184
83	0.136	0.133	0.134	0.130	0.151	0.164	0.145	0.151
84	0.119	0.123	0.113	0.127	0.117	0.123	0.112	0.130
85	0.182	0.177	0.190	0.186	0.191	0.205	0.194	0.204
86	0.213	0.201	0.214	0.209	0.174	0.178	0.171	0.176
87	0.268	0.259	0.276	0.270	0.249	0.264	0.255	0.261
88	0.263	0.265	0.259	0.268	0.203	0.198	0.206	0.194
89	0.312	0.299	0.279	0.307	0.245	0.246	0.247	0.232
90	0.452	0.465	0.393	0.444	0.260	0.252	0.262	0.260
91	0.996	1.018	0.954	0.990	0.541	0.571	0.547	0.561
92	1.457	1.470	1.458	1.448	1.287	1.338	1.297	1.342
93	2.288	2.237	2.434	2.205	2.318	2.483	2.300	2.367
94	1.870	1.831	1.999	1.869	1.268	1.389	1.281	1.324
95	0.929	0.907	0.951	0.996	0.707	0.676	0.756	0.662
96	0.623	0.626	0.624	0.639	0.467	0.458	0.478	0.407
97	0.374	0.343	0.350	0.345	0.403	0.397	0.397	0.401
98	0.392	0.368	0.392	0.384	0.387	0.388	0.387	0.394
99	0.288	0.289	0.299	0.284	0.319	0.322	0.316	0.342
100	0.216	0.211	0.227	0.219	0.214	0.222	0.216	0.220
101	0.210	0.200	0.209	0.207	0.207	0.214	0.209	0.217
102	0.189	0.188	0.185	0.193	0.172	0.174	0.171	0.176
103	0.204	0.198	0.202	0.197	0.205	0.214	0.205	0.222
104	0.172	0.171	0.183	0.177	0.181	0.177	0.177	0.187
105	0.150	0.159	0.155	0.160	0.139	0.142	0.140	0.142
106	0.155	0.154	0.160	0.158	0.150	0.156	0.159	0.145
107	0.163	0.167	0.167	0.164	0.147	0.149	0.147	0.151
108	0.206	0.216	0.218	0.213	0.194	0.187	0.197	0.207
109	0.333	0.355	0.350	0.349	0.275	0.275	0.270	0.304
110	0.329	0.327	0.320	0.319	0.262	0.279	0.260	0.284
111	0.254	0.245	0.248	0.249	0.227	0.240	0.235	0.246
112	0.175	0.188	0.163	0.182	0.143	0.141	0.144	0.144
113	0.157	0.164	0.168	0.169	0.130	0.126	0.131	0.129
114	0.165	0.174	0.165	0.170	0.135	0.136	0.144	0.133
115	0.230	0.243	0.226	0.217	0.200	0.194	0.221	0.205
116	0.329	0.333	0.343	0.322	0.325	0.324	0.340	0.327
117	0.295	0.294	0.316	0.304	0.332	0.342	0.345	0.351
118	0.331	0.315	0.335	0.322	0.328	0.341	0.340	0.351
119	0.281	0.273	0.289	0.281	0.282	0.289	0.279	0.304
120	0.313	0.304	0.320	0.312	0.353	0.360	0.351	0.384

121	0.434	0.430	0.455	0.436	0.480	0.487	0.481	0.519
122	0.434	0.423	0.476	0.436	0.463	0.466	0.465	0.491
123	0.377	0.368	0.380	0.378	0.299	0.280	0.304	0.287
124	0.292	0.277	0.289	0.289	0.273	0.269	0.277	0.291
125	0.329	0.317	0.324	0.311	0.345	0.333	0.342	0.371

Table S9. Cα MDevs for Apo and TSA-bound pseudo-ensembles composed of all structures (42 and 46 KSI molecules, respectively, indicated as 'Full') and pseudo-ensembles from which 30% of the structures have been randomly omitted (12 out of 42 and 14 out of 46 KSI molecules omitted, respectively; random selection and exclusion of molecules was repeated three times to generate three independent sets ($\mathrm{Set}_{1-3}^{\mathrm{omit}}$) for both Apo and TSA-bound).

		Cα ΣMDev entire enzyme (Å)	Cα ΣMDev enzyme core (Å)
Apo	**Full**	47.068	32.547
	$\boldsymbol{Set_1^{omit}}$	46.087	31.722
	$\boldsymbol{Set_2^{omit}}$	46.179	31.555
	$\boldsymbol{Set_3^{omit}}$	46.647	31.992
TSA-bound	**Full**	41.225	29.860
	$\boldsymbol{Set_1^{omit}}$	41.856	30.124
	$\boldsymbol{Set_2^{omit}}$	41.346	30.040
	$\boldsymbol{Set_3^{omit}}$	41.847	30.850

Table S10. Sum of Cα MDev values (ΣMDev, from Table S9) for Apo and TSA-bound pseudo-ensembles composed of all structures (42 and 46 KSI molecules, respectively, indicated as 'Full') and pseudo-ensembles from which 30% of the structures have been randomly omitted (12 out of 42 and 14 out of 46 KSI molecules omitted, respectively; indicated as '$\mathrm{Set}_{1-3}^{\mathrm{omit}}$').

		Cα TSA-bound ΣMDev (Å)			
		Full	Set_1^{omit}	Set_2^{omit}	Set_3^{omit}
Cα Apo ΣMDev (Å)	**Full**	5.843	5.213	5.723	5.221
	Set_1^{omit}	4.862	4.231	4.741	4.240
	Set_2^{omit}	4.954	4.324	4.834	4.333
	Set_3^{omit}	5.422	4.791	5.301	4.800

Table S11. The values represent the differences (ΔMDev) between the sums of Cα MDev values for Apo (Cα Apo ΣMDev from Table S10) and the sums of Cα MDev values for TSA-bound pseudo-ensembles (Cα TSA-bound ΣMDev from Table S10) for the entire enzyme. The 16 values represent all combinations between the Cα Apo ΣMDev from Apo Full and Sets1-3 and TSA-bound Full and Sets1-3.

		Cα TSA-bound ΣMDev (Å)			
		Full	Set_1^{omit}	Set_2^{omit}	Set_3^{omit}
Cα Apo ΣMDev (Å)	**Full**	2.687	2.423	2.507	1.697
	Set_1^{omit}	1.862	1.598	1.682	0.872
	Set_2^{omit}	1.695	1.431	1.515	0.704
	Set_3^{omit}	2.132	1.868	1.952	1.142

Table S12. The values represent the differences (ΔMDev) between the sums of Cα MDev values for Apo (Cα Apo ΣMDev from Table S10) and the sums of Cα MDev values for TSA-bound pseudo-ensembles (Cα TSA-bound ΣMDev from Table S10) for the enzyme core. The 16 values represent all combinations between the Cα Apo ΣMDev from Apo Full and Sets1-3 and TSA-bound Full and Sets1-3.

Cα Apo ΣMDev (Å)		Cα TSA-bound ΣMDev (Å)		$\Delta MDev_{Apo\text{-}TSA}$	$\Delta MDev_{Apo\text{-}TSA} / \Sigma MDev_{Apo}$
Full	47.068	**Full**	41.225	5.843	0.124
		Set_1^{omit}	41.856	5.213	0.111
		Set_2^{omit}	41.346	5.723	0.122
		Set_3^{omit}	41.847	5.221	0.111
Set_1^{omit}	46.087	**Full**	41.225	4.862	0.105
		Set_1^{omit}	41.856	4.231	0.092
		Set_2^{omit}	41.346	4.741	0.103
		Set_3^{omit}	41.847	4.240	0.092
Set_2^{omit}	46.179	**Full**	41.225	4.954	0.107
		Set_1^{omit}	41.856	4.324	0.094
		Set_2^{omit}	41.346	4.834	0.105
		Set_3^{omit}	41.847	4.333	0.094
Set_3^{omit}	46.647	**Full**	41.225	5.422	0.116
		Set_1^{omit}	41.856	4.791	0.103
		Set_2^{omit}	41.346	5.301	0.114
		Set_3^{omit}	41.847	4.800	0.103

Table S13. The values in the far right column represent the conformational heterogeneity dampening in entire Apo enzyme upon TSA binding as obtained by dividing the difference between Cα Apo and TSA-bound MDevs ($\Delta MDev_{Apo\text{-}TSA}$) by the sum of Cα Apo MDevs ($\Sigma MDev_{Apo}$). The values in column 2, 4 and 5 are taken from Tables S10 and S11.

Cα Apo ΣMDev (Å)		Cα TSA-bound ΣMDev (Å)		$\Delta MDev_{Apo\text{-}TSA}$	$\Delta MDev_{Apo\text{-}TSA} / \Sigma MDev_{Apo}$
Full	32.547	**Full**	29.860	2.687	0.083
		Set_1^{omit}	30.124	2.423	0.074
		Set_2^{omit}	30.040	2.507	0.077
		Set_3^{omit}	30.850	1.697	0.052
Set_1^{omit}	31.722	**Full**	29.860	1.862	0.059
		Set_1^{omit}	30.124	1.598	0.050
		Set_2^{omit}	30.040	1.682	0.053
		Set_3^{omit}	30.850	0.872	0.027
Set_2^{omit}	31.555	**Full**	29.860	1.695	0.054
		Set_1^{omit}	30.124	1.431	0.045
		Set_2^{omit}	30.040	1.515	0.048
		Set_3^{omit}	30.850	0.704	0.022
Set_3^{omit}	31.992	**Full**	29.860	2.132	0.067
		Set_1^{omit}	30.124	1.868	0.058
		Set_2^{omit}	30.040	1.952	0.061
		Set_3^{omit}	30.850	1.142	0.036

Table S14. The values in the far right column represent the conformational heterogeneity dampening in Apo enzyme core (excluding 62-65 and 91-96 loops) upon TSA binding as obtained by dividing the difference between Cα Apo and TSA-bound MDevs ($\Delta MDev_{Apo\text{-}TSA}$) by the sum of Cα Apo MDevs ($\Sigma MDev_{Apo}$). The values in column 2, 4 and 5 are taken from Tables S10 and S12.

Residue	Apo Cα MDev (Å)	TSA Cα MDev (Å)
5	0.159	0.138
6	0.140	0.143
7	0.179	0.183
8	0.126	0.141
9	0.106	0.115
10	0.124	0.152
11	0.154	0.147
12	0.121	0.126
13	0.160	0.163
14	0.184	0.178
15	0.186	0.175
16	0.167	0.135
17	0.179	0.160
18	0.215	0.202
19	0.173	0.154
20	0.224	0.186
21	0.238	0.207
22	0.286	0.265
23	0.288	0.241
24	0.272	0.224
25	0.329	0.254
26	0.332	0.313
27	0.216	0.234
28	0.197	0.169
29	0.193	0.203
30	0.222	0.245
31	0.160	0.151
32	0.170	0.175
33	0.208	0.153
34	0.524	0.381
35	0.581	0.392
36	0.192	0.145
37	0.193	0.236
38	0.185	0.252
39	0.164	0.184
40	0.172	0.207
41	0.199	0.227
42	0.216	0.241
43	0.325	0.267
44	0.310	0.279
45	0.363	0.307
46	0.282	0.298
47	0.282	0.226
48	0.260	0.216
49	0.596	0.345
50	0.435	0.284
51	0.425	0.296

52	0.260	0.244
53	0.235	0.242
54	0.243	0.239
55	0.272	0.291
56	0.316	0.324
57	0.358	0.273
58	0.471	0.323
59	0.459	0.328
60	0.518	0.518
61	0.522	0.392
62	1.334	0.774
63	1.914	1.472
64	2.908	2.542
65	1.019	0.877
66	0.460	0.511
67	0.346	0.371
68	0.260	0.232
69	0.233	0.209
70	0.198	0.145
71	0.228	0.242
72	0.202	0.184
73	0.198	0.215
74	0.113	0.124
75	0.114	0.131
76	0.131	0.148
77	0.195	0.202
78	0.182	0.186
79	0.193	0.204
80	0.207	0.183
81	0.183	0.142
82	0.145	0.159
83	0.104	0.116
84	0.105	0.090
85	0.139	0.182
86	0.134	0.144
87	0.192	0.211
88	0.286	0.301
89	0.345	0.238
90	0.607	0.434
91	1.299	0.835
92	1.796	1.540
93	2.679	2.615
94	2.293	1.660
95	1.301	0.953
96	0.816	0.599
97	0.502	0.519
98	0.402	0.434
99	0.243	0.345
100	0.190	0.269

101	0.136	0.168
102	0.127	0.116
103	0.146	0.147
104	0.110	0.124
105	0.134	0.123
106	0.129	0.132
107	0.145	0.148
108	0.190	0.201
109	0.331	0.293
110	0.320	0.252
111	0.227	0.250
112	0.162	0.163
113	0.155	0.139
114	0.145	0.118
115	0.205	0.203
116	0.281	0.289
117	0.202	0.246
118	0.216	0.227
119	0.152	0.150
120	0.157	0.172
121	0.217	0.257
122	0.287	0.362
123	0.326	0.306
124	0.239	0.297
125	0.352	0.410

Table S15. Cα MDevs for Apo and TSA-bound pseudo-ensembles composed of all structures (42 and 46 KSI molecules, respectively) and aligned using and alternative alignment procedure (see Materials and Methods).

	Cα ΣMDev entire enzyme (Å)	Cα ΣMDev enzyme core (Å)
Apo	44.36	27.00
TSA	39.32	25.45
$\Delta MDev_{Apo - TSA}$	5.04	1.55

Table S16. Sum of Cα MDev values (ΣMDev; from Table S15) for Apo and TSA-bound pseudo-ensembles composed of all structures (42 and 46 KSI molecules, respectively) aligned using an alternative alignment procedure (see Materials and Methods). $\Delta MDev_{Apo - TSA}$ indicates the difference between ΣMDev for Apo and ΣMDev for TSA-bound for either the entire enzyme or for the enzyme core (excluding loops 62-65 and 91-96).

	$\Delta MDev_{Apo\text{-}TSA}$ / $\Sigma MDev_{Apo}$
Entire enzyme	0.11
Enzyme core	0.06

Table S17. The values represent the conformational heterogeneity dampening in Apo enzyme core upon TSA binding as obtained by dividing the difference between Cα Apo and TSA-bound MDevs ($\Delta MDev_{Apo\text{-}TSA}$, from Table S16) by the sum of Cα Apo MDevs ($\Sigma MDev_{Apo}$, from Table S16).

Residue	Apo Cβ MDev (Å)	TSA Cβ MDev (Å)
5	0.318	0.290
6	0.247	0.267
7	0.355	0.370
8	0.244	0.252
9	0.182	0.178
10	0.222	0.220
11	-	-
12	0.160	0.189
13	0.176	0.232
14	0.226	0.217
15	0.248	0.248
16	0.216	0.217
17	0.246	0.204
18	0.343	0.247
19	0.266	0.230
20	0.315	0.260
21	0.319	0.283
22	0.342	0.235
23	-	-
24	0.386	0.339
25	0.472	0.390
26	0.567	0.550
27	0.371	0.372
28	0.294	0.264
29	0.293	0.350
30	0.346	0.387
31	0.220	0.217
32	0.207	0.232
33	0.290	0.206
34	0.729	0.497
35	0.755	0.506
36	0.181	0.162
37	0.348	0.357
38	0.269	0.347
39	0.325	0.313
40	0.281	0.374
41	0.382	0.426
42	0.383	0.397
43	-	-
44	0.569	0.482
45	0.563	0.498
46	0.468	0.396
47	0.434	0.380
48	0.471	0.308
49	-	-
50	0.524	0.397
51	0.589	0.453

52	0.347	0.346
53	0.305	0.262
54	0.341	0.363
55	0.383	0.427
56	0.353	0.407
57	0.402	0.296
58	0.516	0.440
59	0.671	0.584
60	-	-
61	0.517	0.326
62	-	-
63	-	-
64	-	-
65	1.219	0.975
66	0.464	0.439
67	0.438	0.476
68	0.272	0.231
69	0.450	0.499
70	0.347	0.248
71	0.359	0.339
72	-	-
73	0.307	0.285
74	0.174	0.150
75	0.172	0.194
76	0.192	0.215
77	0.377	0.353
78	0.291	0.269
79	0.323	0.328
80	-	-
81	0.300	0.237
82	-	-
83	0.206	0.204
84	0.138	0.131
85	0.246	0.264
86	0.203	0.170
87	0.323	0.307
88	0.363	0.270
89	0.421	0.379
90	0.644	0.374
91	1.311	0.776
92	1.767	1.398
93	2.608	2.735
94	-	-
95	1.040	1.083
96	0.778	0.661
97	0.522	0.534
98	0.442	0.404
99	0.317	0.327
100	0.200	0.190

101	0.251	0.240
102	0.209	0.182
103	0.228	0.246
104	0.221	0.225
105	0.186	0.195
106	0.191	0.203
107	0.175	0.152
108	0.237	0.211
109	0.431	0.373
110	0.386	0.287
111	-	-
112	0.249	0.180
113	0.174	0.144
114	0.192	0.174
115	0.355	0.294
116	0.422	0.441
117	0.338	0.346
118	0.347	0.354
119	0.267	0.258
120	0.314	0.343
121	0.463	0.499
122	0.504	0.539
123	0.439	0.284
124	0.288	0.284
125	0.428	0.390

Table S18. Cβ MDevs of residues 5-125 for Apo and TSA-bound pseudo-ensembles composed of all structures (42 and 46 KSI molecules, respectively). Glycine residues lack Cβ and therefore no MDevs could be obtained (indicated with "-").

	Cβ ΣMDev entire enzyme (Å)	Cβ ΣMDev enzyme core (Å)
Apo	43.481	34.759
TSA	39.478	31.851
$\Delta MDev_{Apo - TSA}$	4.003	2.908

Table S19. Sum of Cβ MDev values (ΣMDev; from Table S18) for Apo and TSA-bound pseudo-ensembles composed of all structures (42 and 46 KSI molecules, respectively). $\Delta MDev_{Apo - TSA}$ indicates the difference between ΣMDev for Apo and ΣMDev for TSA-bound for either the entire enzyme or for the enzyme core (excluding loops 62-65 and 91-96).

	$\Delta MDev_{Apo-TSA} / \Sigma MDev_{Apo}$
Entire enzyme	0.092
Enzyme core	0.084

Table S20. The values represent the conformational heterogeneity dampening in Apo enzyme core upon TSA binding as obtained by dividing the difference between Cβ Apo and TSA-bound MDevs ($\Delta MDev_{Apo-TSA}$, from Table S16) by the sum of Cβ Apo MDevs ($\Sigma MDev_{Apo}$, from Table S16).

PDB ID	Mutations	Ligand	Resolution (Å)	Space group	# molecules in AU
1OCV	F116W	-	2.0	$P3_1$	4
1OGZ	P39A	Equilenin	2.3	$P6_522$	1
1OHP	D38N	*5α-Estran-3,17-Dione*	1.53	$P2_1$	4
1OHS	Y14F/D38N	*5α -androstane-3,17-dione*	1.7	$P2_1$	4
1QJG	WT	Equilenin	2.3	$P2_1$	6
3M8C	D99N	Equilenin	2.1	$P6_122$	4
3MHE	P39A	-	1.72	$P2_12_12_1$	2
3MKI	D38E/D99N	-	2.0	$P6_122$	4
3MYT	D38H/D99N	Equilenin	1.96	$P6_122$	4
3NBR	D38N/P39G/D99N	*4-Androstene-3,17-dione*	1.73	$P6_522$	1
3NHX	D99N	*4-Androstene-3,17-dione*	1.59	$P6_522$	1
3NM2	D38E/P39G/V40G/S42G	-	1.89	$P6_522$	1
3NUV	D38N/D99N	*4-Androstene-3,17-dione*	1.76	$P3_112$	2
3NXJ	D99N	-	1.97	$C222_1$	2
3OV4	P39G/V40G/S42G	Equilenin	1.83	$P6_122$	4
3T8U	Y14A/Y55F/D99A	-	2.5	$P6_122$	4
3UNL	F54G	-	2.52	$P6_122$	4
4L7K	D38E	-	2.1	$P6_122$	12
5DRE	D38G/P39G/D99N	-	2.15	$P6_522$	1
5UGI	D38G/F54A	Equilenin	1.8	$P6_522$	1
8CHO	WT	-	2.3	$P6_522$	1

Table S21. All $KSI_{homolog}$ crystal structures available from the PDB (here we use '$KSI_{homolog}$' to refer to the KSI from the organism *C. testosterone,* see Materials and Methods).

PDB ID[#]	Apo	GSA/TSA-bound	Reduced
1OCV	X		
1OGZ			
1OHP		X	X
1OHS	X*	X	X
1QJG		X	X
3M8C	X*	X	X
3MHE			
3MKI	X		
3MYT			
3NBR			
3NHX		X	X
3NM2			
3NUV		X	X
3NXJ	X		X
3OV4			
3T8U	X		X
3UNL	X		
4L7K	X		
5DRE			
5UGI			
8CHO			X

* $KSI_{homolog}$ molecules from these structures contained both ligand-bound and Apo molecules which were included in either the GS/TSA-bound or in the Apo pseudo-ensembles, respectively (see **Table S23**).

Table S22. Different $KSI_{homolog}$ crystal structures included in the various pseudo-ensembles used in this work. Due to the relatively low total number of bound $KSI_{homolog}$ GS- and TSA-bound molecules (9 and 9 molecules, respectively) available from the different bound structures, we did not attempt building separate GS-bound and TSA-bound pseudo-ensembles. $KSI_{homolog}$ Apo structures with molecules in which active site bound ligands were not catalytic cycle analogs (i.e. sulfate or glycerol) were excluded from the pseudo-ensembles (PDB 3MKI, molecules B-D; PDB 4L7K, molecules A, D, F, H, J; PDB 8CHO). $KSI_{homolog}$ GS/TSA-bound structures with molecules lacking any bound ligand (PDB 1OHS, molecule D; PDB 3M8C, molecule A) were included in the Apo pseudo-ensemble. PDB 1OHP, molecule B was excluded from both ensembles, as the GS was not fully bound in the active site and the catalytic state represented by this KSI structure in not defined. $KSI_{homolog}$ crystal structures with mutations that alter the chemical nature of the general base or with mutations in the general base loop (residues 38-43) which are known to substantially increase the local flexibility were also excluded to eliminate artifacts (PDBs 1OGZ, 3MHE, 3MYT, 3NBR, 3NM2, 3OV4, 5DRE, and 5UGI).

Apo	GSA/TSA–bound
1OCV_A	1OHS_A
1OCV_B	1OHS_B
1OCV_C	1OHS_C
1OCV_D	1OHP_A
1OHS_D	1OHP_C
3NXJ_A	1OHP_D
3NXJ_B	1QJG_E
3M8C_A	1GJG_F
3MKI_A	3NHX_A
3T8U_A	3NUV_A
3T8U_B	3NUV_B
3T8U_C	1QJG_A
3T8U_D	1QJG_B
3UNL_A	1QJG_C
3UNL_B	1QJG_D
3UNL_C	3M8C_B
3UNL_D	3M8C_C
4L7K_B	3M8C_D
4L7K_C	
4L7K_E	
4L7K_G	
4L7K_I	
4L7K_K	
4L7K_O	

Table S23. $KSI_{homolog}$ molecules from the PDB crystal structures used to obtain Apo and GSA/TSA–bound pseudo-ensembles.

Residue	Apo Cα MDev (Å)	GSA/TSA Cα MDev (Å)
3	0.338	0.430
4	0.356	0.380
5	0.287	0.326
6	0.183	0.201
7	0.197	0.172
8	0.225	0.151
9	0.212	0.165
10	0.185	0.120
11	0.194	0.154
12	0.259	0.193
13	0.252	0.207
14	0.235	0.166
15	0.237	0.149
16	0.256	0.164
17	0.275	0.176
18	0.255	0.246
19	0.314	0.273
20	0.329	0.289
21	0.305	0.327
22	0.267	0.261
23	0.251	0.322
24	0.288	0.283
25	0.295	0.241
26	0.211	0.204
27	0.231	0.186
28	0.243	0.199
29	0.253	0.178
30	0.220	0.151
31	0.234	0.215
32	0.411	0.343
33	0.368	0.324
34	0.221	0.173
35	0.195	0.178
36	0.205	0.168
37	0.220	0.191
38	0.280	0.325
39	0.218	0.307
40	0.230	0.261
41	0.401	0.381
42	0.380	0.389
43	0.393	0.459
44	0.377	0.354
45	0.329	0.326
46	0.327	0.280
47	0.302	0.233
48	0.241	0.235
49	0.317	0.265

50	0.274	0.217
51	0.236	0.167
52	0.295	0.199
53	0.338	0.236
54	0.242	0.243
55	0.216	0.215
56	0.314	0.271
57	0.354	0.344
58	0.357	0.349
59	0.294	0.339
60	0.361	0.324
61	0.424	0.351
62	0.334	0.411
63	0.270	0.239
64	0.214	0.167
65	0.222	0.174
66	0.340	0.251
67	0.287	0.178
68	0.281	0.191
69	0.261	0.179
70	0.219	0.191
71	0.179	0.155
72	0.193	0.168
73	0.192	0.181
74	0.224	0.221
75	0.298	0.279
76	0.252	0.234
77	0.176	0.138
78	0.175	0.106
79	0.178	0.109
80	0.163	0.113
81	0.167	0.108
82	0.183	0.133
83	0.164	0.167
84	0.170	0.190
85	0.241	0.268
86	0.264	0.299
87	0.423	0.480
88	0.940	1.177
89	1.078	1.607
90	0.874	1.282
91	0.603	0.657
92	0.472	0.412
93	0.300	0.311
94	0.207	0.207
95	0.192	0.179
96	0.167	0.151
97	0.178	0.139
98	0.189	0.131

99	0.178	0.136
100	0.183	0.159
101	0.180	0.149
102	0.149	0.113
103	0.194	0.131
104	0.350	0.260
105	0.462	0.394
106	0.382	0.305
107	0.317	0.214
108	0.246	0.183
109	0.215	0.141
110	0.233	0.158
111	0.228	0.212
112	0.187	0.227
113	0.169	0.161
114	0.209	0.176
115	0.221	0.123
116	0.277	0.198
117	0.302	0.258
118	0.311	0.290
119	0.262	0.301
120	0.228	0.196
121	0.282	0.254
122	0.407	0.333

Table S24. Cα MDev values for Apo and GSA/TSA-bound pseudo-ensembles composed of all Apo or GSA/TSA-bound $KSI_{homolog}$ molecules (from Table S23).

	Cα ΣMDev entire enzyme (Å)	Cα ΣMDev enzyme core (Å)
Apo	33.945	29.555
TSA	31.626	26.012
$\Delta MDev_{Apo - GSA/TSA}$	2.319	3.543

Table S25. Sum of Cα MDev values (ΣMDev; from Table S24) for Apo and GSA/TSA-bound pseudo-ensembles composed of the $KSI_{homolog}$ molecules (24 and 18 KSI molecules, respectively, Table S23). $\Delta MDev_{Apo - GSA/TSA}$ indicates the difference between ΣMDev for Apo and ΣMDev for TSA-bound for either the entire enzyme or for the enzyme core (excluding the 86-92 loop).

	$\Delta MDev_{Apo\text{-}GSA/TSA}$ / $\Sigma MDev_{Apo}$
Entire enzyme	0.068
Enzyme core	0.112

Table S26. The values represent the conformational heterogeneity dampening in Apo enzyme core upon GSA/TSA binding as obtained by dividing the difference between Cα Apo and TSA-bound MDevs ($\Delta MDev_{Apo\text{-}TSA}$, from Table S25) by the sum of Cα Apo MDevs ($\Sigma MDev_{Apo}$, from Table S25).

Bootstrap cycles	Standard deviation (Å)	
	Apo pseudo-ensemble	TSA-bound pseudo-ensemble
2	1.2746	0.82326
5	1.0870	0.47490
10	0.90315	0.40654
20	0.77570	0.44091
30	0.67611	0.41783
40	0.66826	0.41948
50	0.64100	0.43871
100	0.58084	0.44315
200	0.59049	0.41500
300	0.60243	0.41161

Table S27. Standard deviation values from increasing number of bootstrap cycles used to estimate the error associated with Apo and TSA-bound Cα ΣMDev (Fig. 4E from main text and Fig. S7, see also Materials and Methods).

$(1-S^2)$				
Residue #	**Apo**	**GS-bound observed**	**GS-bound corrected**	**TSA-bound**
5	0.566	0.489	0.456	0.414
6	0.473	0.421	0.398	0.399
7	0.842	0.792	0.770	0.577
8	0.506	0.437	0.407	0.398
9	0.382	0.346	0.330	0.384
10	0.461	0.373	0.335	0.349
11	0.395	0.338	0.314	0.342
12	0.374	0.354	0.346	0.306
13	0.337	0.291	0.271	0.283
14	0.396	0.347	0.326	0.396
15	0.397	0.374	0.364	0.392
16	0.336	0.310	0.299	0.294
17	0.383	0.324	0.299	0.332
18	0.658	0.798	0.858	0.790
19	0.384	0.364	0.355	0.318
20	0.374	0.372	0.371	0.295
21	0.390	0.363	0.351	0.338
22	0.550	0.513	0.496	0.476
23	0.405	0.404	0.403	0.346
24	0.440	0.424	0.417	0.428
25	0.527	0.485	0.467	0.529
26	0.564	0.720	0.787	0.738
27	0.379	0.392	0.398	0.342
28	0.337	0.345	0.348	0.301
29	0.460	0.406	0.383	0.448
30	0.669	0.760	0.799	0.748
31	0.383	0.369	0.362	0.326
32	0.331	0.341	0.346	0.324
33	0.436	0.431	0.429	0.430
34	0.623	0.754	0.810	0.728
35	0.672	0.758	0.795	0.775
36	0.414	0.385	0.372	0.345
37	0.621	0.638	0.645	0.606
38	0.393	0.358	0.343	0.331
39	0.369	0.377	0.381	0.326
40	0.380	0.405	0.416	0.357
41	0.454	0.418	0.402	0.343
42	0.401	0.409	0.412	0.323
43	0.417	0.439	0.448	0.329
44	0.588	0.546	0.528	0.458
45	0.704	0.613	0.574	0.714
46	0.696	0.670	0.659	0.681
47	0.691	0.781	0.819	0.726
48	0.749	0.837	0.875	0.783
49	0.433	0.488	0.512	0.447
50	0.484	0.569	0.605	0.580

51	0.522	0.516	0.514	0.473
52	0.460	0.496	0.511	0.486
53	0.380	0.385	0.387	0.373
54	0.440	0.433	0.430	0.397
55	0.470	0.455	0.449	0.509
56	0.457	0.432	0.421	0.437
57	0.399	0.380	0.371	0.331
58	0.862	0.811	0.789	0.687
59	0.774	0.859	0.895	0.642
60	0.630	0.571	0.546	0.533
61	0.606	0.548	0.523	0.517
62	0.803	0.761	0.742	0.650
63	0.964	0.821	0.759	0.830
64	0.975	0.772	0.684	0.784
65	1.045	0.822	0.726	0.852
66	0.663	0.552	0.505	0.413
67	0.597	0.480	0.429	0.453
68	0.414	0.381	0.367	0.346
69	0.717	0.716	0.715	0.764
70	0.356	0.312	0.292	0.352
71	0.391	0.326	0.298	0.336
72	0.369	0.340	0.327	0.340
73	0.556	0.406	0.342	0.517
74	0.343	0.328	0.322	0.286
75	0.300	0.263	0.246	0.348
76	0.461	0.376	0.339	0.401
77	0.473	0.582	0.629	0.378
78	0.468	0.394	0.362	0.355
79	0.491	0.416	0.384	0.380
80	0.402	0.334	0.305	0.324
81	0.370	0.310	0.284	0.313
82	0.303	0.264	0.248	0.246
83	0.287	0.252	0.237	0.254
84	0.304	0.250	0.227	0.252
85	0.296	0.259	0.243	0.256
86	0.302	0.238	0.210	0.252
87	0.469	0.394	0.362	0.390
88	0.437	0.634	0.718	0.769
89	0.540	0.460	0.426	0.419
90	0.721	0.552	0.480	0.621
91	0.916	0.598	0.462	0.684
92	1.090	0.509	0.260	0.660
93	1.123	0.688	0.502	0.721
94	1.131	0.709	0.528	0.825
95	1.078	0.735	0.588	0.884
96	0.884	0.556	0.415	0.718
97	0.857	0.577	0.456	0.687
98	0.539	0.411	0.356	0.412
99	0.384	0.341	0.323	0.316

100	0.364	0.304	0.278	0.263
101	0.304	0.272	0.258	0.224
102	0.276	0.229	0.209	0.219
103	0.333	0.257	0.224	0.363
104	0.319	0.285	0.270	0.259
105	0.333	0.290	0.272	0.287
106	0.390	0.355	0.339	0.318
107	0.392	0.360	0.346	0.332
108	0.550	0.482	0.453	0.533
109	0.924	0.898	0.887	0.889
110	0.857	0.714	0.652	0.649
111	0.558	0.539	0.531	0.431
112	0.492	0.498	0.501	0.496
113	0.353	0.351	0.350	0.289
114	0.474	0.459	0.452	0.431
115	0.588	0.660	0.691	0.542
116	0.429	0.377	0.354	0.402
117	0.366	0.328	0.311	0.317
118	0.346	0.320	0.309	0.260
119	0.279	0.271	0.267	0.229
120	0.337	0.298	0.281	0.300
121	0.432	0.394	0.378	0.385
122	0.770	0.508	0.395	0.600
123	0.611	0.381	0.282	0.434
124	0.357	0.283	0.251	0.267
125	0.572	0.490	0.454	0.541

Table S28. Crystallographic disorder parameters obtained from the 250 K multi-conformer models of KSI Apo, GS-bound and TSA-bound (Table S3) .The values are the average of the two molecules from the crystallographic asymmetric unit. The total occupancy of the GS in the two GS-bound molecules was 1.4 instead of 2.0 (1.0 occupancy for each KSI molecule in the asymmetric unit). The corrected (1-S^2) values were obtained using the relationship $(1-S^2)\ GSA_{corrected} = {((1-S^2)GSA_{observed} - 0.3x(1-S^2)Apo)}/{0.7}$

$\Delta(1-S^2)$			
Residue #	**Apo – GS $_{corrected}$**	**$GS_{corrected}$ – TSA**	**Apo – TSA**
5	0.11	0.042	0.152
6	0.075	-0.001	0.074
7	0.072	0.193	0.265
8	0.099	0.009	0.108
9	0.052	-0.054	-0.002
10	0.126	-0.014	0.112
11	0.081	-0.028	0.053
12	0.028	0.04	0.068
13	0.066	-0.012	0.054
14	0.07	-0.07	0
15	0.033	-0.028	0.005
16	0.037	0.005	0.042
17	0.084	-0.033	0.051
18	-0.2	0.068	-0.132
19	0.029	0.037	0.066
20	0.003	0.076	0.079
21	0.039	0.013	0.052
22	0.054	0.02	0.074
23	0.002	0.057	0.059
24	0.023	-0.011	0.012
25	0.06	-0.062	-0.002
26	-0.223	0.049	-0.174
27	-0.019	0.056	0.037
28	-0.011	0.047	0.036
29	0.077	-0.065	0.012
30	-0.13	0.051	-0.079
31	0.021	0.036	0.057
32	-0.015	0.022	0.007
33	0.007	-0.001	0.006
34	-0.187	0.082	-0.105
35	-0.123	0.02	-0.103
36	0.042	0.027	0.069
37	-0.024	0.039	0.015
38	0.05	0.012	0.062
39	-0.012	0.055	0.043
40	-0.036	0.059	0.023
41	0.052	0.059	0.111
42	-0.011	0.089	0.078
43	-0.031	0.119	0.088
44	0.06	0.07	0.13
45	0.13	-0.14	-0.01
46	0.037	-0.022	0.015
47	-0.128	0.093	-0.035
48	-0.126	0.092	-0.034
49	-0.079	0.065	-0.014
50	-0.121	0.025	-0.096

51	0.008	0.041	0.049
52	-0.051	0.025	-0.026
53	-0.007	0.014	0.007
54	0.01	0.033	0.043
55	0.021	-0.06	-0.039
56	0.036	-0.016	0.02
57	0.028	0.04	0.068
58	0.073	0.102	0.175
59	-0.121	0.253	0.132
60	0.084	0.013	0.097
61	0.083	0.006	0.089
62	0.061	0.092	0.153
63	0.205	-0.071	0.134
64	0.291	-0.1	0.191
65	0.319	-0.126	0.193
66	0.158	0.092	0.25
67	0.168	-0.024	0.144
68	0.047	0.021	0.068
69	0.002	-0.049	-0.047
70	0.064	-0.06	0.004
71	0.093	-0.038	0.055
72	0.042	-0.013	0.029
73	0.214	-0.175	0.039
74	0.021	0.036	0.057
75	0.054	-0.102	-0.048
76	0.122	-0.062	0.06
77	-0.156	0.251	0.095
78	0.106	0.007	0.113
79	0.107	0.004	0.111
80	0.097	-0.019	0.078
81	0.086	-0.029	0.057
82	0.055	0.002	0.057
83	0.05	-0.017	0.033
84	0.077	-0.025	0.052
85	0.053	-0.013	0.04
86	0.092	-0.042	0.05
87	0.107	-0.028	0.079
88	-0.281	-0.051	-0.332
89	0.114	0.007	0.121
90	0.241	-0.141	0.1
91	0.454	-0.222	0.232
92	0.83	-0.4	0.43
93	0.621	-0.219	0.402
94	0.603	-0.297	0.306
95	0.49	-0.296	0.194
96	0.469	-0.303	0.166
97	0.401	-0.231	0.17
98	0.183	-0.056	0.127
99	0.061	0.007	0.068

100	0.086	0.015	0.101
101	0.046	0.034	0.08
102	0.067	-0.01	0.057
103	0.109	-0.139	-0.03
104	0.049	0.011	0.06
105	0.061	-0.015	0.046
106	0.051	0.021	0.072
107	0.046	0.014	0.06
108	0.097	-0.08	0.017
109	0.037	-0.002	0.035
110	0.205	0.003	0.208
111	0.027	0.1	0.127
112	-0.009	0.005	-0.004
113	0.003	0.061	0.064
114	0.022	0.021	0.043
115	-0.103	0.149	0.046
116	0.075	-0.048	0.027
117	0.055	-0.006	0.049
118	0.037	0.049	0.086
119	0.012	0.038	0.05
120	0.056	-0.019	0.037
121	0.054	-0.007	0.047
122	0.375	-0.205	0.17
123	0.329	-0.152	0.177
124	0.106	-0.016	0.09
125	0.118	-0.087	0.031

Table S29. Difference crystallographic disorder parameters ($\Delta(1-S^2)$ values from Table S28).

	Σ(1-S^2) entire enzyme	**Σ(1-S^2) `enzyme core (Å)**
Apo	63.02	53.01
GS-bound observed	56.71	49.74
GS-bound corrected	54.00	48.34
TSA-bound	55.30	47.69

Table S30. Sum of crystallographic disorder parameters (1-S^2) (from Table S29) obtained for Apo, GS-bound (observed and corrected) and TSA-bound 250 K KSI multi-conformer models.

	Δ(1-S^2) entire enzyme	**Δ(1-S^2) `enzyme core (Å)**
Apo – $GS_{observed}$	6.31	3.27
Apo – $GS_{corrected}$	9.04	4.67
$GS_{observed}$ – TSA	1.41	2.05
$GS_{corrected}$ – TSA	-1.30	0.65
Apo – TSA	7.72	5.32

Table S31. Difference crystallographic disorder parameters (Δ(Σ1-S^2) values from Table S30)

	Entire enzyme			Enzyme core		
	$\Delta\Sigma(1-S^2)$	**$\Sigma(1-S^2)_{Apo}$**	**$\Delta\Sigma(1-S^2)$ / $\Sigma(1-S^2)_{Apo}$**	**$\Delta\Sigma(1-S^2)$**	**$\Sigma(1-S^2)_{Apo}$**	**$\Delta\Sigma(1-S^2)$ / $\Sigma(1-S^2)_{Apo}$**
Apo → GS (observed)	6.31	63.02	0.10	3.27	53.01	0.06
Apo → GS (corrected)	9.02		0.14	4.67		0.09
	$\Delta\Sigma(1-S^2)$	**$\Sigma(1-S^2)_{GS}$**	**$\Delta\Sigma(1-S^2)$ / $\Sigma(1-S^2)_{GS}$**	**$\Delta\Sigma(1-S^2)$**	**$\Sigma(1-S^2)_{GS}$**	**$\Delta\Sigma(1-S^2)$ / $\Sigma(1-S^2)_{GS}$**
GS (observed) → TSA	1.41	56.71	0.02	2.05	49.74	0.04
GS (corrected) → TSA	-1.30	54.00	-0.02	0.65	48.34	0.01
	$\Delta\Sigma(1-S^2)$	**$\Sigma(1-S^2)_{Apo}$**	**$\Delta\Sigma(1-S^2)$ / $\Sigma(1-S^2)_{Apo}$**	**$\Delta\Sigma(1-S^2)$**	**$\Sigma(1-S^2)_{Apo}$**	**$\Delta\Sigma(1-S^2)$ / $\Sigma(1-S^2)_{Apo}$**
Apo → TSA	7.72	63.02	0.12	5.32	53.01	0.1

Table S32. The values in the $\Delta\Sigma(1-S^2)$ / $\Delta(1-S^2)$ columns represent the conformational heterogeneity dampening in a given KSI catalytic state relative to the preceding catalytic state – i.e. in the GS-bound state relative to the Apo state and in the TSA-bound state relative to the GS-bound state. The last row indicates the conformational heterogeneity dampening in the TSA-bound state with respect to the Apo state. The conformational heterogeneity dampening for both the entire enzyme or the enzyme core (excluding 62-65 and 91-96 loops) was obtained by dividing the difference of the $(1-S^2)$ sums of two states *x* and *y* ($\Delta\Sigma(1-S^2)$), by the sum of $(1-S^2)$ for *x*. The conformational heterogeneity dampening was calculated using both the observed and corrected $(1-S^2)$ for the GS-bound state. Using either the observed or corrected values led to analogous results and conclusions.

Residue #	Reduced pseudo-ensemble		RT-ensemble	
	Oδ1	O/Nδ1	Oδ1	O/Nδ2
D21	0.270	0.271	0.395	0.524
D24	0.390	0.544	0.679	0.759
D34	1.608	1.564	2.068	1.768
D35	1.005	1.057	2.800	1.405
D40	0.528	0.809	0.337	0.954
N79	1.322	1.294	0.979	1.081
D100	0.226	0.278	0.456	0.461
D103	0.191	0.196	0.271	0.370
D108	0.688	0.688	0.585	0.891
N124	0.256	0.233	0.296	0.355

Table S33. Reduced pseudo-ensemble and RT-ensemble MDev values for all aspartate and asparagine residues Oδ1 and O/Nδ2 atoms (Oδ2 if the residue is aspartate and Nδ2 if the residue is asparagine). Asparagine 93 is situated in the middle of the 91-96 flexible loop and was therefore not included in the comparison.

Residue #	Reduced pseudo-ensemble		RT-ensemble	
	OH	Cζ	OH	Cζ
Y16	0.214		0.335	
Y32	0.305		0.367	
F42		0.436		0.484
F56		0.687		0.668
Y57	0.318		0.321	
F86		0.177		0.234
F107		0.184		0.279
Y119	0.416		0.414	

Table S34. Reduced pseudo-ensemble and RT-ensemble MDev values for all tyrosine and phenylalanine residues OH and Cζ atoms, respectively.

Residue #	Cα MDev (Å)			Cα ΔMDev (Å)	
	Full	Reduced	RT	RT–Full	RT–reduced
5	0.269	0.231	0.278	0.009	0.047
6	0.250	0.203	0.234	-0.016	0.031
7	0.281	0.252	0.286	0.005	0.033
8	0.223	0.210	0.331	0.108	0.121
8	0.164	0.141	0.273	0.109	0.132
9	0.191	0.165	0.243	0.051	0.078
10	0.206	0.179	0.313	0.107	0.134
11	0.171	0.146	0.266	0.095	0.120
12	0.173	0.152	0.170	-0.004	0.017
13	0.187	0.174	0.223	0.036	0.049
14	0.201	0.181	0.232	0.030	0.051
15	0.194	0.180	0.222	0.028	0.042
16	0.201	0.193	0.212	0.010	0.019
17	0.212	0.182	0.289	0.076	0.107
18	0.239	0.202	0.296	0.058	0.094
19	0.279	0.226	0.275	-0.005	0.049
20	0.270	0.222	0.365	0.096	0.143
21	0.265	0.239	0.472	0.207	0.233
22	0.299	0.256	0.366	0.067	0.111
23	0.339	0.300	0.283	-0.056	-0.017
24	0.390	0.309	0.293	-0.096	-0.016
25	0.424	0.320	0.388	-0.035	0.068
26	0.329	0.252	0.313	-0.016	0.060
27	0.251	0.215	0.210	-0.041	-0.005
28	0.273	0.252	0.228	-0.044	-0.023
29	0.285	0.251	0.252	-0.033	0.001
30	0.204	0.183	0.248	0.043	0.065
31	0.191	0.188	0.290	0.099	0.101
32	0.194	0.189	0.332	0.139	0.143
33	0.470	0.502	0.806	0.336	0.304
34	0.511	0.564	0.810	0.298	0.245
35	0.188	0.197	0.421	0.233	0.223
36	0.253	0.239	0.311	0.058	0.072
37	0.279	0.249	0.255	-0.024	0.006
39	0.286	0.251	0.240	-0.046	-0.012
40	0.321	0.283	0.276	-0.045	-0.007
41	0.367	0.349	0.238	-0.129	-0.111
42	0.370	0.334	0.266	-0.104	-0.068
43	0.442	0.392	0.382	-0.060	-0.010
44	0.448	0.424	0.423	-0.025	-0.001
45	0.441	0.430	0.529	0.087	0.099
46	0.356	0.326	0.358	0.002	0.032
47	0.313	0.263	0.372	0.059	0.109
48	0.259	0.220	0.403	0.144	0.183
49	0.506	0.550	0.935	0.429	0.385
50	0.399	0.419	0.655	0.256	0.236
51	0.416	0.420	0.567	0.151	0.147

52	0.316	0.306	0.439	0.122	0.132
53	0.274	0.268	0.252	-0.022	-0.016
54	0.325	0.281	0.323	-0.002	0.042
55	0.381	0.329	0.356	-0.024	0.027
56	0.379	0.325	0.306	-0.073	-0.019
57	0.376	0.296	0.256	-0.120	-0.040
58	0.455	0.335	0.274	-0.181	-0.061
59	0.494	0.377	0.307	-0.187	-0.070
60	0.504	0.448	0.346	-0.158	-0.102
61	0.412	0.359	0.331	-0.080	-0.028
62	0.980	0.803	0.500	-0.480	-0.303
63	1.526	1.264	1.470	-0.056	0.206
64	2.375	2.519	1.861	-0.514	-0.658
65	0.728	0.650	0.804	0.076	0.154
66	0.369	0.376	0.344	-0.025	-0.032
67	0.341	0.333	0.300	-0.041	-0.033
68	0.233	0.212	0.305	0.072	0.093
69	0.291	0.234	0.240	-0.051	0.006
70	0.239	0.199	0.194	-0.045	-0.005
71	0.315	0.253	0.188	-0.127	-0.065
72	0.243	0.212	0.207	-0.037	-0.005
73	0.233	0.209	0.217	-0.015	0.009
74	0.142	0.123	0.147	0.005	0.024
75	0.167	0.137	0.116	-0.050	-0.021
76	0.180	0.168	0.179	-0.001	0.011
77	0.265	0.238	0.215	-0.050	-0.022
78	0.268	0.229	0.257	-0.011	0.028
79	0.267	0.226	0.316	0.049	0.090
80	0.224	0.213	0.323	0.099	0.111
81	0.195	0.163	0.236	0.041	0.073
82	0.181	0.146	0.248	0.067	0.102
83	0.145	0.119	0.114	-0.032	-0.006
84	0.122	0.114	0.137	0.015	0.023
85	0.185	0.157	0.134	-0.051	-0.023
86	0.189	0.162	0.144	-0.045	-0.018
87	0.257	0.220	0.144	-0.113	-0.076
88	0.234	0.237	0.210	-0.023	-0.027
89	0.281	0.214	0.250	-0.032	0.035
90	0.371	0.293	0.414	0.043	0.121
91	0.770	0.670	0.695	-0.075	0.025
92	1.342	1.178	1.090	-0.252	-0.089
93	2.139	2.091	2.341	0.202	0.250
94	1.579	1.470	1.182	-0.397	-0.288
95	0.852	0.802	1.037	0.185	0.234
96	0.539	0.437	0.675	0.136	0.238
97	0.424	0.406	0.405	-0.018	0.000
98	0.393	0.355	0.360	-0.033	0.005
99	0.300	0.281	0.247	-0.053	-0.034
100	0.210	0.201	0.208	-0.002	0.007

101	0.209	0.190	0.142	-0.067	-0.048
102	0.182	0.160	0.122	-0.059	-0.038
103	0.202	0.157	0.179	-0.023	0.022
104	0.172	0.150	0.160	-0.012	0.010
105	0.143	0.124	0.156	0.013	0.032
106	0.154	0.132	0.255	0.102	0.123
107	0.153	0.137	0.307	0.154	0.170
108	0.200	0.187	0.356	0.156	0.169
109	0.305	0.277	0.437	0.132	0.160
110	0.296	0.241	0.518	0.223	0.278
111	0.243	0.208	0.422	0.179	0.214
112	0.162	0.135	0.254	0.092	0.119
113	0.144	0.127	0.291	0.148	0.164
114	0.154	0.133	0.293	0.139	0.160
115	0.210	0.207	0.217	0.007	0.009
116	0.320	0.303	0.207	-0.113	-0.096
117	0.308	0.271	0.167	-0.141	-0.103
118	0.318	0.282	0.219	-0.099	-0.064
119	0.283	0.262	0.185	-0.098	-0.077
120	0.344	0.333	0.206	-0.138	-0.127
121	0.457	0.445	0.289	-0.169	-0.157
122	0.445	0.438	0.325	-0.120	-0.113
123	0.332	0.315	0.305	-0.027	-0.010
124	0.279	0.262	0.187	-0.092	-0.075
125	0.345	0.333	0.294	-0.051	-0.038

Table S35. Full pseudo-ensemble, reduced pseudo-ensemble and RT-ensemble MDev values for Cα atoms of residues 5-125.

Residue #	Cβ MDev (Å)			Cβ ΔMDev (Å)	
	Full	Reduced	RT	RT–Full	RT–reduced
5	0.299	0.260	0.313	0.014	0.053
6	0.263	0.207	0.262	-0.001	0.055
7	0.359	0.321	0.297	-0.062	-0.025
8	0.248	0.242	0.378	0.130	0.136
8	0.177	0.147	0.248	0.071	0.101
9	0.216	0.188	0.267	0.051	0.080
10	-	-	-	-	-
11	0.173	0.149	0.263	0.090	0.114
12	0.202	0.201	0.175	-0.027	-0.026
13	0.223	0.193	0.302	0.079	0.109
14	0.243	0.236	0.310	0.067	0.074
15	0.221	0.220	0.254	0.033	0.034
16	0.226	0.216	0.277	0.050	0.061
17	0.295	0.261	0.330	0.034	0.069
18	0.248	0.210	0.308	0.061	0.099
19	0.292	0.233	0.257	-0.035	0.024
20	0.301	0.230	0.330	0.029	0.100
21	0.298	0.291	0.469	0.170	0.178
22	-	-	-	-	-
23	0.360	0.321	0.336	-0.024	0.015
24	0.424	0.315	0.393	-0.031	0.077
25	0.552	0.421	0.486	-0.066	0.066
26	0.372	0.286	0.368	-0.004	0.082
27	0.278	0.235	0.226	-0.051	-0.009
28	0.320	0.294	0.313	-0.008	0.019
29	0.366	0.319	0.312	-0.054	-0.008
30	0.222	0.193	0.315	0.092	0.122
31	0.222	0.211	0.302	0.080	0.091
32	0.248	0.245	0.433	0.185	0.188
33	0.643	0.632	0.934	0.291	0.302
34	0.648	0.701	0.900	0.252	0.199
35	0.177	0.167	0.398	0.221	0.231
36	0.350	0.330	0.404	0.054	0.074
37	0.308	0.281	0.291	-0.018	0.010
39	0.310	0.268	0.289	-0.022	0.021
40	0.337	0.304	0.325	-0.012	0.021
41	0.395	0.378	0.298	-0.097	-0.080
42	0.379	0.333	0.303	-0.076	-0.030
43	-	-	-	-	-
44	0.514	0.450	0.466	-0.048	0.016
45	0.534	0.538	0.625	0.091	0.088
46	0.419	0.385	0.416	-0.003	0.031
47	0.427	0.368	0.489	0.063	0.121
48	0.399	0.341	0.649	0.250	0.308
49	-	-	-	-	-
50	0.487	0.523	0.773	0.287	0.251
51	0.539	0.554	0.744	0.205	0.190

52	0.348	0.335	0.419	0.071	0.084
53	0.284	0.279	0.284	-0.001	0.005
54	0.352	0.300	0.378	0.025	0.078
55	0.417	0.352	0.413	-0.005	0.061
56	0.411	0.367	0.296	-0.114	-0.070
57	0.380	0.309	0.264	-0.116	-0.044
58	0.468	0.381	0.341	-0.126	-0.040
59	0.636	0.506	0.398	-0.238	-0.108
60	-	-	-	-	-
61	0.440	0.350	0.303	-0.137	-0.046
62	-	-	-	-	-
63	-	-	-	-	-
64	-	-	-	-	-
65	1.127	1.146	1.027	-0.100	-0.119
66	0.445	0.409	0.364	-0.081	-0.045
67	0.441	0.396	0.307	-0.134	-0.089
68	0.260	0.234	0.420	0.161	0.187
69	0.478	0.370	0.336	-0.142	-0.034
70	0.292	0.223	0.244	-0.048	0.021
71	0.341	0.260	0.277	-0.064	0.017
72	-	-	-	-	-
73	0.296	0.251	0.275	-0.020	0.024
74	0.159	0.143	0.132	-0.027	-0.011
75	0.184	0.171	0.160	-0.025	-0.011
76	0.201	0.179	0.261	0.060	0.083
77	0.364	0.320	0.274	-0.090	-0.046
78	0.292	0.254	0.331	0.039	0.077
79	0.326	0.272	0.401	0.075	0.129
80	-	-	-	-	-
81	0.265	0.235	0.241	-0.024	0.007
82	-	-	-	-	-
83	0.210	0.158	0.214	0.004	0.057
84	0.142	0.128	0.221	0.079	0.094
85	0.260	0.207	0.220	-0.040	0.013
86	0.184	0.168	0.162	-0.022	-0.007
87	0.312	0.276	0.195	-0.118	-0.081
88	0.320	0.273	0.355	0.035	0.081
89	0.393	0.304	0.391	-0.002	0.087
90	0.516	0.434	0.446	-0.070	0.012
91	1.018	0.910	0.888	-0.131	-0.022
92	1.529	1.319	1.210	-0.318	-0.109
93	2.529	2.479	2.709	0.179	0.229
94	-	-	-	-	-
95	1.114	1.128	1.346	0.232	0.218
96	0.697	0.537	0.807	0.111	0.270
97	0.550	0.535	0.483	-0.068	-0.052
98	0.440	0.406	0.469	0.029	0.064
99	0.322	0.309	0.271	-0.050	-0.038
100	0.195	0.197	0.262	0.067	0.066

101	0.246	0.224	0.230	-0.015	0.006
102	0.198	0.161	0.147	-0.051	-0.014
103	0.236	0.175	0.303	0.067	0.129
104	0.216	0.178	0.255	0.039	0.078
105	0.187	0.168	0.189	0.002	0.021
106	0.194	0.184	0.281	0.087	0.098
107	0.163	0.146	0.360	0.197	0.214
108	0.220	0.206	0.462	0.242	0.256
109	0.400	0.370	0.569	0.170	0.199
110	0.336	0.268	0.569	0.233	0.301
111					
112	0.221	0.185	0.248	0.027	0.063
113	0.160	0.149	0.295	0.134	0.146
114	0.190	0.184	0.278	0.088	0.095
115	0.322	0.306	0.332	0.010	0.026
116	0.418	0.380	0.317	-0.101	-0.063
117	0.333	0.306	0.231	-0.102	-0.075
118	0.356	0.296	0.261	-0.094	-0.035
119	0.273	0.243	0.204	-0.069	-0.039
120	0.334	0.313	0.207	-0.127	-0.107
121	0.477	0.468	0.381	-0.097	-0.087
122	0.514	0.497	0.408	-0.107	-0.089
123	0.364	0.371	0.361	-0.003	-0.010
124	0.284	0.268	0.214	-0.070	-0.054
125	0.422	0.405	0.413	-0.009	0.008

Table S36. Full pseudo-ensemble, reduced pseudo-ensemble and RT-ensemble MDev values for Cβ atoms of residues 5-125.

Residue #	Cγ2 MDev (Å)		
	Full	Reduced	RT
9	0.191	0.146	0.321
17	0.275	0.243	0.323
20	0.313	0.259	0.309
22	0.898	0.985	1.331
25	0.485	0.375	0.546
28	0.323	0.300	0.292
29	0.382	0.351	0.423
38	0.336	0.319	0.388
47	0.943	0.760	1.036
53	0.306	0.291	0.354
66	0.537	0.505	0.465
74	0.187	0.175	0.251
88	0.645	0.638	1.107
91	1.416	1.417	1.646
101	0.277	0.245	0.282
102	0.213	0.151	0.225
104	0.247	0.198	0.398
113	0.194	0.186	0.308
123	0.665	0.749	0.816

Table S37. Full pseudo-ensemble, reduced pseudo-ensemble and RT-ensemble MDev values for Cγ2 atoms of all KSI isoleucine and valine residues.

Residue #	Cε MDev (Å)		
	Full	Reduced	RT
13	0.228	0.189	0.275
31	0.278	0.233	0.427
84	0.243	0.187	0.402
90	1.651	1.631	1.375
105	0.543	0.530	0.331
116	1.395	1.348	1.017

Table S38. Full pseudo-ensemble, reduced pseudo-ensemble and RT-ensemble MDev values for Cε atoms of all KSI methionine residues.

Residue #	Oγ2/Sγ2 MDev (Å)		
	Full	Reduced	RT
69	1.276	1.370	1.395
77	0.682	0.450	0.907
81	0.370	0.290	0.329
97	1.319	1.373	1.690
121	0.449	0.421	0.626
126	1.138	1.206	1.056

Table S39. Full pseudo-ensemble, reduced pseudo-ensemble and RT-ensemble MDev values for Oγ2 and Sγ2 atoms of all KSI serine and cysteine residues, respectively.

Residue #	Oε2/Nε2 MDev (Å)		
	Full	Reduced	RT
7	1.829	2.140	2.646
8	0.893	0.815	0.670
10	1.289	1.233	0.435
18	2.336	2.705	3.180
26	2.708	2.261	2.733
30	2.670	3.026	3.252
39	1.002	0.900	1.281
44	1.531	1.649	1.645
51	1.880	1.758	1.903
52	1.712	1.846	2.556
59	2.578	2.572	2.493
89	1.104	0.991	1.066
95	2.280	2.359	2.945
109	2.621	2.635	2.367
114	2.103	1.944	2.295
117	1.300	1.346	1.072
122	2.355	2.218	2.610

Table S40. Full pseudo-ensemble, reduced pseudo-ensemble and RT-ensemble MDev values for Oε2 and Nε2 atoms of all KSI glutamate and glutamine residues, respectively.

Structure	Distance (Å)	
	Y16 OH – Equ Ox	D103 Oδ2 – Equ Ox
1W6Y	2.56	2.58
1OH0_A	2.54	2.48
1OH0_B	2.55	2.56
3OWU_D	2.76	2.56
3OWU_A	2.7	2.5
3OWU_B	2.56	2.47
3OWU_C	2.69	2.47
1OGX_A	2.68	2.54
1OGX_B	2.66	2.55
3OWS_A	2.58	2.46
3OWS_B	2.53	2.5
3OWS_C	2.53	2.45
3OWS_D	2.57	2.49
3OWY_A	2.48	2.52
3OWY_B	3.07	2.38
3OWY_C	2.6	2.63
3OWY_D	2.66	2.38
3OWY_E	2.47	2.48
3OWY_H	3.09	2.42
Mean	2.60	2.50

Table S41. Lengths of Y16 and D103 hydrogen bonds made to the transition state analog equilenin in the ensemble of KSI crystal structures of variants with WT-like activity (Table S1-S2). The Y16 OH – Equ Ox distance from PDB 3OWY molecules B and H were not included in the calculation of the mean, because the measured distances of 3.07 and 3.09 Å appear too long for equilenin to be making a hydrogen bond with Y16. However the corresponding D103 Oδ2 – Equ Ox hydrogen bond lengths were included as the distances of 2.38 and 2.42 Å are within the expected range. This observation is onsistent with previous observations that Y16 and D103 hydrogen bonds can be formed independent from one another.

	Packing residue	Packing atom	Y16 atom	Van der Waals sum
1	V20	Cγ2	Cζ	3.4-4.0
2	M105	Cε	Ring	3.4-4.0
3	M84	Cε	Cδ2	3.4-4.0
4	D103	Oδ2	Cε2	3.1-3.7
5	I28	Cγ2	Cε1	3.4-4.0
6	I17	Cδ1	Cδ2	3.4-4.0
7	I113	Cδ1	Cδ1	3.4-4.0
8	M31	Sδ	Cδ1	3.5-3.8
9	M116	Cε	OH	3.1-3.8

Table S42. Y16 packing residues and closest atoms making van der Waals interactions with Y16 identified from KSI crystal structures. Van der Waals sum indicates the sum of the van der Waals radii and is represented as a range because of uncertainty introduced by the absence of hydrogen coordinates in the X-ray structural models and because the oxygen r_{vdw} is orientation-dependent (see **Table S48** for van der Waals radii values).

# distance	1	2	3	4	5	6	7	8	9
1	4.03	3.71	3.84	4.00	4.05	4.03	4.29	6.20	3.83
2	4.14	3.56	3.69	4.02	4.03	4.39	3.96	3.99	3.94
3	3.95	3.66	3.73	3.80	4.32	4.24	4.03	4.23	3.10
4	3.85	3.64	3.55	3.56	4.26	4.08	4.21	4.41	3.49
5	4.12	3.60	3.80	3.89	4.09	3.98	4.10	4.24	2.92
6	4.24	3.60	4.07	4.19	3.91	4.63	3.81	3.98	4.02
7	3.85	3.56	3.57	3.85	4.34	4.04	4.05	4.34	4.05
8	4.02	3.59	3.86	4.03	4.04	4.29	3.94	4.15	3.83
9	3.73	3.55	3.59	3.75	4.11	3.96	4.28	4.43	5.80
10	4.08	3.82	4.38	3.88	3.66	4.54	4.06	3.89	3.89
11	3.62	3.57	3.85	3.52	3.91	4.10	4.24	4.49	3.42
12	3.75	3.56	3.58	3.54	3.85	3.86	4.16	4.54	4.45
13	3.63	3.65	3.68	3.53	4.09	3.91	4.22	4.54	3.29
14	3.68	3.76	3.74	3.45	4.00	3.91	4.43	4.46	4.77
15	3.58	3.72	3.71	3.44	4.08	3.97	4.33	4.62	6.00
16	3.88	3.58	3.77	3.92	3.90	4.02	4.23	4.36	4.27
17	4.01	3.39	3.74	3.62	4.16	4.50	4.30	4.40	3.86
18	3.68	3.61	3.71	3.77	4.01	3.94	4.15	4.63	4.07
19	3.63	3.62	4.13	3.91	3.81	3.99	4.42	4.44	3.88
20	3.81	3.56	3.68	4.25	4.07	3.78	4.12	4.58	3.84
21	3.62	3.63	3.77	3.79	3.94	3.96	4.36	4.51	3.94
22	4.19	3.62	4.35	3.68	3.76	4.48	3.72	4.59	3.45
23	3.75	3.82	3.80	3.55	4.02	3.96	4.22	4.45	3.91
24	3.65	3.67	3.61	3.66	3.93	3.87	4.44	4.54	4.32
25	3.68	3.69	3.97	3.50	4.05	4.13	4.20	6.08	3.55
26	3.75	3.76	3.90	3.75	3.93	4.06	4.31	6.06	4.95
27	4.31	3.66	4.27	3.92	4.06	4.05	3.95	3.98	3.93
28	3.58	5.14	3.79	3.61	3.96	3.88	4.23	4.47	3.37
29	3.64	3.43	3.66	3.62	3.84	3.83	4.42	4.61	5.01
30	3.58	3.59	3.73	3.88	3.83	4.00	4.34	4.35	5.53
31	3.84	4.68	3.98	3.52	3.68	4.33	3.77	4.29	5.09
32	3.64	3.69	3.68	3.66	4.06	4.31	4.18	4.63	4.08
33	3.75	3.67	3.64	3.77	4.11	3.97	4.00	4.44	4.80
34	3.64	3.38	3.65	4.25	3.91	4.11	4.27	6.19	3.73
35	4.53	3.64	4.04	3.74	3.70	4.57	3.73	5.94	3.36
36	3.57	3.53	3.66	3.62	3.88	3.94	4.23	4.60	4.36
37	3.70	3.61	3.91	3.50	4.15	3.98	4.29	4.57	3.70
38	3.77	3.44	3.52	3.63	4.06	4.20	4.00	4.51	3.99
39	3.70	3.64	3.75	3.49	3.96	4.07	4.27	4.44	3.95
40	4.73	3.82	4.31	3.64	4.56	4.27	3.63	4.50	4.07
41	3.72	3.51	3.68	3.83	4.13	3.92	4.21	4.61	3.80
42	3.58	3.50	3.67	3.59	3.99	3.91	4.29	4.52	3.95
43	3.54	3.79	3.99	3.59	3.97	4.12	4.48	4.62	3.98
44	3.65	3.65	3.95	3.62	3.98	4.08	4.49	4.61	4.17
45	4.51	3.76	4.39	3.53	3.79	4.32	3.84	4.07	3.95
46	3.61	3.87	3.76	3.63	4.02	3.93	4.18	4.56	5.31
47	3.55	3.44	3.63	3.75	3.90	3.83	4.24	4.56	4.01

48	3.59	3.64	3.63	3.82	3.88	4.06	4.35	4.61	3.87
49	3.71	3.71	3.91	3.84	3.76	4.41	3.89	4.25	3.62
50	3.64	3.62	3.84	3.63	4.04	4.43	4.34	6.27	4.93
51	3.73	4.89	3.73	3.66	4.05	4.05	4.10	4.74	3.65
52	3.55	4.78	3.71	3.72	4.00	3.77	4.03	4.35	5.48
53	3.67	3.60	3.68	3.65	3.90	4.01	4.31	4.35	4.08
54	3.59	3.54	3.69	3.57	3.93	4.05	4.11	4.38	3.30
55	3.63	3.50	3.63	3.58	4.22	4.05	4.43	4.77	3.87
56	3.44	3.55	3.67	3.58	3.86	3.78	4.23	4.50	3.86
57	3.61	3.52	3.70	3.55	4.13	4.02	4.26	4.56	3.95
58	3.62	3.51	3.69	3.80	3.96	4.04	4.20	4.62	3.85
59	3.60	3.60	3.77	3.60	4.19	4.58	4.23	4.77	5.18
60	3.42	3.42	3.65	3.63	4.04	4.00	4.24	4.47	4.85
61	3.54	3.45	3.56	3.64	4.18	4.23	4.27	4.55	4.86
62	3.48	3.34	3.72	3.72	4.49	4.02	4.36	4.52	5.15
63	3.63	3.44	3.60	3.63	4.05	3.89	4.34	4.55	3.94
64	3.65	3.44	3.64	3.75	4.08	3.93	4.24	4.54	3.94
65	3.67	3.51	3.63	3.69	4.05	3.95	4.30	4.52	3.83
66	3.66	3.90	3.63	3.52	4.09	4.02	4.32	4.72	3.95
67	3.43	3.54	3.70	3.51	4.26	4.08	4.21	4.52	4.02
68	3.51	3.55	3.57	3.50	4.36	4.07	4.28	4.81	5.00
69	3.33	3.95	3.51	3.52	3.97	4.14	4.27	4.51	4.25
70	3.55	3.55	3.51	3.69	3.95	4.24	4.19	4.68	4.24
71	3.51	3.98	3.52	3.68	4.17	4.00	4.27	4.70	3.95
72	3.49	3.52	3.51	3.69	4.18	4.20	4.26	4.64	3.65
73	3.30	3.89	3.53	3.69	4.19	3.94	4.39	4.62	3.73
74	3.37	4.78	3.61	3.96	3.92	4.16	4.25	4.57	3.62
75	3.62	4.41	3.68	3.92	3.98	4.19	4.35	4.63	3.88
76	3.64	4.74	3.66	3.92	4.00	4.20	4.40	4.67	3.53
77	3.68	4.43	3.66	3.97	3.98	4.15	4.32	4.63	3.71
78	3.62	4.32	3.73		3.89	4.16	4.37	4.61	3.63
79	3.78	4.30	3.68		3.90	3.95	4.27	4.59	3.56
80	3.75	4.79	3.69		3.83	4.00	4.26	4.63	3.53
81	3.76	4.48	3.66		3.84	4.02	4.27	4.64	3.48
82	3.75	3.46	3.69		3.98	4.00	4.29	4.51	3.50
83	3.67	3.43	3.69		4.10	4.42	4.24	4.51	4.57
84	3.53	3.40	3.72		4.08	4.46	4.14	4.52	4.55
85	3.53	3.48	3.73		4.01	4.46	4.13	4.53	4.60
86	3.65	3.40	3.65			4.40	4.26		4.63
87		3.40							4.10
88		3.42							4.16
89		3.42							4.14
90		3.65							4.07
91		3.65							
92		3.63							
93		3.66							
94									

Table S43. Full pseudo-ensemble distances between Y16 atoms and packing residues closest atoms from **Table S42**. The number of distances varies depending on the packing group as a result of the presence of various mutations and, in some cases, alternative conformations for some residues.

	Packing residue	Packing atom	D103 atom	Van der Waals sum
1	D103	NH	Oδ1	2.95-3.25*
2	A118	Cβ	Oδ1	3.1-3.7
3	F86	Cε1	Oδ1	3.1-3.7
4	V101	Cγ1	Oδ1	3.1-3.7
5	Y16	Cε2	Oδ2	3.1-3.7
6	M84	Cε	Cβ	3.4-4.0
7	M84	Cε	Oδ2	3.1-3.7
8	M105	Cε	Oδ2	3.1-3.7
9	M116	Cε	Oδ2	3.1-3.7
10	M116	Sδ	Oδ2	3.2-3.5

* The r_{vdw} for N was used instead of NH.

Table S44. D103 packing residues and closest atoms making van der Waals interactions with D103 identified from KSI crystal structures. Van der Waals sum indicates the sum of the van der Waals radii and is represented as a range because of uncertainty introduced by the absence of hydrogen coordinates in the X-ray structural models and because the oxygen r_{vdw} is orientation-dependent (see **Table S48** for van der Waals radii values).

# distance	1	2	3	4	5	6	7	8	9	10
1	3.13	3.52	3.40	3.25	4.00	4.08	4.46	4.51	3.59	3.63
2	3.25	3.34	3.64	3.62	4.02	4.14	4.17	4.02	4.02	3.86
3	3.44	3.19	3.78	3.85	3.80	3.93	3.99	3.90	3.73	3.86
4	3.32	3.26	3.59	3.65	3.56	3.82	3.98	4.29	4.03	3.86
5	3.32	3.24	3.67	3.65	3.89	3.99	4.12	4.41	3.91	3.88
6	3.26	3.46	3.46	3.62	4.19	3.99	3.97	3.93	4.06	4.06
7	3.26	3.56	3.37	3.55	3.85	3.93	3.98	4.28	4.00	4.00
8	3.28	3.36	3.58	3.62	4.03	4.16	4.05	4.16	4.21	3.76
9	3.23	3.26	3.53	3.58	3.75	4.19	4.30	4.08	4.00	3.92
10	3.34	3.01	3.84	3.83	3.88	4.46	4.21	4.35	4.14	4.23
11	3.18	3.25	3.53	3.45	3.52	4.13	4.08	4.08	3.90	4.09
12	3.22	3.21	3.56	3.46	3.54	4.03	4.14	4.29	3.64	3.43
13	3.20	3.15	3.51	3.45	3.53	4.08	4.05	3.74	3.65	3.68
14	3.33	3.21	3.59	3.68	3.45	3.97	3.87	4.08	4.02	3.94
15	3.24	3.17	3.46	3.61	3.44	3.84	4.08	3.72	3.80	3.09
16	3.28	3.30	3.31	3.70	3.92	3.84	4.64	3.99	3.17	4.71
17	3.20	3.21	3.46	3.42	3.62	4.10	4.05	4.07	3.57	3.83
18	3.20	2.98	3.65	3.91	3.77	3.94	4.12	4.30	3.99	3.90
19	3.24	3.12	3.69	3.48	3.91	4.11	4.34	3.74	3.77	4.58
20	3.35	3.26	3.97	4.03	4.25	3.88	3.93	4.13	3.86	4.39
21	3.28	3.37	3.50	3.73	3.79	4.10	3.78	4.04	4.04	4.01
22	3.22	3.21	3.41	3.56	3.68	3.65	4.02	5.46	3.93	3.94
23	3.18	3.19	3.39	3.54	3.55	3.84	3.93	4.09	3.26	3.26
24	3.21	3.26	3.49	3.41	3.66	3.92	4.06	3.94	3.69	3.80
25	3.21	3.16	3.48	3.49	3.50	4.16	4.04	4.35	4.04	3.19
26	3.26	3.04	3.29	3.40	3.75	4.14	4.19	4.22	4.51	4.30
27	3.23	3.16	3.48	3.45	3.92	4.40	4.08	3.87	4.61	3.88
28	3.21	3.19	3.54	3.53	3.61	3.96	4.01	4.01	3.72	3.95
29	3.15	3.20	3.46	3.58	3.62	4.04	4.01	4.06	4.19	4.19
30	3.13	3.19	3.55	3.51	3.88	4.04	4.05	4.04	4.02	3.73
31	3.37	3.16	3.68	3.80	3.52	3.93	3.96	4.13	4.24	3.96
32	3.23	3.65	3.36	3.68	3.66	4.11	3.87	3.64	4.34	4.28
33	3.23	3.13	3.55	3.54	3.77	3.91	4.26	4.03	4.10	3.89
34	3.24	2.84	3.88	4.04	4.25	3.94	4.57	4.07	3.98	3.90
35	3.36	3.31	3.58	3.62	3.74	3.99	4.00	4.00	3.86	4.02
36	3.24	3.18	3.43	3.51	3.62	3.86	4.13	4.16	4.01	3.95
37	3.20	3.15	3.38	3.43	3.50	4.25	4.12	4.25	3.80	3.89
38	3.19	3.39	3.46	3.42	3.63	3.90	4.09	3.94	2.89	3.54
39	3.16	3.18	3.48	3.40	3.49	4.04	4.20	4.12	3.31	3.30
40	3.32	3.02	3.26	3.59	3.64	4.03	3.81	6.21	3.83	4.40
41	3.20	3.18	3.45	3.50	3.83	3.94	4.06	5.76	4.97	3.58
42	3.22	3.23	3.51	3.52	3.59	3.96	4.02	4.09	4.27	4.09
43	3.23	3.22	3.45	3.60	3.59	4.21	3.99	3.97	4.42	4.42
44	3.20	3.22	3.53	3.53	3.62	4.26	4.05	4.12	3.03	4.75
45	3.34	3.32	3.72	3.83	3.53	4.24	3.91	4.06	3.22	4.91
46	3.23	3.25	3.55	3.60	3.63	4.04	4.20	3.97	3.25	4.98
47	3.15	3.38	3.44	3.53	3.75	4.08	3.99	3.93	3.18	4.84

48	3.22	3.18	3.43	3.57	3.82	4.02	4.33	4.05	4.54	4.54
49	3.23	3.24	3.51	3.59	3.84	3.93	4.07	4.14	4.38	4.38
50	3.14	3.17	3.39	3.33	3.63	4.01	4.10	4.46	4.27	4.27
51	3.16	3.24	3.53	3.38	3.66	3.90	3.87	4.51	4.49	4.49
52	3.10	3.11	3.55	3.37	3.72	3.80	3.85	4.50	3.84	4.11
53	3.06	3.23	3.19	3.33	3.65	3.87	4.00	4.40	3.97	3.97
54	3.23	3.33	3.53	3.42	3.57	3.82	4.21	3.48	3.88	4.07
55	3.20	3.31	3.58	3.50	3.58	3.96	4.28	3.94	3.98	4.09
56	3.21	3.28	3.58	3.40	3.58	3.91	4.18	3.95	3.61	3.80
57	3.21	3.27	3.48	3.42	3.55	4.07	4.24	3.96	3.87	3.84
58	3.32	3.30	3.45	3.55	3.80	3.90	4.01	4.03	3.78	3.89
59	3.36	3.36	3.27	3.42	3.60	3.91	3.82	4.08	3.65	3.70
60	3.38	3.40	3.32	3.45	3.63	3.72	3.80	4.07	2.70	3.60
61	3.34	3.34	3.32	3.53	3.64	4.00	3.78	3.92	2.78	3.83
62	3.22	2.99	3.56	3.44	3.72	3.84	4.19	4.42	2.85	4.02
63	3.14	3.06	3.36	3.50	3.63	4.23	3.78	4.41	2.69	3.82
64	3.19	3.05	3.57	3.58	3.75	4.24	3.65	4.45	3.03	4.12
65	3.11	3.15	3.39	3.63	3.69	4.28	3.89	4.46	2.76	3.82
66	3.21	3.26	3.47	3.60	3.52	4.28	3.62	4.11	2.91	3.93
67	3.19	3.19	3.55	3.65	3.51	4.01	3.97	4.11	2.94	3.96
68	3.13	3.01	3.53	3.45	3.50	3.84	4.06	4.10	4.19	4.62
69	3.14	3.16	3.42	3.48	3.52	3.81	3.71	4.12	4.14	4.54
70	3.04	3.56	3.39	3.34	3.69	3.71	3.89	3.95	4.19	4.59
71	3.06	3.55	3.44	3.29	3.68	3.90	3.90	4.04	4.16	4.61
72	3.09	3.55	3.52	3.34	3.69	3.64	3.90	4.06	4.16	4.16
73	3.16	3.56	3.44	3.31	3.69	3.92	3.85	3.96	4.17	4.17
74	3.22	3.05	3.67	3.67	3.96	3.89	4.12		4.21	4.21
75	3.18	3.09	3.60	3.67	3.92	3.70	4.13		4.16	4.16
76	3.16	3.10	3.62	3.65	3.92	3.88	4.08		3.83	3.78
77	3.18	3.06	3.65	3.71	3.97	3.88	4.11		3.64	3.73
78	3.18	3.26	3.43	3.42		3.69	4.01		3.65	3.73
79	3.17	3.19	3.42	3.44		3.91	4.22		3.81	3.77
80	3.21	3.18	3.44	3.42		3.88	4.21			
81	3.17	3.50	3.44	3.43		3.93	4.01			
82						3.86				
83						3.85				
84						3.89				
85						3.86				
86						3.86				
87						4.15				
88						4.18				
89						4.08				
90						4.16				
91						4.06				
92						4.17				
93						4.18				
94						4.07				

Table S45. Full pseudo-ensemble distances between D103 atoms and packing residues closest atoms from **Table S44**. The number of distances varies depending on the packing group as a result of the presence of various mutations and, in some cases, alternative conformations for some residues.

	Packing residue	Packing atom	General base atom	Van der Waals range
1	F56	Cγ	Xδ2	3.1-3.7*
2	A118	Cβ	Xδ2	3.1-3.7*
3	V38	Cγ1	Cβ	3.4-4.0
4	M116	Cε	Xδ2	3.1-3.7*

* A r_{vdw} range of 1.4-1.7 Å was used for both O and NH_2 groups; The average N r_{vdw} is ~ 1.55 Å, close to the average O r_{vdw} of 1.5 Å. Xδ2 indicates either Nδ2 (asparagine) or Oδ2 (aspartate).

Table S46. General base packing residues and closest atoms making van der Waals interactions with general base identified from KSI crystal structures. Van der Waals sum indicates the sum of the van der Waals radii and is represented as a range because of uncertainty introduced by the absence of hydrogen coordinates in the X-ray structural models and because the oxygen r_{vdw} is orientation-dependent (see **Table S48** for van der Waals radii values).

# distances	1	2	3	4
1	3.93	3.48	4.06	3.92
2	3.67	3.67	3.95	4.01
3	4.01	3.30	3.90	4.48
4	3.81	3.37	3.91	4.20
5	3.80	3.53	4.03	5.03
6	3.75	3.39	3.96	4.04
7	3.54	3.68	4.05	5.14
8	4.31	3.06	4.12	3.65
9	3.71	3.51	3.98	3.84
10	4.08	3.04	4.00	3.42
11	3.46	3.94	4.00	4.22
12	3.19	3.64	3.75	3.87
13	3.44	3.62	3.77	6.85
14	3.38	3.52	3.75	7.80
15	3.49	3.55	3.70	3.89
16	3.72	3.45	3.87	4.59
17	3.71	3.60	4.24	5.65
18	3.49	3.67	3.94	3.96
19	3.77	4.05	4.03	4.29
20	3.24	4.24	3.90	3.73
21	3.21	3.48	3.90	3.94
22	3.57	3.41	4.19	3.89
23	4.08	3.82	3.81	3.85
24	3.12	3.88	3.82	4.01
25	3.55	3.24	4.13	3.74
26	4.04	3.66	3.98	3.76
27	3.57	3.90	3.95	6.49
28	4.17	3.69	3.74	6.17
29	3.55	5.35	3.96	6.28
30	3.60	3.46	3.90	3.96
31	3.53	3.58	3.90	4.46
32	3.41	3.57	3.77	4.04
33	4.31	3.71	3.66	3.97
34	3.74	3.69	4.14	4.39
35	3.63	4.28	3.81	2.83
36	3.50	3.76	4.14	4.00
37	4.14	4.33	3.87	4.33
38	4.80	3.73	4.02	4.05
39	3.58	3.70	4.08	3.75
40	3.27	3.71	3.69	3.95
41	3.63	3.99	3.89	3.69
42	3.35	3.75	3.80	3.70
43	3.84	3.56	3.93	3.66
44	3.18	3.62	3.88	4.07
45	3.60	3.90	4.24	3.90
46	3.74	3.77	3.70	6.52
47	3.80	5.46	4.04	3.66
48	4.32	3.42	3.83	5.92

49	3.45	3.65	3.86	6.53
50	3.52	3.56	3.90	3.82
51	3.56	3.82	3.68	4.39
52	3.63	3.70	4.05	3.67
53	4.14	3.44	3.81	2.85
54	3.53	3.67	4.14	3.66
55	3.53	3.61	4.01	3.82
56	3.67	3.66	3.95	3.73
57	3.95	3.55	4.03	3.65
58	3.64	3.56	3.93	3.59
59	3.41	3.81	4.00	4.17
60	3.21	3.76	3.92	4.09
61	3.15	3.65	3.96	3.92
62	3.15	3.58	3.80	3.94
63	3.17	3.81	3.81	4.08
64	3.34	3.77	3.68	4.14
65	3.23	3.88	3.84	4.09
66	3.35	3.81	3.77	7.02
67	3.34	3.70	3.70	6.81
68	3.48	3.72	3.91	6.71
69	3.64	3.59	3.88	6.55
70	3.19	3.61	3.89	6.94
71	3.58	3.79	4.03	6.45
72	3.27	3.75	4.11	6.41
73	3.57	3.86	4.04	6.95
74	3.67	3.71	3.93	4.14
75	3.21	3.85	4.07	4.04
76	3.53	3.62	4.00	4.13
77	3.61	3.45	4.01	4.07
78	3.61	3.89	4.03	3.98
79	3.57	3.74	4.00	3.81
80	3.67	3.69	3.91	4.09
81	3.66	3.70	3.98	3.95
82	3.73	3.72	3.99	4.10
83	3.67	3.41	3.96	3.95
84	3.45	3.42	3.95	4.00
85	3.33	3.34	3.98	4.06
86	4.69	3.42	3.98	
87	3.56	3.63	3.77	
88	3.49	3.40	3.86	
89	3.17	3.87	3.76	
90	3.16	3.59	3.80	
91	3.32	3.76	3.65	
92		3.74	3.73	
93		3.74	3.79	
94		3.73	3.63	

Table S47. Full pseudo-ensemble distances between general base D40 atoms and packing residues closest atoms from **Table S46**. The number of distances varies depending on the packing group as a result of the presence of various mutations and, in some cases, alternative conformations for some residues.

Atom/group	r_{vdw} (Å)	Reference
C	1.70	(51)
N	1.55	(51)
O	1.40-1.70	(51)
S	1.8	(51)
CH_3	2.0	(52)

Table S48. Van der Waals radii of elements and groups.

Structure	Y16 – Y57 hydrogen bond length (Å)
1C7H	2.47
1DMQ	2.73
1OPY	2.66
1W6Y	2.33
2INX	2.43
3CPO	2.54
3RGR	2.57
3SED	2.59
5D81	2.42
1OH0_A	2.51
1OH0_B	2.53
3VSY_A	2.59
3VSY_A	2.52
1CQS_A	2.7
1E3R_A	2.52
1E3V_A	2.67
1OGX_A	2.59
1VZZ_A	2.58
1W00_A	2.6
3FZW	2.43
3VGN_A	2.55
5D82_A	2.41
5D83_A	2.61
5KP3_A	2.43
5G2G_A	2.33
1CQS_B	2.42
1E3R_B	2.51
1E3V_B	2.71
1OGX_B	2.42
1VZZ_B	2.52
1W00_B	2.61
3FZW_B	2.4
3VGN_B	2.55
5D82_B	2.49
5D83_B	2.45
5KP3_B	2.31
5KP4_B	2.76
5G2G_B	2.43
3OWS_A	2.5
3OWS_B	2.55
3OWS_C	2.43
3OWS_D	2.45
3OWU_A	2.44
3OWU_B	2.49

3OWU_C	2.46
3OWU_D	2.53
2PZV_A	2.51
2PZV_B	2.53
2PZV_C	2.49
2PZV_D	2.5
3OWY_A	2.59
3OWY_B	2.54
3OWY_C	2.69
3OWY_D	2.65
3OWY_E	2.56
3OWY_F	2.62
3OWY_G	2.73
3OWY_H	2.6
3OX9_A	2.55
3OX9_B	2.57
3OX9_C	2.55
3OX9_D	2.56
3OXA_A	2.63
3OXA_B	2.61
3OXA_C	2.57
3OXA_D	2.59
5KP1_A	2.48
5KP1_B	2.47
5KP1_C	2.46
5KP1_D	2.46

Table S49. Lengths of the Y16 – Y57 hydrogen bond in all KSI crystal structures that contain intact Y16 and Y57 (n=70, **Table S1**). 5KP4 molecule B was not included, as in this molecule, Y16 and Y32 instead Y57 make a hydrogen bond.

Structure	D/N 40 Xδ1 – W120 Nε1 Hydrogen bond length (Å)
1C7H	2.56
1DMM	2.81
1DMN	2.92
1DMQ	2.94
1E97	2.68
1EA2	2.71
1GS3	2.68
1OHO	2.74
1OPY	2.89
1W02	2.83
1W6Y	2.64
2INX	2.86
3CPO	2.81
3RGR	2.81
3SED	2.84
4K1V	2.75
5AI1	2.84
5D81	2.84
1CQS_A	2.79
1E3R_A	2.75
1E3V_A	2.91
1K41_A	2.85
1OGX_A	2.82
1OH0_A	2.83
1VZZ_A	2.77
1W00_A	2.68
1W01_A	2.79
3FZW_A	2.80
3VGN_A	2.77
3VSY_A	2.84
4K1U_A	2.72
5D82_A	2.81
5D83_A	2.82
5KP3_A	2.76
5KP4_A	2.77
5G2G_A	2.93
1CQS_B	2.89
1E3R_B	2.82
1E3V_B	2.78
1K41_B	2.98
1OGX_B	2.77
1OH0_B	2.86
1VZZ_B	2.77
1W00_B	2.94
1W01_B	2.68
3FZW_B	2.86

3VGN_B	2.79
3VSY_B	2.90
4K1U_B	2.67
5D82_B	2.87
5D83_B	2.85
5KP3_B	2.85
5KP4_B	2.81
5G2G_B	2.85
3OWU_A	2.74
3OWU_B	2.72
3OWU_C	2.69
3OWU_D	2.78
3OWS_A	2.90
3OWS_B	2.80
3OWS_C	2.68
3OWS_D	2.89
2PZV_A	2.88
2PZV_B	2.82
2PZV_C	2.80
2PZV_D	2.84
3IPT_A	2.80
3IPT_B	2.80
3IPT_C	2.79
3IPT_D	2.68
3OWY_A	2.78
3OWY_B	2.64
3OWY_C	2.98
3OWY_D	2.67
3OWY_E	2.69
3OWY_F	2.64
3OWY_G	2.82
3OWY_H	2.68
3OX9_A	2.94
3OX9_B	2.97
3OX9_C	2.91
3OX9_D	2.94
3OXA_A	2.99
3OXA_B	3.00
3OXA_C	3.02
3OXA_D	3.02
3T8N_A	2.81
3T8N_B	2.84
3T8N_D	2.82
3T8N_F	2.81
5KP1_A	2.82
5KP1_A	2.91
5KP1_C	2.89
5KP1_D	2.81

Table S50. Lengths of the D/N40 – W120 hydrogen bond in all KSI crystal structures (n=94, **Table S1**).

Structure	Distance (Å)	
	M84 – Y16	M31 – Y16
1C7H	3.84	4.43
1DMQ	3.55	4.41
1OPY	3.58	4.43
1W6Y	3.85	4.49
2INX	3.58	4.54
3CPO	3.67	4.54
3RGR	3.74	4.46
3SED	3.71	4.62
5D81	3.71	4.63
1OH0_A	3.61	4.54
1OH0_B	3.67	4.52
3VSY_A	3.73	4.35
3VSY_B	3.63	4.61
1CQS_A	4.13	4.44
1E3R_A	3.68	4.58
1E3V_A	3.77	4.51
1OGX_A	3.80	4.45
1VZZ_A	3.97	4.41
1W00_A	3.90	4.34
3FZW_A	3.79	4.47
3VGN_A	3.66	4.61
5D82_A	3.68	4.63
5D83_A	3.64	4.44
5KP3_A	3.65	4.71
5G2G_A	3.66	4.60
1CQS_B	3.91	4.57
1E3R_B	3.52	4.51
1E3V_B	3.75	4.44
1OGX_B	3.68	4.61
1VZZ_B	3.99	4.62
1W00_B	3.95	4.61
3FZW_B	3.76	4.56
3VGN_B	3.63	4.56
5D82_B	3.84	4.24
5D83_B	3.73	4.69
5KP3_B	3.71	4.74
5KP4_B	3.68	4.35
5G2G_B	3.69	4.35
3OWS_A	3.63	4.38
3OWS_B	3.67	4.77
3OWS_C	3.70	4.50
3OWS_D	3.69	4.56
3OWU_A	3.77	4.62
3OWU_B	3.65	4.77
3OWU_C	3.55	4.47
3OWU_D	3.72	4.55

2PZV_A	3.60	4.51
2PZV_B	3.64	4.55
2PZV_C	3.63	4.54
2PZV_D	3.63	4.52
3OWY_A	3.70	4.72
3OWY_B	3.57	4.52
3OWY_C	3.51	4.81
3OWY_D	3.51	4.50
3OWY_E	3.52	4.68
3OWY_F	3.51	4.70
3OWY_G	3.53	4.64
3OWY_H	3.61	4.62
3OX9_A	3.68	4.57
3OX9_B	3.66	4.63
3OX9_C	3.66	4.67
3OX9_D	3.73	4.63
3OXA_A	3.68	4.61
3OXA_B	3.69	4.59
3OXA_C	3.66	4.63
3OXA_D	3.69	4.64
5KP1_A	3.68	4.51
5KP1_B	3.72	4.51
5KP1_C	3.73	4.52
5KP1_D	3.65	4.53
Mean	3.69	4.55

Table S51. Y16 Cδ2 – M84 Cε and Y16 Cδ1 – M31 Sδ distances in all KSI crystal structures with intact Y16-Y57 hydrogen bond (n=70, see **Table S1 and S2**).

Structure	Distance (Å)	
	M84 – Y16	M31 – Y16
1DMM	3.69	3.99
1DMN	3.73	4.23
1E97	3.80	4.24
1EA2	4.07	3.98
1GS3	3.57	4.34
1OHO	3.86	4.15
1W02	4.38	3.89
4KIV	3.77	4.36
5AI1	3.74	4.40
1K41_A	4.35	4.59
1W01_A	4.27	3.98
4K1U_A	3.98	4.29
1K41_B	4.31	4.50
1W01_B	4.39	4.07
4K1U_B	3.91	4.25
Mean	3.99	4.22

Table S52. Y16 Cδ2 – M84 Cε and Y16 Cδ1 – M31 Sδ distances in all KSI crystal structures in which the Y16-Y57 hydrogen bond has been ablated (i.e. crystal structures with Y16F and Y57X mutations, in which X is any residue (n=15, see **Table S1 and S2**).

Structure	Side chain χ1 angle (°)									
	D21	D24	D34	D35	D40	N79	D100	D103	D108	N124
1E97	-171.07	-160.35	74.26	58.44	-169.88	67.72	-68.74	-93.21	68.12	-56.11
1EA2	-175.87	-163.34	71.30	60.17	-164.16	66.61	-64.25	-87.88	63.33	-58.86
1OHO	-175.17	-164.57	63.22	58.08	-155.61	63.44	-62.30	-84.39	66.07	-59.84
1OPY	-174.66	-164.75	67.48	62.03	-172.13	66.06	-64.05	-87.95	64.79	-59.48
2INX	-174.86	-164.45	62.74	64.23	-175.99	70.89	-62.19	-78.58	63.46	-64.24
3CPO	-176.99	-165.41	64.60	60.38	-175.15	66.23	-65.98	-79.28	64.37	-65.17
3RGR	-173.70	-165.41	64.60	60.38	-173.51	70.80	-63.05	-82.54	68.09	-64.01
3SED	-177.11	-167.98	63.13	63.48	-178.03	73.17	-66.08	-86.14	67.90	-63.85
4K1V	-176.03	-165.01	62.59	58.71	-173.04	67.58	-69.17	-87.67	63.46	-57.32
5D81	-175.46	-165.47	62.71	66.37	-175.61	69.32	-63.48	-81.35	65.77	-62.99
1OH0_A	-175.11	-163.84	67.70	67.21	178.81	68.69	-63.13	-83.82	64.58	-60.38
1OH0_B	-175.11	-163.84	67.70	67.21	178.81	68.69	-63.13	-83.82	64.58	-60.38
3VSY_A	-176.65	-165.77	-69.90	55.08	-173.80	72.19	-65.03	-79.25	68.53	-60.87
3VSY_B	-176.16	-168.88	59.33	62.11	-174.21	70.43	-64.03	-77.23	69.72	-62.06
1E3V_A	-174.48	-167.10	66.02	61.67	-170.46	71.34	-61.53	-85.93	62.51	-57.05
1OGX_A	-168.62	-167.92	62.35	62.31	-176.81	66.49	-65.66	-82.48	61.73	-58.48
3FZW_A	-174.86	-170.30	63.69	56.97	-177.17	67.03	-62.27	-79.56	68.41	-60.26
3VGN_A	-178.84	-162.20	62.67	57.77	176.43	68.73	-65.47	-77.56	65.07	-64.82
4K1U_A	-174.57	-167.14	116.05	57.60	-177.16	64.54	-66.19	-86.95	62.93	-57.52
5D82_A	-175.45	-168.29	62.09	64.09	-175.57	68.55	-64.75	-80.74	64.79	-62.91
5D83_A	-168.86	-165.75	53.93	62.78	-171.10	63.03	-64.35	-83.76	62.15	-63.95
5KP3_A	176.68	-163.74	60.41	61.78	-173.24	66.83	-64.69	-80.01	66.37	-61.16
5G2G_A	179.67	-167.29	62.68	61.01	177.35	65.70	-64.33	-88.33	64.15	-61.55
1E3V_B	-175.67	-164.13	-83.58	61.60	-171.84	75.79	-65.42	-84.79	65.40	-60.27
1OGX_B	-175.67	-164.13	-83.58	61.60	-171.84	75.79	-65.42	-84.79	65.40	-60.27
3FZW_B	-172.99	-165.80	-83.58	71.16	-174.90	68.34	-66.99	-81.14	66.86	-63.12
3VGN_B	-178.22	-167.63	60.72	64.78	177.78	71.74	-65.27	-76.77	65.28	-65.56
4K1U_B	-174.79	-162.99	-76.62	50.39	-174.54	66.89	-58.83	-79.15	56.34	-60.55
5D82_B	-172.94	-161.87	-66.63	66.57	-172.66	68.24	-63.43	-83.99	65.17	-60.64
5D83_B	-176.75	-170.43	64.55	56.53	-171.97	68.59	-59.37	-83.38	62.82	-61.27
5KP3_B	176.00	-167.54	43.30	66.11	-172.65	62.35	-65.92	-87.78	59.79	-63.21
5KP4_B	-171.60	-165.72	-56.37	57.47	-174.17	60.32	-66.13	-82.65	57.69	-61.44
5G2G_B	-174.20	-165.43	-73.41	40.27	177.17	65.10	-63.36	-86.54	67.33	-64.87
3OWS_A	-168.11	-163.97	22.95	54.68	-177.42	84.59	-60.86	-85.77	69.53	-57.00
3OWS_B	179.44	-162.58	35.48	62.51	-176.69	83.02	-59.34	-79.84	67.14	-58.09
3OWS_C	-173.40	-164.92	40.53	52.35	-175.04	73.73	-63.00	-85.76	65.43	-64.83
3OWS_D	-173.36	-166.94	25.51	55.79	-178.82	79.97	-59.50	-87.27	67.42	-64.52
2PZV_A	-177.68	-168.20	61.60	64.27	-174.67	67.98	-66.63	-82.50	74.32	-62.02
2PZV_B	-174.82	-169.22	63.26	61.58	-173.80	70.58	-66.10	-82.83	66.98	-63.12
2PZV_C	-177.37	-167.37	59.08	63.20	-178.41	63.26	-66.67	-78.40	70.69	-64.18
2PZV_D	-178.52	-169.64	60.73	62.26	-172.54	66.15	-61.97	-80.71	67.37	-66.15
3IPT_A	177.06	-178.32	60.71	60.91	-178.63	62.34	-65.40	-83.23	60.25	-62.99
3IPT_B	-175.62	-174.14	61.03	59.06	178.25	63.02	-67.70	-88.35	59.76	-57.27
3IPT_C	-177.74	-171.01	61.28	57.06	-170.16	65.37	-62.06	-84.40	64.42	-61.61
3IPT_D	-176.46	-175.11	60.35	59.35	-172.47	60.00	-56.31	-90.61	60.77	-58.71
3OXA_A	-171.92	-167.32	44.46	64.09	-170.32	80.60	-64.49	-87.07	66.56	-60.02
3OXA_B	-171.17	-167.64	44.69	63.60	-171.30	80.50	-61.97	-84.84	67.33	-59.17
3OXA_C	-172.20	-167.51	44.07	62.32	-172.12	80.43	-62.07	-84.78	66.79	-60.51
3OXA_D	-170.61	-168.96	43.57	63.37	-171.15	79.11	-63.58	-85.88	68.47	-59.25
5KP1_A	-173.20	-170.56	66.80	61.42	-173.89	69.24	-64.10	-76.09	71.97	-58.82
5KP1_B	-171.72	-166.80	66.80	68.26	-172.69	68.44	-63.57	-76.01	66.42	-63.31
5KP1_C	-171.73	-165.94	66.80	69.49	-173.62	66.00	-65.05	-74.93	65.57	-62.16
5KP1_D	-173.35	-169.47	68.31	62.38	-173.79	68.82	-61.58	-76.83	71.38	-59.43

Table S53. Side chain χ1 dihedral angles for all aspartate and asparagine residues in KSI from the reduced pseudo-ensemble. Asparagine residues at position 2 and position 93 have been excluded from the analysis, because these residues are situated in the highly flexible N-terminus of the protein and the 91-96 loop, respectively.

Structure	Side chain χ1 angle (°)							
	Y16	Y32	F42	F56	Y57	F86	F107	Y119
1OPY	170.46	-76.03	177.96	164.93	-78.58	66.91	-65.80	-67.48
2INX	170.59	-77.61	-172.79	172.35	-78.19	63.32	-68.42	-70.77
3CPO	169.66	-79.43	-175.94	174.96	-78.21	61.84	-68.12	-73.40
3RGR	168.38	-77.54	-175.33	171.22	-73.99	57.90	-67.40	-71.06
3SED	169.33	-76.54	-178.03	176.45	-77.83	63.90	-70.43	-74.11
5D81	168.81	-80.65	-171.25	179.82	-77.83	60.51	-68.86	-68.90
1OH0_A	165.56	-78.96	-178.52	-179.44	-80.43	62.59	-68.74	-74.03
1OH0_B	165.56	-78.96	-178.52	-179.44	-80.43	62.59	-68.74	-74.03
3VSY_A	171.44	-79.73	-173.63	167.92	-76.91	58.74	-70.79	-71.29
3VSY_B	171.44	-81.29	-172.57	170.33	-77.28	61.48	-71.10	-67.73
1E3V_A	169.50	-78.01	-172.43	169.03	-77.21	61.70	-64.57	-70.17
1OGX_A	167.16	-75.87	-176.29	175.44	-67.06	64.39	-66.51	-68.47
3FZW_A	168.05	-82.40	-175.78	175.30	-74.50	58.45	-66.79	-77.47
3VGN_A	166.98	-79.76	-174.61	162.71	-75.71	60.39	-69.68	-74.32
5D82_A	171.10	-81.24	-171.07	174.00	-81.76	62.58	-67.90	-67.60
5D83_A	169.87	-85.81	-170.19	171.97	-78.93	60.59	-71.23	-68.74
5KP3_A	164.43	-83.31	-171.69	179.06	-85.64	60.86	-69.03	-67.85
5G2G_A	164.86	-80.46	-174.00	176.11	-79.25	62.77	-68.33	-72.22
1E3V_B	168.49	-77.56	-176.53	169.41	-75.66	62.65	-62.98	-67.93
1OGX_B	168.49	-77.56	-176.53	169.41	-75.66	62.65	-62.98	-67.93
3FZW_B	167.00	-79.08	-173.10	178.34	-74.20	58.74	-66.58	-72.10
3VGN_B	167.36	-77.10	-175.20	164.89	-74.07	58.17	-71.34	-75.93
5D82_B	172.63	-79.60	-174.23	171.21	-82.27	61.10	-67.34	-71.58
5D83_B	166.27	-90.05	-174.22	176.60	-80.48	61.59	-68.74	-68.83
5KP3_B	166.01	-80.05	-172.54	178.50	-83.11	61.21	-69.81	-71.73
5KP4_B	167.41	-75.54	-169.70	169.93	-77.70	60.35	-66.68	-72.31
5G2G_B	170.83	-78.43	-167.68	171.79	-78.76	58.98	-66.03	-72.78
3OWS_A	164.40	-84.79	-174.59	168.34	-79.14	60.92	-68.10	-66.76
3OWS_B	164.39	-83.04	178.64	165.19	-80.10	62.57	-65.45	-69.10
3OWS_C	168.01	-80.78	179.77	169.66	-80.39	59.81	-67.94	-73.61
3OWS_D	166.91	-85.77	-179.50	167.76	-80.86	61.59	-71.71	-74.66
2PZV_A	173.73	-73.12	-175.54	174.28	-77.53	58.01	-66.34	-64.18
2PZV_B	172.17	-77.10	-174.88	167.98	-81.25	59.04	-70.18	-69.43
2PZV_C	171.08	-75.39	-173.36	173.42	-77.83	61.09	-66.25	-70.21
2PZV_D	174.47	-76.64	-170.00	172.49	-78.49	63.39	-69.91	-68.21
3OXA_A	170.71	-83.52	178.90	173.25	-79.99	62.06	-64.25	-64.98
3OXA_B	171.42	-82.65	179.49	172.94	-79.08	61.91	-64.06	-68.17
3OXA_C	170.67	-82.41	178.78	171.74	-79.09	62.70	-64.23	-66.43
3OXA_D	167.93	-82.38	179.27	171.78	-80.75	60.59	-63.48	-66.44
5KP1_A	169.14	-78.28	-175.00	-175.07	-76.05	60.92	-67.74	-79.93
5KP1_B	167.79	-79.35	-168.98	170.79	-70.80	62.37	-68.22	-69.06
5KP1_C	167.82	-78.85	-167.59	171.69	-72.29	61.33	-68.14	-69.34
5KP1_D	168.37	-78.74	-175.84	178.53	-76.42	62.40	-67.70	-78.31

Table S54. Side chain χ1 dihedral angles for all tyrosine and phenylalanine residues in KSI from the reduced pseudo-ensemble. χ1 angles for position 16 include Tyrosine residues only (phenylalanine substitutions have been omitted).

	Angle OH(X) – TSA ring plane (°)		Transformed angle	
Structure	X=Y16	X=D103	180° - angle (Y16–TSA)	Angle (D103–TSA)*(-1)
1GS3	145.4	-21	34.6	21
1W6Y	149.2	-48	30.8	48
3CPO	163.7	-52.4	16.3	52.4
5AI1	149.4	4.3	30.6	-4.3
1OGX_A	151.3	-55.4	28.7	55.4
1OGX_B	153.8	-35.2	26.2	35.2
1OH0_A	143.1	-42.6	36.9	42.6
1OH0_B	150	-36.5	30	36.5
3FZW_A	154.8	-45.8	25.2	45.8
3FZW_B	156.2	-33.1	23.8	33.1
3OWS_A	155.5	-32	24.5	32
3OWS_B	146.9	-26.6	33.1	26.6
3OWS_C	151.7	-27.9	28.3	27.9
3OWS_D	149.2	-17.6	30.8	17.6
3OWU_A	149.4	-20.9	30.6	20.9
3OWU_B	146.7	-34.1	33.3	34.1
3OWU_C	154.9	-31.7	25.1	31.7
3OWU_D	148.6	-31.2	31.4	31.2
3VGN_A	135.4	-34.4	44.6	34.4
3VGN_B	140	-34.7	40	34.7
5KP3_A	144.2	-33.8	35.8	33.8
5KP3_B	139.1	-25.9	40.9	25.9
2PZV_A	162.4	-51.8	17.6	51.8
2PZV_B	167.4	-47	12.6	47
2PZV_C	166.9	-47.7	13.1	47.7
2PZV_D	168.6	-38	11.4	38
3OWY_A	153.3	-31.3	26.7	31.3
3OWY_B	160	-13	20	13
3OWY_C	146.9	-54.1	33.1	54.1
3OWY_D	160.6	-34.7	19.4	34.7
3OWY_E	147.2	-42.8	32.8	42.8
3OWY_H	140.3	-69.8	39.7	69.8
5PK1_A	160	-48.7	20	48.7
5PK1_B	161.4	-44.9	18.6	44.9
5PK1_C	161.5	-44	18.5	44
5PK1_D	161.2	-48.9	18.8	48.9

Table S55. Angles between the hydrogen bond donors Y16 and D103 and the plane of the A ring of transition state analogs bound to KSI (see Tables S1 and S2). Dihedral angle is measured between Y16 or D103 OH atom and Ox, C1, C2 atoms of the bound transition state analog (OH – Ox – C1 – C2, two columns on the left). In the two columns on the right the values have been transformed mathematically for clarity of presentation.

Structure	Residue at position 40 (X)	Distance D40 – TSA (Å)			Bound Ligand
		Xδ2 - C2	Xδ2 - C4	Xδ2 - C10	
1GS3	N	3.23	3.92	3.19	Equ
1W6Y	D	3.29	4.21	3.06	Equ
3CPO	N	3.18	4.1	-	Phe
5AI1	N	3.09	4.02	3.33	Equ
1OGX_A	N	3.08	4.17	3.31	Equ
1OH0_A	D	3.47	4.51	3.52	Equ
3FZW_A	N	3.28	4.34	3.68	Equ
3VGN_A	N	5.21	4.86	-	Phe
5KP3_A	N	3.24	4.37	3.65	Equ
1OGX_B	N	3.42	4.24	3.57	Equ
1OH0_B	D	3.31	4.37	3.67	Equ
3FZW_B	N	3.33	4.35	3.86	Equ
3VGN_B	N	5.58	5.27	-	Phe
5KP3_B	N	3.21	4.16	3.47	Equ
3OWS_A	N	3.19	4.12	3.65	Equ
3OWS_B	N	3.36	4.2	3.49	Equ
3OWS_C	N	3.15	3.98	3.3	Equ
3OWS_D	N	3.26	4.03	3.5	Equ
3OWU_A	N	3.45	3.96	3.8	Equ
3OWU_B	N	3.35	4	3.53	Equ
3OWU_C	N	3.35	4.01	3.8	Equ
3OWU_D	N	3.14	4.03	3.66	Equ
2PZV_A	N	3.18	4.27	-	Phe
2PZV_B	N	3.13	3.48	-	Phe
2PZV_C	N	3.25	4.17	-	Phe
2PZV_D	N	3.18	3.89	-	Phe
3OWY_A	N	3.19	3.89	3.27	Equ
3OWY_B	N	3.47	3.78	3.77	Equ
3OWY_C	N	3.34	4.19	3.42	Equ
3OWY_D	N	3.21	3.77	3.39	Equ
3OWY_E	N	3.52	3.89	3.23	Equ
3OWY_H	N	3.08	4.04	3.23	Equ
5KP1_A	N	3.24	4.31	3.52	Equ
5KP1_B	N	3.17	4.36	3.85	Equ
5KP1_C	N	3.19	4.35	3.85	Equ
5KP1_D	N	3.22	4.28	3.53	Equ

Table S56. Distances between the Xδ2 (Oδ2 and Nδ2 for aspartate and asparagine at position 40, respectively) and the carbon positions between which protons are shuffled in KSI reactions from KSI crystal with WT-like activity (see Table S1 and S2).

Structure	Angle (°)		
	Oδ1-Nε1-Cζ2	O/Nδ2-Oδ1-Nε1-Cζ2	O/ND2-OD1-Nε1
1C7H	97.0	130.7	121.7
1DMM	93.1	133.4	127.98
1DMN	97.1	148.4	130.71
1DMQ	99.0	145.8	130.8
1E 97	99.2	131.1	125.26
1EA2	93.5	140.9	125.55
1GS3	93.9	131.6	134.05
1OHO	89.5	156.7	119.08
1OPY	94.3	137.6	128.51
1W02	79.9	156.7	114.76
1W6Y	91.9	99.5	127.11
2INX	93.3	133.6	129.42
3CPO	95.9	133.5	132.51
3RGR	93.8	144.7	134.02
3SED	97.0	135.2	130.69
4K1V	94.9	135.1	130.2
5AI1	94.4	135.0	129.93
5D81	96.2	128.9	133.05
1CQS_A	86.8	108.8	137.41
1E3R_A	101.2	79.6	135.32
1E3V_A	94.7	134.8	127.23
1K41_A	77.8	144.0	103.11
1OGX_A	89.2	123.6	133.45
1OH0_A	98.3	118.4	137.17
1VZZ_A	89.9	145.1	122.16
1W00_A	97.3	124.4	131.8
1W01_A	98.1	105.4	139.96
3FZW_A	98.6	124.3	133.79
3VGN_A	100.2	13.2	121.01
3VSY_A	97.1	132.2	132.2
4K1U_A	89.3	135.8	127.79
5D82_A	94.5	134.9	131.17
5D83_A	98.8	125.7	134.37
5KP3_A	96.9	120.7	133.2
5KP4_A	99.4	99.7	148.16
5G2G_A	98.6	130.1	138.33
1CQS_B	95.4	97.2	143.14
1E3R_B	104.0	102.3	132.76
1E3V_B	91.6	125.2	124.95
1K41_B	90.4	137.0	136.41
1OGX_B	95.4	109.3	138.99
1OH0_B	97.4	121.5	136.22
1VZZ_B	92.9	132.1	134.42
1W00_B	90.2	135.8	127.77
1W01_B	89.7	123.9	127.11
3FZW_B	100.4	119.1	136.46
3VGN_B	99.1	3.3	113.37

3VSY_B	91.6	138.3	129.75
4K1U_B	87.4	138.5	127.86
5D82_B	98.2	132.4	133.38
5D83_B	95.7	124.1	137.34
5KP3_B	89.8	124.8	128.14
5KP4_B	91.5	136.9	125.38
5G2G_B	97.1	129.6	134.73
3OWS_A	89.0	131.4	125.93
3OWS_B	94.1	124.3	129.02
3OWS_C	92.8	128.8	129.5
3OWS_D	95.4	137.2	124.4
3OWU_A	90.8	129.3	135.38
3OWU_B	88.6	122.6	134.31
3OWU_C	94.1	127.9	134.83
3OWU_D	90.5	128.3	129.63
2PZV_A	94.6	131.3	137.25
2PZV_B	96.0	128.3	133.94
2PZV_C	95.2	124.4	136.87
2PZV_D	96.9	124.7	135.56
3IPT_A	98.9	117.5	140.06
3IPT_B	95.4	123.8	135.88
3IPT_C	95.1	126.1	131.62
3IPT_D	93.1	133.6	135.52
3OWY_A	85.6	123.5	116.96
3OWY_B	82.1	129.2	113.16
3OWY_C	84.6	124.4	115.63
3OWY_D	86.5	127.3	117.32
3OWY_E	88.9	118.3	123.75
3OWY_F	87.8	119.8	118.27
3OWY_G	87.6	131.1	116.78
3OWY_H	86.7	119.0	124.97
3OX9_A	95.4	119.7	128.44
3OX9_B	97.2	120.4	130.38
3OX9_C	97.3	119.1	130.47
3OX9_D	96.1	122.2	129.33
3OXA_A	94.8	139.1	130.44
3OXA_B	95.4	138.9	131.4
3OXA_C	93.6	142.8	126.57
3OXA_D	93.9	142.1	129.15
3T8N_A	105.8	123.3	141.52
3T8N_B	105.0	121.9	135.48
3T8N_C	100.4	112.5	139.09
3T8N_D	102.1	120.4	136.46
5KP1_A	100.4	112.1	135.16
5KP1_B	100.3	121.8	136.68
5KP1_C	100.9	120.3	137.55
5KP1_D	99.8	114.7	135.06

Table S57. Angles characterizing the general base and W120 relative sidechain orientations obtained from the full pseudo-ensemble (see Table S1 and S2).

Enzyme	k_{cat} s^{-1}	K_M µM	k_{cat} rel	K_M rel	[E] nM
KSI WT	9.7[a]	29	(1)	(1)	-
KSI W120F	33.6	168.1	3.5	5.8	15
	34.8	174.7	3.6	6.0	40
KSI W120F Average	34.2 ± 0.6	171.4 ± 3.3	3.5	5.9	
$KSI_{homolog}$ WT	37[a]	28	(1)	(1)	-
$KSI_{homolog}$ F120W	4.9	20.4	0.13	0.7	40
	4.5	20.2	0.12	0.7	80
$KSI_{homolog}$ F120W Average	4.7 ± 0.2	20.3 ± 0.1	0.13	0.7	

[a] from (16)

Table S58. Michaelis-Menten kinetic parameters for KSI WT and W120F variant and $KSI_{homolog}$ WT and F120W obtained in this study. Kinetics have been measured with the substrate 5(10)-Estrene-3,17-dione as the chemical step for this substrate is rate limiting. Note that W120F mutation in KSI results in an enzyme which is more efficient than the natural (WT) variant.

Enzyme	k_{cat} (s^{-1})	K_M (μM)	K_M^{rel}	Reference
WT	9.9 ± 0.9	19 ± 4	(1)	(53)
Y16A	4.8 ± 0.4 x 10^{-2}	30 ± 10	1.6 ± 0.6	(53)
Y16G	4.0 ± 0.4 x 10^{-2}	23 ± 2	1.2 ± 0.3	(53)
Y16S	3.8 ± 0.5 x 10^{-2}	18 ± 6	0.95 ± 0.4	(53)
Y16T	5.2 ± 0.3 x 10^{-2}	19 ± 3	1 ± 0.3	(53)
Y16F	5.4 ± 0.1 x 10^{-4}	41 ± 6	2.15 ± 0.6	(53)
WT	9.9 ± 0.9	30 ± 4	1 ± 0.2	(16)
D103L	5.9 ± 0.1 x 10^{-2}	39 ± 5	1.3 ± 0.2	(16)
D103A	6.6 ± 0.2 x 10^{-2}	52 ± 4	1.7 ± 0.3	(16)
D103G	3.1 ± 0.3 x 10^{-1}	51 ± 13	1.7 ± 0.5	(16)
Y16F/D103L	8.0 ± 2.0 x 10^{-6}	25 ± 4	0.8 ± 0.2	(16)
Y16A/D103A	1.1 ± 0.1 x 10^{-4}	32 ± 1	1.1 ± 0.2	(16)
Y16G/D103G	1.3 ± 1.2 x 10^{-3}	36 ± 8	1.2 ± 0.3	(16)
D103N	7.8 ± 0.1 x 10^{-1}	-	-	(19)

Table S59. Effects of various KSI oxyanion hole mutations on K_M for the substrate 10-EST.

KSI W120F	$KSI_{homolog}$ F120W
TTTTGTTTAACTTTAAGAAGGAGATATACAT ATGAACCTACCGACTGCGCAGGAAGTCCA GGGCCTGATGGCCCGTTACATCGAGCTGG TCGATGTCGGGGATATCGAGGCGATCGTG CAGATGTACGCCGATGACGCCACGGTCGA AGACCCGTTTGGCCAGCCGCCGATCCACG GCCGCGAGCAGATTGCCGCGTTCTATCGC CAGGGTTTGGGCGGAGGCAAGGTCCGCGC CTGCCTGACCGGGCCGGTACGGGCCAGCC ATAACGGCTGCGGGGCGATGCCGTTTCGC GTCGAGATGGTCTGGAACGGCCAGCCCTG TGCACTGGATGTCATCGATGTGATGCGCTT TGATGAGCACGGCCGGATCCAGACGATGC AAGCCTACTTTAGCGAGGTCAACCTCAGCG TGCGCGAGCCGCAGTAGTGAAAGCTTGCG GCCGCACTCGAGCACCACCACCACCACCA CTGAGATCCGGCTGCTAACAAAGCCCGAAA GGAAGCTGAGTTGGCTGCTGCCACCGCTG AGCAATAACTAGCATAACCCCTTGGGGCCT CTAAACGGGTCTTGAGGGGTTTTTTGCTGA AAGGAGGAACTATATCCGGATTGGCGAATG GGACGCGCCCTGTAGCGGCGCATTAAGCG CGGCGGGTGTGGTGGTTACGCGCAGCGTG ACCGCTACACTTGCCAGCGCCCTAGCGCC CGCTCCTTTCGCTTTCTTCCCTTCCTTTCTC GCCACGTTCGCCGGCTTTCCCCGTCAAGC TCTAA	TTTTGTTTAACTTTAAGAAGGAGATATACAT ATGAATACCCCAGAACACATGACCGCCGTG GTACAGCGCTATGTGGCTGCGCTCAATGC CGGCGATCTGGACGGCATCGTCGCGCTGT TTGCCGATGACGCCACGGTGGAAGACCCC GTGGGTTCCGAGCCCAGGTCCGGTACGGC TGCGATTCGTGAGTTTTACGCCAACTCGCT CAAACTGCCTTTGGCGGTGGAGCTGACGC AGGAGGTACGCGCGGTCGCCAACGAAGCG GCCTTCGCTTTCACCGTCAGCTTCGAGTAT CAGGGCCGCAAGACCGTGGTTGCGCCCAT CGATCACTTTCGCTTCAATGGCGCCGGCAA GGTGGTGAGCATGCGCGCCTTGTGGGGCG AGAAGAATATTCACGCTGGCGCCTGAAGCT TGCGGCCGCACTCGAGCACCACCACCACC ACCACTGAGATCCGGCTGCTAACAAAGCCC GAAAGGAAGCTGAGTTGGCTGCTGCCACC GCTGAGCAATAACTAGCATAACCCCTTGGG GCCTCTAAACGGGTCTTGAGGGGTTTTTTG CTGAAAGGAGGAACTATATCCGGATTGGCG AATGGGACGCGCCCTGTAGCGGCGCATTA AGCGCGGCGGGTGTGGTGGTTACGCGCAG CGTGACCGCTACACTTGCCAGCGCCCTAG CGCCCGCTCCTTTCGCTTTCTTCCCTTCCT TTCTCGCCACGTTCGCCGGCTTTCCCCGTC AAGCTCTAAATCGGGGGCTCCCTTTAGGGT TCCGA

Table S60. DNA sequencing results for KSI W120F and $KSI_{homolog}$ F120W (KSI numbering) mutants.

References

1. P. V. Burra, Y. Zhang, A. Godzik, B. Stec, Global distribution of conformational states derived from redundant models in the PDB points to non-uniqueness of the protein structure. *Proc. Natl. Acad. Sci.* **106**, 10505–10510 (2009).

2. R. B. Best, K. Lindorff-Larsen, M. A. DePristo, M. Vendruscolo, Relation between native ensembles and experimental structures of proteins. *Proc. Natl. Acad. Sci.* **103**, 10901–10906 (2006).

3. J. E. Kohn, P. V. Afonine, J. Z. Ruscio, P. D. Adams, T. Head-Gordon, Evidence of Functional Protein Dynamics from X-Ray Crystallographic Ensembles. *PLoS Comput. Biol.* **6**, e1000911 (2010).

4. V. Zoete, O. Michielin, M. Karplus, Relation between sequence and structure of HIV-1 protease inhibitor complexes: a model system for the analysis of protein flexibility11Edited by R. Huber. *J. Mol. Biol.* **315**, 21–52 (2002).

5. R. Elber, M. Karplus, Multiple conformational states of proteins: a molecular dynamics analysis of myoglobin. *Science* **235**, 318–321 (1987).

6. Zhang, Protein Flexibility and Adaptability Seen in 25 Crystal Forms of T4 Lysozyme. 26.

7. H. Frauenfelder, *et al.*, Thermal expansion of a protein. *Biochemistry* **26**, 254–261 (1987).

8. D. A. Keedy, *et al.*, Mapping the conformational landscape of a dynamic enzyme by multitemperature and XFEL crystallography. *eLife* **4**, e07574 (2015).

9. B. Halle, Biomolecular cryocrystallography: Structural changes during flash-cooling. *Proc. Natl. Acad. Sci.* **101**, 4793–4798 (2004).

10. J. S. Fraser, *et al.*, Hidden alternative structures of proline isomerase essential for catalysis. *Nature* **462**, 669–673 (2009).

11. D. H. Juers, B. W. Matthews, Reversible lattice repacking illustrates the temperature dependence of macromolecular interactions. *J. Mol. Biol.* **311**, 851–862 (2001).

12. T. Sandalova, G. Schneider, H. Käck, Y. Lindqvist, Structure of dethiobiotin synthetase at 0.97 Å resolution. *Acta Crystallogr. D Biol. Crystallogr.* **55**, 610–624 (1999).

13. E. Lolis, G. A. Petsko, Transition-state analogues in protein crystallography: probes of the structural source of enzyme catalysis. *Annu. Rev. Biochem.* **59**, 597–630 (1990).

14. R. Wolfenden, Transition State Analog Inhibitors and Enzyme Catalysis. *Annu. Rev. Biophys. Bioeng.* **5**, 271–306 (1976).

15. V. L. Schramm, ENZYMATIC TRANSITION STATES AND TRANSITION STATE ANALOG DESIGN. *Annu. Rev. Biochem.* **67**, 693–720 (1998).

16. J. P. Schwans, F. Sunden, A. Gonzalez, Y. Tsai, D. Herschlag, Correction to "Evaluating the Catalytic Contribution from the Oxyanion Hole in Ketosteroid Isomerase." *J. Am. Chem. Soc.* **138**, 7801–7802 (2016).

17. D. C. Hawkinson, R. M. Pollack, N. P. Ambulos, Evaluation of the Internal Equilibrium Constant for 3-Oxo-.DELTA.5-steroid Isomerase Using the D38E and D38N Mutants: The Energetic Basis for Catalysis. *Biochemistry* **33**, 12172–12183 (1994).

18. I. P. Petrounia, R. M. Pollack, Substituent Effects on the Binding of Phenols to the D38N Mutant of 3-Oxo-Δ^{5}-steroid Isomerase. A Probe for the Nature of Hydrogen Bonding to the Intermediate †. *Biochemistry* **37**, 700–705 (1998).

19. V. Lamba, F. Yabukarski, M. Pinney, D. Herschlag, Evaluation of the Catalytic Contribution from a Positioned General Base in Ketosteroid Isomerase. *J. Am. Chem. Soc.* **138**, 9902–9909 (2016).

20. A. Radzicka, R. Wolfenden, A proficient enzyme. *Science* **267**, 90–93 (1995).

21. I. K. McDonald, J. M. Thornton, Satisfying Hydrogen Bonding Potential in Proteins. *J. Mol. Biol.* **238**, 777–793 (1994).

22. D. Herschlag, M. M. Pinney, Hydrogen Bonds: Simple after All? *Biochemistry* **57**, 3338–3352 (2018).

23. S. O. Shan, D. Herschlag, Hydrogen bonding in enzymatic catalysis: analysis of energetic contributions. *Methods Enzymol.* **308**, 246–276 (1999).

24. S. W. Kim, C. Y. Kim, W. F. Benisek, K. Y. Choi, Cloning, nucleotide sequence, and overexpression of the gene coding for delta 5-3-ketosteroid isomerase from Pseudomonas putida biotype B. *J. Bacteriol.* **176**, 6672–6676 (1994).

25. D. A. Kraut, *et al.*, Testing electrostatic complementarity in enzyme catalysis: hydrogen bonding in the ketosteroid isomerase oxyanion hole. *PLoS Biol.* **4**, e99 (2006).

26. D. L. Turner, Binomial solvent suppression. *J. Magn. Reson. 1969* **54**, 146–148 (1983).

27. R. B. Fenwick, H. van den Bedem, J. S. Fraser, P. E. Wright, Integrated description of protein dynamics from room-temperature X-ray crystallography and NMR. *Proc. Natl. Acad. Sci.* **111**, E445–E454 (2014).

28. H. van den Bedem, A. Dhanik, J.-C. Latombe, A. M. Deacon, Modeling discrete heterogeneity in X-ray diffraction data by fitting multi-conformers. *Acta Crystallogr. D Biol. Crystallogr.* **65**, 1107–1117 (2009).

29. M. M. Pinney, *et al.*, Structural Coupling Throughout the Active Site Hydrogen Bond Networks of Ketosteroid Isomerase and Photoactive Yellow Protein. *J. Am. Chem. Soc.* **140**, 9827–9843 (2018).

30. W. Kabsch, XDS. *Acta Crystallogr. D Biol. Crystallogr.* **66**, 125–132 (2010).

31. Collaborative Computational Project, Number 4, The CCP4 suite: programs for protein crystallography. *Acta Crystallogr. D Biol. Crystallogr.* **50**, 760–763 (1994).

32. Evans, Murshudov, How good are my data and what is the resolution? *Acta Crystallogr. D Biol. Crystallogr.* **69**, 1204–1214 (2013).

33. S. French, K. Wilson, On the treatment of negative intensity observations. *Acta Crystallogr. Sect. A* (1978) https:/doi.org/10.1107/S0567739478001114 (August 12, 2019).

34. A. J. McCoy, *et al.*, Phaser crystallographic software. *J. Appl. Crystallogr.* **40**, 658–674 (2007).

35. G. Langer, S. X. Cohen, V. S. Lamzin, A. Perrakis, Automated macromolecular model building for X-ray crystallography using ARP/wARP version 7. *Nat. Protoc.* **3**, 1171–1179 (2008).

36. P. Emsley, K. Cowtan, Coot: model-building tools for molecular graphics. *Acta Crystallogr. D Biol. Crystallogr.* **60**, 2126–2132 (2004).

37. P. V. Afonine, *et al.*, Towards automated crystallographic structure refinement with phenix.refine. *Acta Crystallogr. D Biol. Crystallogr.* **68**, 352–367 (2012).

38. V. B. Chen, *et al.*, MolProbity: all-atom structure validation for macromolecular crystallography. *Acta Crystallogr. D Biol. Crystallogr.* **66**, 12–21 (2010).

39. D. A. Keedy, J. S. Fraser, H. van den Bedem, Exposing Hidden Alternative Backbone Conformations in X-ray Crystallography Using qFit. *PLOS Comput. Biol.* **11**, e1004507 (2015).

40. D. A. Keedy, *et al.*, An expanded allosteric network in PTP1B by multitemperature crystallography, fragment screening, and covalent tethering. *eLife* **7**, e36307 (2018).

41. W. Doster, S. Cusack, W. Petry, Dynamical transition of myoglobin revealed by inelastic neutron scattering. *Nature* **337**, 754 (1989).

42. H. Frauenfelder, G. A. Petsko, D. Tsernoglou, Temperature-dependent X-ray diffraction as a probe of protein structural dynamics. *Nature* **280**, 558–563 (1979).

43. J. R. Lewandowski, M. E. Halse, M. Blackledge, L. Emsley, Protein dynamics. Direct observation of hierarchical protein dynamics. *Science* **348**, 578–581 (2015).

44. R. F. Tilton, J. C. Dewan, G. A. Petsko, Effects of temperature on protein structure and dynamics: X-ray crystallographic studies of the protein ribonuclease-A at nine different temperatures from 98 to 320 K. *Biochemistry* **31**, 2469–2481 (1992).

45. P. Emsley, B. Lohkamp, W. G. Scott, K. Cowtan, Features and development of Coot. *Acta Crystallogr. D Biol. Crystallogr.* **66**, 486–501 (2010).

46. H. M. Berman, *et al.*, The Protein Data Bank. *Nucleic Acids Res.* **28**, 235–242 (2000).

47. S. W. Kim, *et al.*, High-Resolution Crystal Structures of Δ5-3-Ketosteroid Isomerase with and without a Reaction Intermediate Analogue. *Biochemistry* **36**, 14030–14036 (1997).

48. J. P. Schwans, D. A. Kraut, D. Herschlag, Determining the catalytic role of remote substrate binding interactions in ketosteroid isomerase. *Proc. Natl. Acad. Sci.* **106**, 14271–14275 (2009).

49. R. M. Pollack, S. Bantia, P. L. Bounds, B. M. Koffman, pH dependence of the kinetic parameters for 3-oxo-delta 5-steroid isomerase. Substrate catalysis and inhibition by (3S)-spiro[5 alpha-androstane-3,2'-oxiran]-17-one. *Biochemistry* **25**, 1905–1911 (1986).

50. D.-H. Kim, *et al.*, Contribution of the Hydrogen-Bond Network Involving a Tyrosine Triad in the Active Site to the Structure and Function of a Highly Proficient Ketosteroid Isomerase from *Pseudomonas putida* Biotype B [†,‡]. *Biochemistry* **39**, 4581–4589 (2000).

51. A. Bondi, van der Waals Volumes and Radii. *J. Phys. Chem.* **68**, 441–451 (1964).

52. L. Pauling, The Nature of the Chemical Bond. *Cornell Univ. Press* (1960).

53. D. A. Kraut, P. A. Sigala, T. D. Fenn, D. Herschlag, Dissecting the paradoxical effects of hydrogen bond mutations in the ketosteroid isomerase oxyanion hole. *Proc. Natl. Acad. Sci. U. S. A.* **107**, 1960–1965 (2010).